


2014

Green Technologies and Sensor Networks for BMP Evaluation in Stormwater Retention Ponds and Wetlands.

Anthony Crawford
University of Central Florida

 Part of the [Environmental Engineering Commons](#)
Find similar works at: <https://stars.library.ucf.edu/etd>
University of Central Florida Libraries <http://library.ucf.edu>

This Masters Thesis (Open Access) is brought to you for free and open access by STARS. It has been accepted for inclusion in Electronic Theses and Dissertations, 2004-2019 by an authorized administrator of STARS. For more information, please contact STARS@ucf.edu.

STARS Citation

Crawford, Anthony, "Green Technologies and Sensor Networks for BMP Evaluation in Stormwater Retention Ponds and Wetlands." (2014). *Electronic Theses and Dissertations, 2004-2019*. 1209.
<https://stars.library.ucf.edu/etd/1209>

**GREEN TECHNOLOGIES AND SENSOR NETWORKS FOR BMP
EVALUATION IN STORMWATER RETENTION PONDS AND
WETLANDS**

by

ANTHONY JAMES CRAWFORD
B.S. University of Central Florida, 2010

A thesis submitted in partial fulfillment of the requirements
for the degree of Master of Science
in the Department of Civil, Environmental, and Construction Engineering
in the College of Engineering and Computer Science
at the University of Central Florida
Orlando, Florida

Fall Term
2014

Major Professor: Ni-Bin Chang

© 2014 A. James Crawford

ABSTRACT

The aim of this thesis is to examine and develop new techniques in stormwater Best Management Practices (BMP) for nutrient and erosion reduction and monitoring by incorporation of low impact green technologies and sensor networks. Previous research has found excessive nutrient loading of nitrogen and phosphorus species from urban stormwater runoff can lead to ecological degradation and eutrophication of receiving lakes and rivers (Fareed and Abid, 2005). In response, the Florida Department of Environmental Protection (FDEP) has set forth reduction goals as established in Total Maximum Daily Load (TMDL) reports to reduce nutrient loading and restore, or maintain, Florida water bodies to reasonable conditions. Often times current stormwater management practices are not sufficient to attain these goals and further improvements in system design are required. In order to reach these goals, affordable technologies designed for both nutrient reduction and monitoring of system performance to deepen and improve our understanding of stormwater processes are required.

Firstly this thesis examines the performance of three types of continuous-cycle Media Bed Reactors (MBRs) using Bio-activated Adsorptive Media (BAM) for nutrient reduction in three retention ponds located throughout the Central Florida region. Chapter 2 examines the use of a Sloped and Horizontal MBRs arranged in a baffling configuration, whereas Chapter 3 examines the field performance of a Floating MBR arranged in an upflow configuration. Each MBR was analyzed for performance in reducing total phosphorus, soluble reactive phosphorus, total nitrogen, organic nitrogen, ammonia, nitrates + nitrites, turbidity and chlorophyll *a* species as measured from the influent to effluent ends of the MBR. The results of the experiments indicate that MBRs may be combined with retention ponds to provide “green technology”

alternatives for inter-event treatment of nutrient species in urban stormwater runoff by use of recyclable sorption media and solar powered submersible pumps.

Secondly the thesis focusses on three new devices for BMP monitoring which may be integrated into wireless networks, including a Groundwater Variable Probe (GVP) for velocity, hydraulic conductivity and dispersion measurements in a retention pond bank (Chapter 4), an affordable Wireless Automated Sampling Network (WASN) for sampling and analysis of nutrient flux gradients in retention ponds (Chapter 5), and finally an Arc-Type Automated Pulse Tracer Velocimeter (APTV) for low velocity and direction surface water measurements in retention ponds and constructed wetlands (Chapter 6).

The GVP was integrated with other environmental sensing probes to create a remote sensing station, capable of real-time data analysis of sub-surface conditions including soil moisture, water table stage. Such abilities, when synced with user control capabilities, may help to increase methods of monitoring for applications including erosion control, bank stability predictions, monitoring of groundwater pollutant plume migration, and establishing hydraulic residence times through subsurface BMPs such as permeable reactive barriers. Advancement of this technology may be used by establishing additional sub-stations, thereby creating sensing networks covering broader areas on the kilometer scale. Two methods for velocity calculation were developed for the GVP for low flow ($P_e < 0.2$) and high flow ($P_e > 0.6$) conditions. The GVP was found to operate from a 26-505 cm d^{-1} range in the laboratory to within $\pm 26\%$ of expected velocities for high-flow conditions and effectively measure directional flow angles to within $\pm 14^\circ$ of expected. Hydraulic conductivity measurements made by the GVP were confirmed to within $\pm 12\%$ as compared to laboratory measurements. The GVP was found capable of measuring the dispersion coefficient in the laboratory, however turbulent interferences

caused during injection was found to occur. Further advancement of the technology may be merited to improve dispersion coefficient measurements.

Automated water sampling can provide valuable information of the spatial and temporal distribution of pollutant loading in surface water environments. This ability is expanded with the development of the WASN, providing an affordable, ease-of-use method compared to conventional automated water samplers currently on the market. The WASN was found to effectively operate by text activation via GSM cellular networks to an activation module. Propagation of the signal was distributed to collection units via XBee modules operating on point-to-point star communication using an IEEE 802.15.4 protocol. Signal communications effectively transmitted in the field during a storm event to within a range of 200 feet and collected 50 ± 4 ml samples at synced timed increments. A tracer study confirmed that no mixing of samples occurs when a factor of safety of 2 is applied to flush times. This technology provides similar abilities to current market devices at down to 10% of the cost, thereby allowing much more sampling locations for a similar budget.

The Arc-Type APTV is useful in establishing both low range horizontal velocity fields and expanding low range velocity measurements below detection ranges of mechanical velocity meters. Installation of a field station showed system functionality, which may be integrated with other environmental sensing probes for surface water testing. This may assist in nutrient distribution analysis and understanding the complex behavior of hydraulic retention times within wetland systems. The device was found to work effectively in both lab and field environments from a $0.02 - 5.0 \text{ cm s}^{-1}$ range and measure velocity within approximately $\pm 10\%$ of an acoustic Doppler velocimeter and within an average of $\pm 10^\circ$ of directional measurements. A drop in accuracy was measured for velocity ranges $>4.5 \text{ cm s}^{-1}$. The field station operated on 3G CDMA

cellular network two-way communication by installation of a Raven cellular modem. Use of LoggerNet software allowed control and data acquisition from anywhere with an internet connection.

This thesis also introduces brief discussions on expanding these “point” measurement technologies into sensing networks. Installation of sub-stations with communication protocols to one central master node station may broaden the sensing system into much larger kilometer-scale ranges, thus allowing large spatial analysis of environmental conditions. Such an integration into controllable sensing networks may help bridge the gap and add calibration and verification abilities between fine-resolution “point” measurements and large scale technologies such as Electrical Resistivity Tomography and satellite remote sensing. Furthermore, application of sensing networks may assist in calibration and verification of surface and groundwater models such as ModFlow, SVFlux and FEHM.

ACKNOWLEDGMENTS

I would like to express my outstanding gratitude to my advisors, Dr. Ni-Bin Chang and Dr. Marty Wanielista for their assistance in developing this thesis. Their support and guidance has been a great asset in my developing career. I would additionally like to thank my co-workers for their assistance in this work including Bastien Clouet, Jamie Jones, Benjamin Vannah, and Golam Mohuiddin. I would also especially like to thank Tyler Petresky for his outstanding work in developing the circuitry and programming of the WASN.

TABLE OF CONTENTS

LIST OF FIGURES	xii
LIST OF TABLES	xviii
CHAPTER 1 : INTRODUCTION	1
1.1 Importance of Stormwater Management.....	1
1.2 Media Bed Reactors	4
1.3 Application of Bio-activated Adsorptive Media	5
1.4 First Flush Phenomenon.....	8
1.5 TMDL and NPDES Permitting	8
1.6 Wireless Sensor Networks for Environmental Monitoring.....	10
1.7 Research Objectives	11
1.8 Limitations	12
1.9 References	13
CHAPTER 2 : STORMWATER NUTRIENT REDCTION USING SLOPED AND HORIZONTAL MEDIA BED REACTORS	15
2.1 Introduction	15
2.1.1 Chapter Objectives.....	16
2.2 Methodology	17
2.2.1 Location	17
2.2.2 Design	18
2.2.3 Installation.....	23
2.3 Results and Discussion.....	26
2.3.1 Source Water Quality.....	26
2.3.2 SMBR Field Performance.....	27
2.3.3 HMBR Field Performance	31
2.3.4 Hydraulics	34
2.4 Final Remarks	35
2.5 References	35
CHAPTER 3 : STORMWATER NUTRIENT REDUCTION USING UPFLOW FLOATING MEDIA BED REACTOR.....	38

3.1	Introduction	38
3.1.1	Chapter Objectives.....	41
3.2	Methodology	41
3.2.1	Location	41
3.2.2	Source Water Quality.....	42
3.2.3	Floating Media Bed Reactor Design.....	43
3.2.4	Nutrient Removal.....	45
3.2.5	Hydraulics	46
3.3	Results and Discussion.....	46
3.4	Final Remarks	51
3.5	References	51
CHAPTER 4 : EROSION CONTROL MONITORING USING INTEGRATED SOIL MOISTURE AND GROUNDWATER VELOCIMETER SYSTEM		54
4.1	Introduction	54
4.1.1	Chapter Objectives.....	56
4.2	Methodology	56
4.2.1	Volumetric Water Content.....	61
4.3	GVP Theory	62
4.3.1	Directional Calculations.....	62
4.3.2	Velocity Magnitude and Dispersion Coefficient	64
4.3.3	Hydraulic Conductivity.....	67
4.4	Methodology	67
4.4.1	Operation and Laboratory Set-up.....	67
4.4.2	Field Measurements	70
4.5	Results	72
4.5.1	Laboratory Testing.....	72
4.5.2	Field Testing	76
4.5.3	Communications & Sensor Network Design	81
4.5.4	Tri-Lock Block.....	83
4.6	Final Remarks	86
4.7	References	87

CHAPTER 5 : NUTRIENT FLUX MONITORING USING AUTOSAMPLER WIRELESS NETWORKS	89
5.1 Introduction	89
5.1.1 Chapter Objectives.....	90
5.2 Methodology	90
5.2.1 Location	90
5.2.2 Wireless Autosampler Network Development	91
5.3 Results and Discussion.....	101
5.4 Final Remarks	103
5.5 References	103
CHAPTER 6 : MEASURING THE LOW VELOCITY FIELD WITH AN ARC-TYPE AUTOMATIC PULSE TRACER VELOCIMETER IN WETLANDS AND PONDS	105
6.1 Introduction	105
6.1.1 Wetland Applications.....	107
6.1.2 Stormwater Pond Applications	110
6.1.3 Chapter Objectives.....	111
6.2 Methodology	111
6.2.1 Study Sites	111
6.2.2 STA 3B – Everglades, Florida.....	111
6.2.3 APTV Operation and Laboratory Set-up	114
6.2.4 APTV Velocity Calculations	118
6.2.5 APTV Field Measurements.....	119
6.3 Results and Discussion.....	122
6.3.1 Laboratory Performance	122
6.3.2 Velocity Comparison	124
6.3.3 Field Testing	131
6.4 APTV Sensor Network and Other Potential Applications	135
6.5 Final Remarks	139
6.6 References	141
CHAPTER 7 : CONCLUSIONS	146
APPENDIX A: HMBR RESULTS.....	149

APPENDIX B: SMBR RESULTS	152
APPENDIX C: FMBR RESULTS	155
APPENDIX D: ZOLFO POND RESULTS.....	159
APPENDIX E: ORLANDO POND RESULTS	162
APPENDIX F: PALATKA POND RESULTS.....	165

LIST OF FIGURES

Figure 1-1 Particle size distribution curve of nutrient sorption media mix 2. (Jones, 2013).....	7
Figure 2-1 Design layout of a SMBR including solar powered submersible recycling pump. A roughing filter is placed in the first chamber to reduce clogging and prolong the life cycle of the filter.....	20
Figure 2-2 Design layout of a HMBR including solar powered submersible recycling pump. Due to close proximity to the inlet of the pond and associated high turbidity amounts only a 5/8ths expanded clay mixture is utilized.	20
Figure 2-3 Theoretical battery drainage graph for a 60 Ah battery connected to a 12V pump running continuously at 330mA with (a) no solar panel, (b) 7 watt solar panel and (c) 15 watt solar panel.	23
Figure 2-4 Installation of SMBR on the pond bank at Zolfo Springs with (a) without roughing media in the 1 st chamber and (b) with a 5/8ths expanded clay roughing media mix added to the 1 st chamber.	24
Figure 2-5 Exterior view of installation of SMBR on the pond bank at Zolfo Springs. The SMBR is powered by two 15W solar panels in parallel.	24
Figure 2-6 High turbidity near the inlet of the Orlando Pond (left) which caused the premature clogging of the HMBR filled with Media Mix 2 (right).	25
Figure 2-7 HMBR re-filled with 50% 5/8 th expanded clay and 50% tire chunk.	25
Figure 2-8 Drop in DO levels comparing the first week (blue columns) to the third week of operation (red bars). An initial aerating throughout the chamber occurs which gradually ..	29
Figure 2-9 Chl- <i>a</i> concentrations through the SMBR between influent and effluent sampling locations.	30
Figure 2-10 Turbidity measurements comparing influent and effluent concentrations measured in the SMBR.	30
Figure 2-11 DO concentrations in the HMBR one day following the initial run of the HMBR and shortly following a storm event.	32
Figure 2-12 TN comparison between influent and effluent sampling locations on the HMBR. .	33
Figure 2-13 Turbidity comparison between influent and effluent sampling locations on the HMBR.	33
Figure 3-1 Theoretical flow rate comparison of gravity vs. pump filters for one week duration with one major storm event.	40
Figure 3-2 Palatka pond site layout with FMBR placement and photo.	43
Figure 3-3 Design layout of a FMBR including solar powered submersible recycling pump. Pond water initially is routed into a settling chamber before advancing through the upflow filter filled with sorption Media Mix #2.	45
Figure 3-4 TP (<i>left</i>) and TN (<i>right</i>) concentrations taken at the influent and effluent sampling locations within the FMBR.	48

Figure 3-5 TP (<i>left</i>) and TN (<i>right</i>) measurements taken at the inlet and outlet sampling locations of the Palatka pond prior and after FMBR installation.	49
Figure 3-6 Laboratory head loss testing of Media Mix #2 in an upflow filter. Results display the increase in head loss measured over four runs conducted over a six month period.	50
Figure 4-1 Inlet #2 displaying erosion occurring around support wall, picture taken June 2 nd , 2012.	58
Figure 4-2 Inlet #2 displaying erosion occurring around support wall following refilling of the bank, picture taken March 1 st , 2014.	58
Figure 4-3 Inlet #2 shortly following re-filling of the bank, picture taken March 25 th , 2014.	59
Figure 4-4 Inlet #2 erosion re-occurring around support wall three months following re-filling, picture taken March 17 th , 2014.	59
Figure 4-5 Area placement of Tri-Lock Blocks around Inlet #2. Also depicted are locations of test holes for pressure transducers, soil moisture probes and GVP installation.	60
Figure 4-6 Typical slope placement specifications for Tri-Lock Blocks.	61
Figure 4-7 Electronics enclosure casing for field station control of GVP, soil moisture probes and pumps for water sample collection.	62
Figure 4-8 Example of a tracer response curve. The peak change in the resistance ratio is denoted by Δr	63
Figure 4-9 Flow diagram for calculation procedure of flow direction, velocity, dispersion coefficient and dispersivity from tracer curves for $P_e > 1$	65
Figure 4-10 Front- and bottom-view schematic of a 6cm diameter GVP. Detectors are comprised of eight sets of 18 gauge copper wires (with an 8.5cm portion stripped) built upon a 3D printed support frame.	69
Figure 4-11 GVP set up in a hydraulic flume for laboratory testing. Sand is contained between two perforated retention walls to produce uniform, lateral, flow across the flume. The hydraulic gradient is measured by dh/dx	70
Figure 4-12 GVP field station installation on a pond bank including a GVP probe, pressure transducer wells and EC-5 soil moisture probes.	72
Figure 4-13 Layered response curve for five consecutive pulses at an expected velocity of 80 cm d^{-1} . The overall shape and Δr between each pulse remains similar indicating little variation between pulse measurements.	73
Figure 4-14 <i>Left</i> - agreement between v_{EXPECTED} (eq. 1) and v_{GVP} (eq. 4). The expected velocity is used as the independent variable whereas v_{GVP} is used as the dependent variable, the dashed lines represent the linear regression of the v_{GVP} measurements. <i>Right</i> – agreement between v_{GVP} and the change in hydraulic head (dh).	74
Figure 4-15 Simultaneous plot of all eight tracer response curves measured by each detector for a salt injection with probe set at a 45 ⁰ angle to the direction of flow and velocity set to 270 cm d^{-1}	75
Figure 4-16 Soil moisture readings and precipitation data for the Royal Palm pond bank.	77

Figure 4-17 Correlation of head differential from pond to PT-W1 measured by pressure transducer (cm) of the pond bank and precipitation data (cm) for the Royal Palm Pond. Water table elevations are in reference to centimeters above the pond outlet drawdown orifice.....	78
Figure 4-18 Correlation of head differential measured by pressure transducer readings (cm) of the pond bank and precipitation data (cm) for the Royal Palm Pond. Water table elevations are in reference to centimeters above the pond outlet drawdown orifice.	79
Figure 4-19 GVP measurements following a four second injection (5.2ml) of 15mg ^l ⁻¹ NaCl at the Royal Palm pond bank. A general spreading of the tracer is witnessed with close correlation of precipitation events to decreases in Δr by the 135 ⁰ , 180 ⁰ , and 225 ⁰ detectors, representative of an overall shifting of tracer plume away from these detectors.	80
Figure 4-20 Measurement of the tracer plume edge using resistance measurements by the 180 ⁰ detector correlated with the hydraulic gradient ($\Delta h/\Delta x$). As seen, an increase in $\Delta h/\Delta x$ results in an increase in resistance ratio, relating to the pulse moving away from the pond. Daily fluctuations in detector readings are believed to be a combined cause of pulse movement and pulse spreading caused by temperature dependent molecular diffusion.....	80
Figure 4-21 GVP communications diagram for a field station including pressure transducers for measurement of upstream and downstream groundwater elevations and soil moisture probes. The station is remotely controllable from anywhere with an internet connection by using a laptop and <i>LoggerNet</i> software or 3G network using a smartphone and <i>LoggerLink</i> software.	81
Figure 4-22 GVP sensing network. Two master station nodes communicate via point-to-point spread spectrum radio frequencies, whereas master to substation nodes are operated on point-to-multipoint communications. Final relay is sent via a cell modem and 3G CDMA cellular signals back to the user. All telecommunications are two-way for data retrieval and transmittal.	82
Figure 4-23 Inlet #1 two months following installation of TriLock Blocks, picture taken August 30 th , 2014.	84
Figure 4-24 Inlet #2 two months following installation of TriLock Blocks, picture taken August 30 th , 2014.	84
Figure 4-25 Minor erosion of fill soil between blocks occurring at the headwall edge of Inlet #2. Despite the loss of fill soil the blocks appear to retain their structural integrity.	85
Figure 4-26 Vegetative regrowth between blocks approximately 2 months following installation.	85
Figure 5-1 Communications diagram for activation of the WASN. Activation may be accomplished anywhere with a working phone signal.	92
Figure 5-2 Basic circuit diagram for connection of WASN collection units. The microprocessor, XBee, voltage regulator, transistor and bread board are located within the electronics enclosure whereas the battery, peristaltic pumps, and servomotor are located in the main enclosure.	94

Figure 5-3 GSM module used for receiving text command and transmittal to XBee Pro.	95
Figure 5-4 AutoCAD layout of the WASN sampling tray. The servo motor sits at the center of the tray and rotates at 20° increments to fill sample bottles via an attached arm. Two flush holes are included to flush the tubes in-between samples.	97
Figure 5-5 Photograph displaying the WASN sampling tray, servo motor and arm for holding influent tubes. The tray may hold up to 12 bottles (only two are pictured for clarity).	97
Figure 5-6 Adafruit high torque peristaltic pumps used for sample collection. Pumps operate on 12volt DC power and are directly powered by a battery.	98
Figure 5-7 XBee radio transmitter/receiver used for communications between the GSM shield module and the sampling units. Each XBee has a maximum 1-mile transmittal radius.	99
Figure 5-8 Arduino Uno microprocessor used for programming and control of the WASN collection units and peristaltic pumps.	100
Figure 5-9 Field application of WASN networked system. The GSM unit is comprised of an enclosure case, GSM module, XBee radio transmitter, microprocessor and 12 volt battery; each WASN is comprised of an enclosure case, XBee, microprocessor, sampling tray, one servo motor, two peristaltic pumps, tubing, and 12 volt battery.	101
Figure 5-10 Rhodamine WT tracer test conducted for 12' section of tubing to establish the degree of spreading within the intake tubes. As seen a relatively large spread occurs due to frictional forces acting near the walls of the tube.	103
Figure 6-1 Map displaying Lake Okeechobee, the EAA, the STAs and the Northern Everglades. The STAs were strategically located to intercept runoff from the EAA prior to entering the Everglades (Source: SFWMD, 2012).	113
Figure 6-2 Front-view schematic of an APTV cross-type detector. Detectors are comprised of four sets of 18 gauge copper wires (with 5 cm stripped) built upon a 3/4-inch support frame.	115
Figure 6-3 Side-view schematic of a 1 st generation (left) and 2 nd generation (right) APTV arc-type detector. The 2nd generation APTV attaches the injection port physically to the body, includes a slimmer frame, moves the injection port closer to the detectors, and has an improved hydrofoil design.	116
Figure 6-4 Top view (cross section A) of APTV detector body and injection port. Five detector wire pairs are located equidistant from the injection port to allow 180 degree detectable range. The field prototype APTV detector was placed with the center detector wire pair oriented to capture southern flow velocities.	116
Figure 6-5 Picture of the Engineering Laboratory Design hydraulic flume used for the laboratory study. An APTV detector and Flow Tracker ADV are seen setup approximately three fourths from the beginning of the flume.	117
Figure 6-6 Example pulse tracer response curve generated by the APTV in the hydraulic flume. Sodium chloride tracer used at 15gL ⁻¹ concentration. Injection of the pulse occurred at zero seconds. The correlating peak detection time (Δt_{peak}) was measured at 4.5 seconds.	119

Figure 6-7 APTV field station system communications diagram and photograph displaying support structure, tracer reservoir, electronics enclosure box, cell modem antennae, profiling detectors, 12V battery and pump enclosure box. An additional portable “satellite” detector was set up approximately 4 meters from the station next to a Vector ADV (<i>not pictured</i>). Picture was taken at Site 1 facing south.	120
Figure 6-8 Standard deviation values for APTV vs ADV measurements in the flume. The effects of the calibration equation on the standard deviation is seen to increase at velocities $>4.5\text{cms}^{-1}$	124
Figure 6-9 Calibration curve developed from direct comparison of APTV raw velocity low regime (left) and high regime (right) data using Δt_{peak} method to Sontek Flow Tracker ADV velocity data for the 1 st generation APTV.	125
Figure 6-10 Calibration curve developed from direct comparison of APTV raw velocity data using Δt_{peak} method to Sontek Flow Tracker ADV velocity data for the 2 nd generation APTV (left) and correlation between APTV calibrated and ADV velocity measurements.	126
Figure 6-11 Effect of pulse averaging on correlation with ADV velocity measurements for 2 nd Generation APTV.	127
Figure 6-12 Detector response curves conducted in the flume using the 2 nd Generation APTV for 0° (top), 56° to the left (middle) and 75° to the right (bottom) flow directions.	128
Figure 6-13 Variable velocity flume test comparing ADV with 2 nd Generation APTV velocity measurements.	130
Figure 6-14 Variable velocity flume test comparing ADV with 2 nd Generation APTV flow direction measurements.	130
Figure 6-15 Correlation between ADV and 2 nd Generation APTV velocity magnitude measurements.	131
Figure 6-16 Field comparison of Vector ADV and calibrated APTV velocities for Site 1. Field measurements were conducted in Cell 3B of the STA located in the northern portion of the Everglades, FL.	132
Figure 6-17 Field comparison of Vector ADV and calibrated APTV velocities for Site 1. Field measurements were conducted in Cell 3B of the STA located in the northern portion of the Everglades, FL.	133
Figure 6-18 Field comparison of Vector ADV and calibrated APTV velocities for Site 2. Field measurements were conducted in Cell 3B of the STA located in the northern portion of the Everglades, FL.	134
Figure 6-19 Field comparison of Vector ADV and calibrated APTV velocities for Site 2. Field measurements were conducted in Cell 3B of the STA located in the northern portion of the Everglades, FL. Positive results indicate degrees west of southern axis while negative results indicate degrees east of southern axis.	134
Figure 6-20 Communications diagram for full-scale remote APTV system designed for horizontal velocity field, water & soil quality and environmental measurements.	136

Figure 6-21 Theoretical field installation of APTV sensing network with seven velocity sensors positioned to capture horizontal velocity profile.....	137
Figure 6-22 Side-view schematic of an APTV arc-type detector for operation in an estuary environment.	138

LIST OF TABLES

Table 1-1. Material Characterization BAM Mixture #2 Nutrient Sorption Media (Jones, 2013).	6
Table 1-2 Florida Surface Water Quality Standards (FDEP, 2014)	9
Table 2-1 Field Site Identification Numbers and Geographic Coordinates	17
Table 2-2 Identified Pollutant Issues	18
Table 2-3 MBR Design Comparison	19
Table 2-4 Pump Specifications	21
Table 2-5 Zolfo Springs Pond pre-BMP Nutrient Concentrations	26
Table 2-6 Orlando Pond pre-BMP Nutrient Concentrations	27
Table 2-7 SMBR Mean Reduction Performance	27
Table 2-8 SMBR Mean Reduction Performance	28
Table 2-9 HMBR Mean Removal Efficiencies	31
Table 2-10 HMBR Mean Removal Efficiencies	31
Table 3-1. Field Site Identification Numbers and Geographic Coordinates	41
Table 3-2. Field Site Basin and Pond Characteristics	41
Table 3-3. Palatka Pre-BMP Nutrient Concentrations	42
Table 3-4. FMBR design specifications	44
Table 3-5. Mean Reduction of Tested Parameters by the FMBR	47
Table 3-6. Concentration Comparison between Influent and Effluent Concentrations of the FMBR	47
Table 4-1 Field Site Identification Numbers and Geographic Coordinates	57
Table 4-2 Field Site Pond Characteristics	57
Table 4-3 Statistical summary of v_{GVP} and K measurements as compared with the expected values	73
Table 4-4 Statistical summary of GVP velocity directional measurements versus the expected direction of flow	75
Table 5-1 Field Site Identification Numbers and Geographic Coordinates	91
Table 6-1 Velocity Meter Specification Comparison	106
Table 6-2 Velocity meters used for surface water measurements	108
Table 6-3 Statistical summary of velocity magnitude measurements made by the 2 nd Generation APTV	123
Table 6-4 Statistical summary of velocity magnitude measurements made by the 2 nd Generation APTV	129

CHAPTER 1: INTRODUCTION

1.1 Importance of Stormwater Management

The hydrologic cycle is a continuous process, cycling water from the atmosphere to the ground and back. Movement of water occurs through many different phenomena including precipitation, runoff, evapo-transpiration, infiltration, groundwater recharge, and stream base flow, all of which contain important properties of both water quantity as well as water quality. The development of urban settings may alter this water cycle in several ways, which if not adjusted by stormwater management practices, could lead to increases in flooding, erosion of banks, eutrophication of lakes as well as other detrimental impacts to water bodies such as rivers, lakes, streams and the ocean.

Chemical and biological water quality characteristics may be altered as a result of the urbanization of land. During development portions of pervious land are altered to impervious areas, thereby reducing the retention time of stormwater remaining on the land. As a result a more rapid transport of runoff from the site occurs, thus allowing less time for natural settling processes of suspended solids and other pollutants. Without proper management to attenuate the runoff leaving the site, the increased pollutant loading may lead to detrimental environmental and economic impacts downstream. Additionally, pollutant loading to water bodies is increased from the deposition of pollutants and nutrients to land surfaces, which become entrained and transported in runoff during storm events to downstream water bodies. Excessive nutrient loading, such as fertilizer application to lawns and agricultural lands, has become a growing issue, leading to eutrophic conditions developing downstream water bodies. Other sources of

non-point pollutant sources may also include vehicle exhaust, vehicle wear and tear (Vitousek et al., 1997; German, 1989), leaking underground septic storage tanks, industrial and commercial site runoff and atmospheric deposition.

One common technique utilized in areas of high water table such as Central Florida are retention basins, otherwise known as retention ponds or wet detention basins. Wet retention ponds are installed to intercept and attenuate runoff exiting urbanized areas in order to match pre-developed flow characteristics to post-developed flows. Wet retention ponds are a commonly found throughout Central Florida and have been a successful means in attenuating stormwater flow and reducing total suspended solids through settling processes (Wanielista, 1978; Harper and Herr, 1993; Harper, 1995; Mallen et al, 2002) from urban runoff in order to meet an 80% average annual load reduction as per Chapter 62-40 of the Florida Administrative Code (F.A.C.). The F.A.C. currently only pertains to TSS reductions, however recent attention has been focused on nutrient reduction. Studies have shown a somewhat variable ability of retention ponds in reducing nutrient species, with TP reductions reported as 30-90% (Schueler, 1992), 51% (Riner, 2000), and 69% (Harper and Baker, 2007); soluble nutrients as 40-80% (Schueler, 1992), 50-70 (Hartigan, 1988), 79% (OP only) (Harper and Baker, 2007). TN species appear to show a lesser degree of removal compared to TP with some values being reported as 37% (Harper and Baker, 2007), 12-15% (Cullom, 1984), and 35% (Yousef et al, 1986). Martin M.H. (1988) found that a pond was capable of removing from less than 0% to 72% of total nutrient species. If regulations progress to include >80% removal efficiencies for nutrient species similar to those required of TSS reductions, additional treatment measures will be required to meet these regulations. Stormwater Best Management Practices

A best management practice (BMP) is defined as “a control technique used for a given set of conditions to achieve water quality and quantity at a minimum price” (MRI, 2003). BMPs primarily focus on improving both water quality and reducing the volume of stormwater runoff, which in itself may also improve the water quality by decreasing erosion downstream or infiltrate the nutrient laden first-flush volumes of stormwater runoff. The type and functionality of BMPs vary over a wide range, each with benefits and drawbacks. Listed below are examples of typical BMPs used in Floridian environments:

- Wet Detention Basin / Wet Pond
- Retention Basin / Infiltration Basin
- Exfiltration Trenches
- Vegetative Swales / Grass Swales
- Vegetated Filter Strips
- Constructed Filters
- Bioretention Basins / Landscape Retention
- Check Dams
- Baffle Boxes
- Floating Treatment Wetlands
- “Soft Armor” Erosion Controls - Turf Reinforcement Mats, Vegetated Banks, etc
- “Hard Armor” Erosion Controls – Concrete Reinforcement, TriLock Blocks, etc

Constructed filters are structures designed for the physical filtration of stormwater through a filtration media such as sand or sorption media. A wide variety of filtration media has been used in previous studies from natural media including sand (Urbonas, B, 1999; Harris et al, 1996; Tufenkji et al, 2002), mulch and wood chips (Ray et al, 2006; Kim et al, 2006) to man-made or man processed materials such as crushed piping materials (Li et al, 2000). Filters may be built as large in-place structures or prefabricated and installed at location. Traditional filters typically are installed on the outlet of a wet retention/detention ponds and are event driven, e.g. only operate under flow conditions when an increase in hydraulic gradient occurs, during and shortly following storm events.

With filtration media there exists an inherent maximum hydraulic loading capacity per area ($L^3L^{-2}t^{-1}$). When this loading capacity increases beyond the maximum loading capacity particulate matter dislodges from the media and becomes entrained in the effluent stream, leading to possible increased concentrations in the effluent. Due to the relative sparse amount of time traditional filters may be in operation, large filter areas are typically required in order to produce reasonable hydraulic loading rates through the filter. This may lead to high installation and maintenance costs.

1.2 Media Bed Reactors

Currently, most stormwater BMPs treat stormwater runoff during, or closely following, storm events. Such BMPs include: grass swales, constructed filters, baffle boxes, filter strips, exfiltration trenches, etc, which operate only when runoff flow is present. Conversely, few BMPs are capable of treating stormwater runoff in between storm events, also known as inter-event periods, which may present a significant amount of potential treatment time. Such inter-event treatment methods such as wet retention ponds, floating treatment wetlands, and stormwater reuse have the distinct advantage of treating stormwater for longer durations.

MBRs present a “green technology” addition to stormwater treatment options by pumping stormwater via solar powered submersible pumps from wet retention ponds through a media bed containing a bio-activated adsorptive media (BAM), and returning the treated pond water either directly to the pond, to downstream waterways, or potentially upstream portions of the pond. The Media Bed Reactors examined in this thesis differ from traditional filters by operating on an inter-event continuous nature. Whereby traditional filters only operate when natural hydraulic gradients form, most commonly during an immediately after storm events, MBRs cycle water through the media beds continuously. Using this method may improve filtration operability functions by allowing consistent, long, hydraulic residence times, allowing sufficient contact time for adsorptive

processes as well keep shear stresses across the media constant and within reasonable levels. MBRs may also treat a greater volume of water per total square footage of media compared to “event driven” filters. As an example suppose a design was required to treat $1,000\text{m}^3$ of stormwater in a week with a maximum media loading rate of $5\text{ m}^3\text{m}^{-2}\text{day}^{-1}$. Supposing only one storm event occurred, and the traditional event-driven filter only received significant head to operate for one day of the week, then a total filter area of 200m^2 would be required to meet the treatment volume. However by use of a continuous running filter which could operate for the full seven days, a filter area of only 28.6m^2 would be required, or one seventh of the area, presenting a significant decrease in price and space.

Three types of MBRs are covered in this thesis. Chapter 2 discussed horizontal and sloped MBRs configured in a baffling structure, whereas Chapter 3 discusses a floating type MBR constructed as an upflow filter configuration. Each of the MBRs was field installed and examined for effective reduction in nutrient species, as well as changes in turbidity, pH, chlorophyll *a* and dissolved oxygen. All media utilized within this study are made from inexpensive recycled or natural material including expanded clay, tire crumb, tire chip, sand and limestone

1.3 Application of Bio-activated Adsorptive Media

Bio-activated Adsorptive Media (BAM) has been used as a filtration media to reduce nutrient concentrations in stormwater over the last several years (Hossain, F., 2009; Ryan, P, et al, 2010; Hood, D., 2013). BAM utilizes recycled, cost-effective, natural materials to form mixtures of adsorptive media. BAM primarily operates by three processes, first an adsorptive process in which nutrient species such as OP and NO_x are adsorbed to the surface of the media through Van Der Waals forces, secondly a physical filtration and precipitation process whereby particulate matter with bound phosphorus and nitrogen species is captured between pore spaces, and finally a biological

process in which nutrients are reduced or incorporated into bacterial cells and retained within the media.

Previous laboratory studies have been conducted to establish adsorptive properties of the BAM media for adsorption of SRP, NO₃, and NH₄. Jones et al (2013) conducted several laboratory studies using a BAM mixture comprised of 50% sand, 25% tire crumb and 25% fine expanded clay. Conducting Langmuir isotherm experiments using deionized water (DI) spiked with 1mg l⁻¹ OP, they found that the media had a q_{max} value of 11.6 µgOPg⁻¹_{media} resulting in a linear fit equation of 1/q = 625.93(1/C_e) + 73.95. Using column studies run at 1hr HRT the study found that an adsorptive phase lasted for approximately 150 minutes using DI water spiked with 1mg l⁻¹ of OP, but lasted for approximately 200 hours when using pond water.

The degree of removal due to filtration and precipitation processes may vary depending on the source water properties and physical characteristics of the media including porosity, surface area and particle size distribution. Table 1-1 and Figure 1-1 display properties of media mix #2 conducted by Jones (2013) used in the work of this thesis.

Table 1-1. Material Characterization BAM Mixture #2 Nutrient Sorption Media (Jones, 2013).

	Nutrient Sorption Mix 2
Dry Density (kg·m⁻³)	1387.5
Void Ratio (dimensionless)	0.3696
Porosity (dimensionless)	0.2699
Specific Gravity (G_s)	2.208
Surface Area (m²·g⁻¹)	0.446

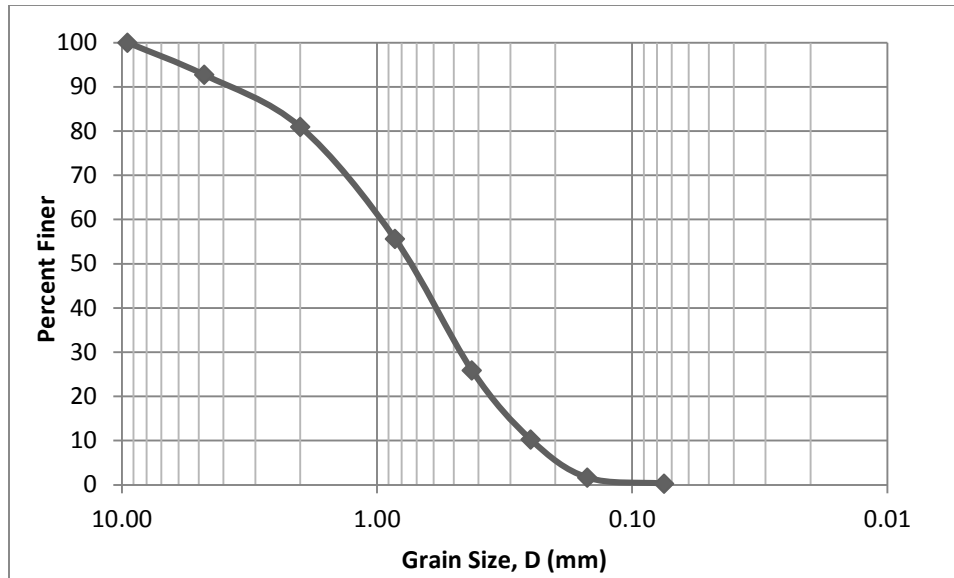
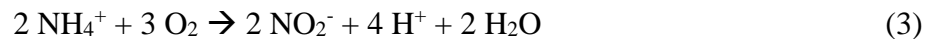
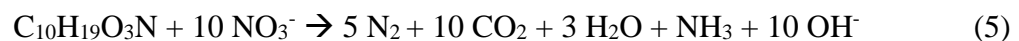


Figure 1-1 Particle size distribution curve of nutrient sorption media mix 2. (Jones, 2013)

Following the exhaustion of adsorptive processes, a biofilm may develop on the media surface, whereby chemical and biological removal processes continue to remove the nutrients. The removal of nitrogen species by biological processes undergoes several chemical steps. Firstly hydrolysis of urea and amino acids to ammonia occurs with conversion to nitrite and nitrate species by nitrifying bacteria under aerobic conditions (Sawyer *et al.*, 2003):



Under anaerobic conditions, denitrification may then proceed to reduce nitrate to nitric oxide or nitrogen gas with the use of a carbon source as an electron donor (Sawyer *et al.*, 2003). The portion of nitrogen converted to gaseous form then exits the aquatic system and enters the atmosphere.



1.4 First Flush Phenomenon

The first-flush phenomenon in stormwater relates to the increased concentrations of pollutants commonly found during the initial “flush” of runoff from a storm event. During inter-event dry periods, a dry deposition build-up of pollutants from sources such as atmospheric deposition, fertilizer applications, vehicle wear and exhaust, spills, etc, will accumulate within a watershed. Then during the first storm following this dry period, much of these pollutants are incorporated in the watershed runoff and eventually transported to ponds, rivers and lakes. As a result, the first-flush of runoff has been found to contain higher pollutant concentrations of heavy metals, suspended solids and nutrients as compared to the remaining runoff from the storm (Deletic, A. 1998; Bertrand-Krajewski, J et al, 1998; Lee J.H. et al, 2001). By using BMPs designed to specifically capture and treat the first-flush of storms, much of the pollutant loading may be reduced without the need to treat the entire volume of runoff. Additionally BMPs should typically be designed to provide treatment control for smaller rainfall events. In Florida, nearly 90 percent of the storm events in a given year produce one inch or less of rainfall and contribute to 75 percent of the total volume of rain fall (Wanielista, 1977). Therefore by designing BMPs to treat one inch storms or less rather than peak expected amounts, cost-effective sizing of the BMPs may be obtained.

1.5 TMDL and NPDES Permitting

In order to manage pollutant loading entering the waterways of the United States Congress enacted the National Pollutant Discharge Elimination System (NPDES) as established by the Federal Water Pollution Control Act Amendments of 1972. Under this program all facilities which discharge pollutants from any point source into waters of the United States must

obtain a NPDES permit. Under this spectrum stormwater discharges from urban areas are considered point sources and nutrients (i.e. ammonia, nitrogen, phosphorus) are considered non-conventional pollutants.

Within the NPDES a description of the pollutant loading capacity of the water body which is receiving the discharge must be established, known as a Total Maximum Daily Load (TMDL). TMDLs are described in 40 CFR 130.2 and 130.7 and Section 303(d) of the Clean Water Act CWA, as well as in U.S. Environmental Protection Agency guidance (U.S. EPA, 1991). A TMDL is defined as “the sum of the individual waste load allocations for point sources and load allocations for nonpoint sources and natural background” (40 CFR 130.2) such that the capacity of the water body to assimilate pollutant loadings (the loading capacity) is not exceeded. BMPs may be included in NPDES permitting to help achieve water quality goals. Discharges may also depend on what water body the pollutant is being discharged into, as specified in Table 1-2 below.

Table 1-2 Florida Surface Water Quality Standards (FDEP, 2014)

CLASS I - Potable Water Supplies	Includes fourteen general areas throughout the state with tributaries, certain lakes, rivers.
CLASS II - Shellfish Propagation or Harvesting	Generally coastal waters where shellfish harvesting occurs.
CLASS III - Fish Consumption, Recreation, Propagation and Maintenance of a Healthy, Well Balanced Population of Fish and Wildlife	The surface waters of the state are Class III unless described in rule <u>62-302.400, F.A.C.</u>
CLASS III - Limited - Fish Consumption, Recreation or Limited Recreation; and/or Propagation and Maintenance of a Limited Population of Fish and Wildlife	This classification is restricted to waters with human-induced physical or habitat conditions that, because of those conditions, have limited aquatic life support and habitat that prevent attainment of Class III uses.
CLASS IV - Agricultural Water Supplies	Generally located in agricultural areas around Lake Okeechobee.
CLASS V - Navigation, Utility and Industrial Use	Currently there are no designated Class V bodies of water.

1.6 Wireless Sensor Networks for Environmental Monitoring

Every BMP method has, to some extent, variability in operation caused by changes in environmental conditions, changes in source water, seasonal changes, rare events, etc. Such variability may be of a consistent nature such as the reduction of TSS in a vegetation slope, may follow a trend, such as the build-up of pollutants within a filter, leading to eventual breakthrough point, or follow an unpredictable nature such as the flow patterns through a wetland. In order to increase our understanding of BMPs there exists a continued need for monitoring of BMP systems to further our understanding with respect to; how they operate, determine which variables effect performance, calculate the efficiency, all of which may add to the collective scientific knowledge in these research areas. However with locations often difficult, time consuming, or expensive to reach, obtaining continuous sampling may become a difficult challenge.

Fortunately with advances in wireless technology over the last few decades, several new techniques have been developed in obtaining environmental data wirelessly. Applications of wireless networks allows a single area to be monitored by several devices, all relaying into a central master terminal which may communicate directly to an operator using radio, cellular or blue tooth signal technologies. Such methods have been used to expand the range of measurements, which when temporally synced, may broaden the spectrum to display large scale trends such as nutrient fluxes or hydraulic retention times within wetlands (Rundel et al, 2009). Furthermore such sensing networks may be deployed in remote areas or difficult to reach areas such as wetlands, allowing the collection of data which may otherwise not be attainable.

Applications of such wireless sensor networks are helping to bridge the gap between small scale and large remote sensing scale measurements, thus broadening the scientific

understanding of natural phenomena. Monitoring of sub-surface conditions is an example of where wireless networks have proven to be beneficial. Soil moisture measurements are used in understanding the infiltration of precipitation, determining groundwater recharge and measuring the partitioning of energy fluxes. Groundwater velocity may also be useful in understanding transport behavior patterns of pollutants in tracking plumes, or determining the hydraulic residence times of permeable reactive barriers. Development of wireless sensor networks continues to grow as technologies become more accurate while providing energy efficient processes.

1.7 Research Objectives

The research efforts of this study are to investigate the performance of new technologies developed for treatment and monitoring of stormwater systems. Scientific outlines and questions pertaining to this study per chapter are as follows:

- **Chapter 2&3** – Examine the application of BAM media in reducing pollutants in a field environment by utilizing three different media bed configurations run at 1 hour HRT and operated in a continuous cycling manner. How does each MBR operate in reducing concentrations of total phosphorus, orthophosphate, total nitrogen, ammonia, nitrates + nitrites, organic nitrogen, turbidity and chlorophyll *a* from stormwater retention ponds. To what degree will total loading reduction be achieved using MBRs and to what cost? And finally do dissolved oxygen measurements indicate any transitions from aerobic to anaerobic zones?
- **Chapter 4** – Lab and field test the operability of a Groundwater Variability Probe station installed in a pond bank to monitor environmental conditions relating to erosion issues including precipitation, soil moisture content, water elevation and groundwater

fluctuations in; velocity, direction, hydraulic conductivity and dispersion. How does precipitation events alter the subaqueous environment below the pond bank? Is soil moisture content effected more by overland flow or groundwater table fluctuations? And finally can a GVP station be effectively operated remotely via wireless communications?

- **Chapter 5** – Develop and test an affordable new wireless automated sampling network for examination of the nutrient flux gradient within a retention pond. Can the system be built for text activation? What factor of safety is necessary for flush intervals to isolate samples to set time increments. To what distance is the system capable of operation?
- **Chapter 6** – Develop an affordable velocimeter to measure low range velocities below the detection range of traditional mechanical velocimeters ($<5\text{cms}^{-1}$) in constructed wetlands and pond like conditions by use of NaCl pulses and conductivity measurements. To what degree of accuracy and detection range can the device attain? How many pulses are necessary in order to obtain accuracy goals? And finally can the device be integrated into a wireless sensing station for remote applications?

1.8 Limitations

The limitations of this research are related to the climate conditions in central Florida and the surrounding areas. The time lime of the research conducted includes February to August, 2014 for the MBRs and August to October, 2013 for wetland studies. Performance of devices tested in the laboratory are representative of the conditions tested in. Further details of specific limitations with respect to the work conducted for specific devices are summarized at the end of each chapter.

1.9 References

- Bertrand-Krajewski, J., Chebbo, G., Saget, A., 1998. Distribution of pollutant mass vs volume in stormwater discharges and the first flush phenomenon, *Water Resources* (32) 2341-2356.
- Chojnacka, Katarzyna. 2010. Biosorption and bioaccumulation – the prospects for practical applications: Elsevier, April 2010, *Environment International*, Vol. 36, pp. 299-307.
- Cullum, M.G., 1984. Evaluation of the Water Management System at a Single-Family Residential Site: Water Quality Analysis for Selected Storm Events at Timbercreek Subdivision in Boca Raton, Florida. South Florida Water Management District, Technical Publication No 84-11, Volume 11, West Palm Beach, FL, 116 pages.
- Deletic, A., 1998. The first flush load of urban surface runoff, *Water Resources* (32) 2462-2470.
- Harper, H.H., and Herr, J.L., 1993. Treatment Efficiency of retention with Filtration Systems. Final Report Submitted to St. Johns River Water Management District, Project No. 90B103.
- Harper, H.H., 1995. Treatment Efficiencies for Typical Stormwater Management Systems in Florida. Environmental Research & Design, Inc., Orlando, FL.
- Hartigan, J.P., 1988. Basis design of wet retention basin BMPs. Design of Urban Runoff Quality Control, American Society of Engineers 1988.
- Lee, J.H., Bang, K.W., Ketchum L.H., Choe J.S., Yu M.J., 2001. First flush analysis of urban storm runoff, *The Science of the Total Environment* (293) 163-175.
- Martin, E.H., Smoot J.L, 1986. Constituent-load changes in urban stormwater runoff routed through a retention pond-wetlands system in Central Florida: US Geological Survey, Water-Resources Investigations Report 85-4310.

- Rundel, P.W., Graham, E.A., Allen, M.F., Fisher, J.C., Harmon, T.C., 2009. Environmental sensor networks in ecological research. *New Phytologist* 182(3) 589-607.
- Schueler, T.R., 1992. A Current Assessment of Urban Best Management Practices. Metropolitan Washington Council of Governments.
- Wanielista, M.P., 1978. Stormwater Management: Quantity and Quality, Ann Arbor, MI: Ann Arbor Science.
- Winer, R., 2000. National pollutant removal performance database for stormwater treatment practices: US Geological Survey: Center for Watershed Protection.
- Yousef, Y.A., Wanielista, M.P., Harper H.H., Hvitved-Jacobsen, T., 1986. Best management practices: effectiveness of retention/detention ponds for control of contaminants in highway runoff. Florida Department of Transportation, Bureau of Environment – Environmental Research. Report No. FL-ER-34-86.

CHAPTER 2: STORMWATER NUTRIENT REDCTION USING SLOPED AND HORIZONTAL MEDIA BED REACTORS

2.1 Introduction

Stormwater retention ponds are commonly used BMP strategies used in Florida for the capture and attenuation of stormwater runoff. Wet retention ponds are very effective at controlling the volumetric flow of stormwater to prevent flooding downstream and have been shown to effectively remove above 80% of the TSS from stormwater runoff prior to entering downstream water sources. Although these BMPs are quite effective in TSS removal, they are not always capable of reaching high nutrient removal efficiencies and may require additional BMP installed in series or within the pond to attain higher nutrient removal performance.

For discharge to sensitive water bodies, existing wet retention ponds may not be sufficient in attaining reducing nutrient loading to the water body and further reductions may be necessary. Obtaining nutrient removal efficiencies beyond the pond capacity may be accomplished by the installation of additional BMP measures in series upstream or downstream of the pond such as vegetative swales, baffle boxes, exfiltration trenches, or constructed filters. This however may not present a viable option in urban environments due to space limitations or high property values, leading to “in pond” treatment methods. Currently there are only a few “in pond” treatment options including; natural vegetation in riparian zone, use of chemical coagulants such as alum, floating treatment wetlands and constructed filters at the influent or effluent sections of the pond (however such filters only operate during and shortly after storm events). Use of hydrated potassium aluminum sulfate, or more commonly known as “alum” is largely the most commonly used chemical coagulant, however may not be a suitable method due to the chemical addition to natural water sources, depending on the need of the user.

This chapter examines two new BMP techniques known as media bed reactors (MBRs) which serve as inter-event treatment methods of wet retention ponds. The MBRs operate by cycling pond water through baffling filters filled with bioactivated adsorptive media (BAM). Pollutant reduction is accomplished within the filtration media by adsorptive, physical and biological reactions. Two pilot scale MBRs are designed in horizontal (HMBR) and sloped (SMBR) configurations. Analysis was conducted on the removal capacity of nutrient species including TP, TN, NO_x, as well as turbidity and chl-*a* concentrations from the pond water. Further analysis was conducted to determine changes in dissolved oxygen levels throughout the MBRs to gain insights in whether aerobic or anaerobic processes were occurring.

Although a host of filtration media may be used in MBRs, this study incorporates “Green Technology” practices by incorporating a natural, recycled BAM filtration media using tire crumbs, sand, fine expanded clay and limestone. As such, the technology does not rely on chemical dosing which may increase both costs and offer a more environmentally friendly option.

Science Questions: To what degree will MBRs operate in field environments using continuous cycled filtration run at 1 hour hydraulic residence time with respect to adsorption, physical straining and biological removal of nutrient species? How does the baffling configuration effect DO levels within the MBR?

2.1.1 Chapter Objectives

- Identify the long-term performance of the MBR's in order to establish recommended replacement frequencies.

- Quantify the total removal of TN, TP, NO_x, turbidity and chl-*a* with respect to time.
Analyze the data for correlations with predicted adsorption rates based on laboratory studies.
- Determine maintenance or operation concerns.

2.2 **Methodology**

2.2.1 **Location**

Two wet retention ponds were selected for the installation of the MBRs. The HMBR was installed in a pond located in Orlando, Florida, whereas the SMBR was installed in a pond in Zolfo Springs, Florida. Table 2-1 below presents information regarding the ponds acreage and coordinates.

Table 2-1 Field Site Identification Numbers and Geographic Coordinates

Pond Site	Pond Size (acre)	Pond ID	Coordinates
Zolfo Springs	0.49	F06010-3501-01	27.497928°, -81.7957305°
Orlando	0.98	75037-3501-02	28.591550°, -81.208487°

During pre-BMP deployment a baseline study on existing pollutant problems was conducted and analysis performed as of possible sources of the pollutants. The Zolfo pond is located in a mix rural/urban environment, with surroundings consisting of highway, residential, commercial and agricultural. The surroundings of the Orlando pond in contrast are more comprised of mixed residential & commercial and highways. Identified characteristics pertaining to the Zolfo pond included; close proximity to cattle field, overgrown nearby forest and close proximity of metal piping factory, while the Orlando pond included; overgrown littoral

decay within pond, copper sulfate algaecide applications, and attachment to SR 434. A summary of these findings is included in Table 2-2.

Table 2-2 Identified Pollutant Issues

Pollutant	Study Pond	Characteristics
Total Nitrogen	Zolfo Springs (2248 $\mu\text{g}\cdot\text{L}^{-1}$), Orlando (1967 $\mu\text{g}\cdot\text{L}^{-1}$)	-Zolfo- Close proximity to cattle field, over grown forest -Orlando- Adjacent to SR 434, overgrown littoral decay
Nitrates	Zolfo Springs (442 $\mu\text{g}\cdot\text{L}^{-1}$)	Close proximity to cattle field, over grown forest providing littoral zone decay
Total Phosphorus	Zolfo Springs (1132 $\mu\text{g}\cdot\text{L}^{-1}$)	Close proximity to cattle field, over grown forest providing littoral zone decay, high phosphate soils
Soluble Reactive Phosphorus	Zolfo Springs (512 $\mu\text{g}\cdot\text{L}^{-1}$)	Close proximity to cattle field, over grown forest providing littoral zone decay, high phosphate soils
E. coli	Zolfo Springs (799 $\mu\text{g}\cdot\text{L}^{-1}$)	All highly variable between seasons and location in ponds -Zolfo Springs- Close proximity to cattle field and over grown forest
Copper	Orlando (9.7 $\mu\text{g}\cdot\text{L}^{-1}$), Zolfo Springs (9.3 $\mu\text{g}\cdot\text{L}^{-1}$)	Orlando- Copper sulfate algaecide treatment, adjacent to SR 434 Zolfo Springs- close proximity to State Road 35 and Metal piping warehouse
Zinc	Zolfo Springs (66.3 $\mu\text{g}\cdot\text{L}^{-1}$)	Zolfo Springs- close proximity to State Road 35 and Metal piping warehouse
Chromium	Orlando (39.7 $\mu\text{g}\cdot\text{L}^{-1}$)	Much higher concentrations found after the rainy season. Orlando- adjacent to SR 434

2.2.2 Design

Both the SMBR and HMBR are designed to hold filtration media within an enclosure. Pond water is pumped by a submersible pump through a screened intake and into the influent end of the MBR. Initially water enters a sedimentation chamber whereby any potentially larger

particles may settle out, rather than enter the filtration media. Following the settling chamber water travels through varying baffling chambers containing sorption media. For the HMBR a three chambered design is utilized whereas the SMBR utilizes a four chamber design. The first chamber is typically used as a roughing filter to prevent premature clogging of the small pores of Media Mix #2. For the SMBR water is routed under a baffling wall to the next chamber, then over a second baffle, and finally under a third baffling wall. The baffling walls serve to create a non-linear pathway for water to travel through, thus increasing contact of the water with filtration media and decrease the effects of linear short circuiting which may occur through the media. A summary of the design specifications for each MBR is summarized in Table 2-3 below and diagrams of the MBRs are displayed in Figure 2-1 and Figure 2-2.

Table 2-3 MBR Design Comparison

Parameter	SMBR	HMBR
Type	Sloped	Horizontal
Number of Chambers	4	3
Sorption Media	Mix #2	5/8ths Exp. Clay and Tire Chunks
Media Volume Capacity	16.6 L	8.4 L
Filter Loading Rate	3.46 L·min·m ⁻²	3.21 L·min·m ⁻²
Hydraulic Residence Time	1 hour	1 hour
Flow Rate	0.13 L·min ⁻¹	0.26 L·min ⁻¹
Installation Locations	Mid Pond	Inlet Pond

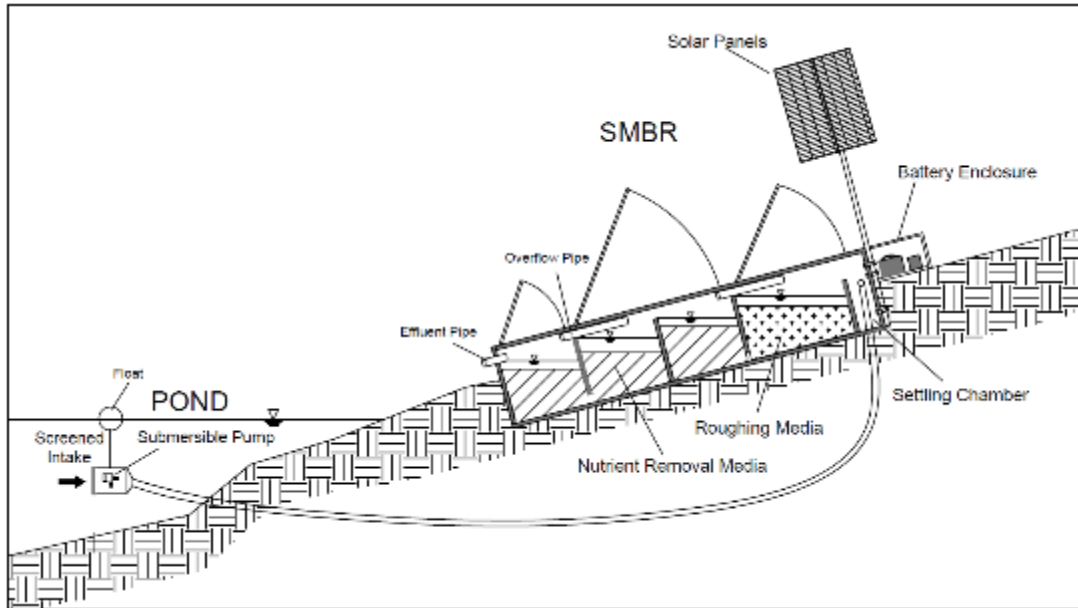


Figure 2-1 Design layout of a SMBR including solar powered submersible recycling pump. A roughing filter is placed in the first chamber to reduce clogging and prolong the life cycle of the filter.

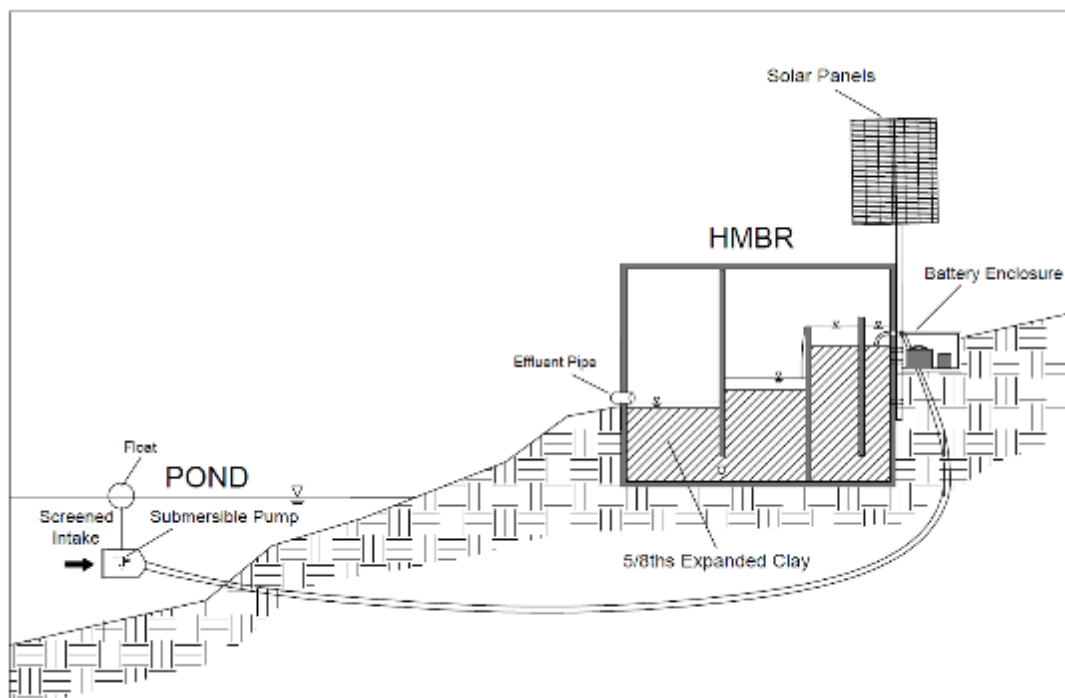


Figure 2-2 Design layout of a HMBR including solar powered submersible recycling pump. Due to close proximity to the inlet of the pond and associated high turbidity amounts only a 5/8ths expanded clay mixture is utilized.

An enclosure was built for containment of the submersible pump. The enclosure was constructed using a 4-inch PVC segment, one end connected to the influent of the MBR with a meshed screen attached to the other end. The screening is added to prevent the intake of larger particles which may prematurely clog the filtration media. A float was attached to one end of the pump enclosure and a weight attached to the other. This allowed the pump to be maintained at a constant elevation and prevent the intake end from dropping into the sediment below. A small submersible pump rated at 3.6 Lmin^{-1} was utilized for the MBRs. It should be noted that the pump was specifically sized for the MBRs which were pilot scale and any pumps on a full field-scale would require different specifications. Pump specifications are presented Table 2-4 below.

Table 2-4 Pump Specifications

Pump Type	Brushless Submersible
Rated Flow rate	$3.6 \text{ L} \cdot \text{min}^{-1}$
Power Source	12V DC
Vertical Lift	3m
Current	320mA
Intake	6mm ID / 8.7mm OD
Outlet	5.38 mm ID / 8.7mm OD

Power system designs for the MBR included the total power draw by the submersible pump, energy loss through the voltage regulator, energy loss charging the battery, energy drain losses through wiring and output power generated by the solar panel. The daily consumption of joules by the pump can be calculated when the voltage and current draw from the pump are known using the following equation:

$$\text{Daily Joules Consumed} = (\text{Watts}) \left(\frac{60 \text{ sec}}{\text{min}} \right) \left(\frac{60 \text{ min}}{\text{hour}} \right) \left(\frac{24 \text{ hours}}{\text{day}} \right) \quad (6)$$

Similarly the total battery capacity in joules may be calculated using the following equation:

$$\text{Battery Capacity in Joules} = (\text{Amphours})(\text{Voltage}) \left(\frac{60\text{min}}{\text{hour}} \right) \left(\frac{60\text{sec}}{\text{min}} \right) \quad (7)$$

The daily energy converted per area and total required area of solar panels may be calculated using the following equations:

$$J_{\text{area}} = (\psi)(\eta)(\text{Hours Daylight}) \left(\frac{60\text{min}}{\text{hour}} \right) \left(\frac{60\text{sec}}{\text{min}} \right) \left(\frac{1}{100} \right) \quad (8)$$

Where:

J_{area} = daily energy converted per unit area ($\text{Jm}^{-2}\text{h}^{-1}$)
 ψ = local Annual Average Solar Irradiance (Wm^{-2})
 η = solar panel efficiency

$$A = \frac{J_c (24 - t_r)}{h_d t_r} \quad (9)$$

Where:

A = required area of solar panels
 J_c = hourly energy converted per unit area
 t_r = time available to recharge batteries
 h_d = hours of daylight

Using the above equations, a theoretical battery capacity with respect to time may be developed, Figure 2-3. The figure displays a weekly scenario in which a 33 mA submersible pump is operated continuously for a 110 hour period using a 60 Amp-hour battery with (a) no solar panels (b) a 7 Watt solar panel and (c) a 15 Watt solar panel. It should be noted that for real field applications the wattage of the solar panels must be increased to account for time periods where cloud cover may reduce the output current of the solar panels and reduce charging.

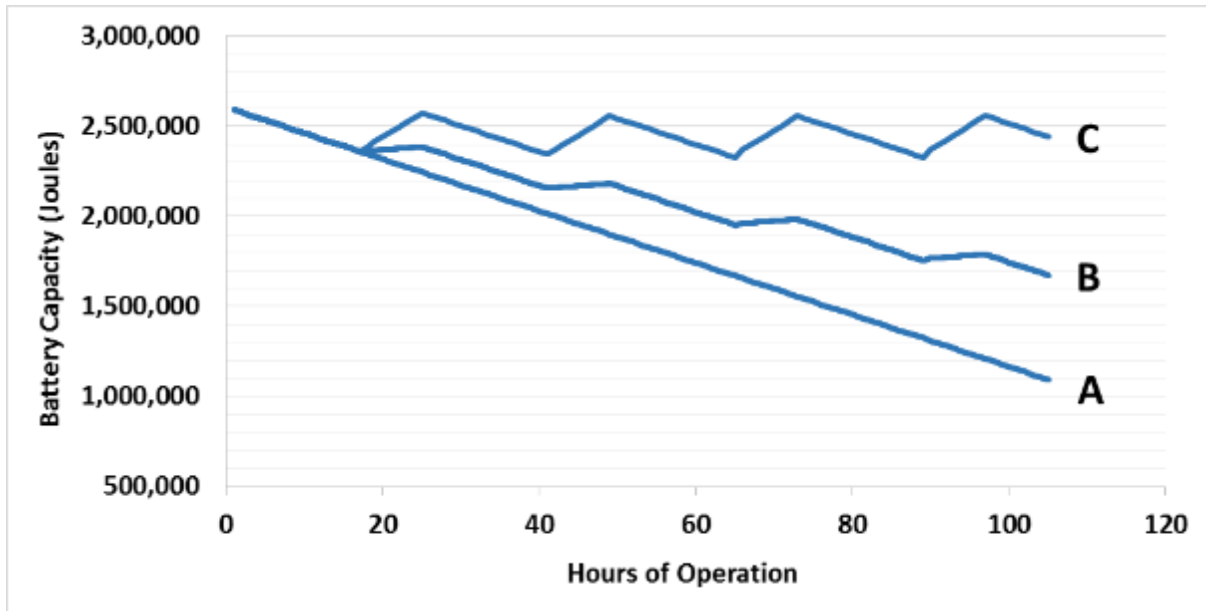


Figure 2-3 Theoretical battery drainage graph for a 60 Ah battery connected to a 12V pump running continuously at 330mA with (a) no solar panel, (b) 7 watt solar panel and (c) 15 watt solar panel.

2.2.3 Installation

An SMBR with all chambers filled with Media Mix #2 was installed on a wet retention pond in the city of Zolfo Springs on February 13th, 2014. The SMBR was operated continuously for a two month duration. During the first two month run period all chambers of the SMBR were filled with Media Mix #2 composed of 50% sand, 20% fine expanded clay, 20% tire crumb and 10% limestone (Figure 2-4a). Within the first two months excessive head loss due to clogging of the pores was experienced in the first chamber, leading to a bypassing of the 1st chamber. Following this, a second run of the SMBR was taken which included a roughing filter in the 1st chamber comprised of 5/8ths expanded clay (Figure 2-4b), with the remaining three chamber being refilled with Media Mix #2. The replacement occurred on April 10th, 2014. Figure 2-5 displays the exterior of the SMBR with a temporary wooden enclosure and dual 15 watt solar panels wired in parallel.



Figure 2-4 Installation of SMBR on the pond bank at Zolfo Springs with (a) without roughing media in the 1st chamber and (b) with a 5/8ths expanded clay roughing media mix added to the 1st chamber.



Figure 2-5 Exterior view of installation of SMBR on the pond bank at Zolfo Springs. The SMBR is powered by two 15W solar panels in parallel.

An HMBR with all chambers filled with Media Mix #2 was installed on a wet retention pond in the city of Orlando on February 13th, 2014. The HMBR was operated continuously for a two month duration. During the first two month run period all chambers of the HMBR were filled with Media Mix #2 composed of 50% sand, 20% fine expanded clay, 20% tire crumb and 10% limestone. However, similar to the SMBR, within the first two months excessive head loss due to clogging of the pores was experienced in the first chamber, leading to a bypassing of the

1st and 2nd chambers. Unfortunately roadway construction activities coincided with this time period which could explain the rapid clogging and high turbidities near the inlet, Figure 2-6. As the HMBR was installed very near to the inlet and the pond did not have sufficient time to settle out heavy particles, the HMBR was filled with 50% 5/8ths expanded clay and 50% tire chunks, Figure 2-7.

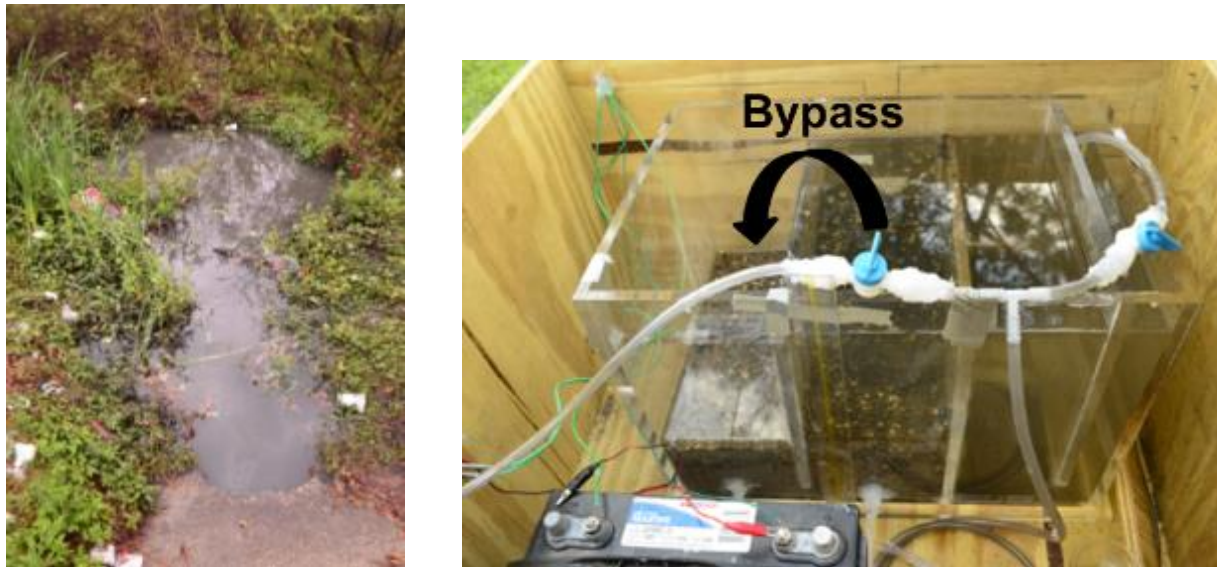


Figure 2-6 High turbidity near the inlet of the Orlando Pond (left) which caused the premature clogging of the HMBR filled with Media Mix 2 (right).



Figure 2-7 HMBR re-filled with 50% 5/8th expanded clay and 50% tire chunk.

2.3 Results and Discussion

2.3.1 Source Water Quality

Background concentrations in the pond were analyzed during a pre-BMP campaign. For the Zolfo Springs Pond, samples were collected from the inlet, center and outlet of the pond on September 21st, 2012 and May 30th, 2013. For the Orlando Pond samples were collected at the inlet, center and outlet of the pond on September 21st, 2012 and May 28th, 2013. As depicted in Table 2-5 and Table 2-6 below, the Zolfo Pond had significantly higher levels of all nutrient species in the influent and as well as better performance reductions with mean values of 12% TP reduction and 37% TN reduction compared with Orlando Pond mean values of -46% reduction in TP and -14% reduction in TN.

Table 2-5 Zolfo Springs Pond pre-BMP Nutrient Concentrations

Parameter	Location	8/21/2012	5/30/2013	Average	SD	95% CI
TP ($\mu\text{g}\cdot\text{L}^{-1}$)	Inlet	1723	911	1317	406	± 563
	Center	787	414	601	187	± 258
	Outlet	885	1445	1165	280	± 388
TN ($\mu\text{g}\cdot\text{L}^{-1}$)	Inlet	1885	3204	2545	660	± 914
	Center	1151	1239	1195	44	± 61
	Outlet	888	2303	1596	708	± 981
SRP ($\mu\text{g}\cdot\text{L}^{-1}$)	Inlet	742	340	541	201	± 279
	Center	411	394	403	8.5	± 12
	Outlet	381	368	375	6.5	± 9.0
NH ₄ ($\mu\text{g}\cdot\text{L}^{-1}$)	Inlet	160	1.5	81	79	± 110
	Center	38	1.5	20	18	± 25
	Outlet	2.5	1.5	2.0	0.5	± 0.7
NO _x ($\mu\text{g}\cdot\text{L}^{-1}$)	Inlet	1112	52	582	530	± 735
	Center	97	91	94	3.0	± 4.2
	Outlet	118	30	74	44	± 61

Table 2-6 Orlando Pond pre-BMP Nutrient Concentrations

Parameter	Location	8/21/2012	5/28/2013	Average	SD	95% CI
TP ($\mu\text{g}\cdot\text{L}^{-1}$)	Inlet	18	28	23	5.0	± 6.9
	Center	37	758	398	361	± 500
	Outlet	20	47	34	14	± 19
TN ($\mu\text{g}\cdot\text{L}^{-1}$)	Inlet	694	628	661	33	± 46
	Center	728	4330	2529	1801	± 2496
	Outlet	566	944	755	189	± 262
SRP ($\mu\text{g}\cdot\text{L}^{-1}$)	Inlet	15	5	10	5.0	± 6.9
	Center	9	141	75	66	± 91
	Outlet	15	9	12	3.0	± 4.2
NH ₄ ($\mu\text{g}\cdot\text{L}^{-1}$)	Inlet	39	49	44	5.0	± 6.9
	Center	5	1.5	3	1.8	± 2.4
	Outlet	81	1.5	41.3	40	± 55
NO _x ($\mu\text{g}\cdot\text{L}^{-1}$)	Inlet	449	62	256	194	± 268
	Center	101	79	90	11	± 15
	Outlet	154	88	121	33	± 46

2.3.2 *SMBR Field Performance*

The SMBR was found to reduce mean concentrations of TP, SRP, TN, NH₄, NO_x, Org-N, Turbidity and chl-*a* fairly consistently throughout the study, as displayed in Table 2-7. A one tailed t-test ($\alpha=0.05$) concluded that there was a decrease between the means of the influent and effluent concentrations for Turbidity ($p=0.0312$) and chl-*a* ($p=0.004$) when tested at a 95% confidence interval and assuming normality. TP was found to have a reduction when tested at the 85% confidence interval ($p=0.0148$). Table 2-8 provides a summary of mean concentrations as measured at the influent and effluent of the SMBR and respective standard deviations.

Table 2-7 SMBR Mean Reduction Performance

SMBR Average Removal Efficiencies					
TP	TN	No _x	Org. N	Turb	Chl-a
21.5%	28.0%	63.0%	26.5%	32.5%	64.8%

Table 2-8 SMBR Mean Reduction Performance

Parameter	Influent		Effluent	
	Mean	Std Dev	Mean	Std Dev
Total P, $\mu\text{g}\cdot\text{L}^{-1}$	618	281	486	178
Total N, $\mu\text{g}\cdot\text{L}^{-1}$	1052	1004	757	427
Nitrates + Nitrites, $\mu\text{g}\cdot\text{L}^{-1}$	38	61	14	17
Organic Nitrogen, $\mu\text{g}\cdot\text{L}^{-1}$	844	912	620	493
Chlorophyll <i>a</i>, $\mu\text{g}\cdot\text{L}^{-1}$	10.1	3.9	3.7	1.3
Turbidity, NTU	6.6	3.2	3.9	2.3

Figure 2-8 displays the change in DO levels comparing the 1st week to the 3rd week of operation. As seen there is an initial aeration throughout the chambers as influent water travels through the baffled system of the SMBR. Following three weeks of operation, DO levels remain significantly low throughout the filter with mean values equal to $0.67 \text{ mg}\cdot\text{L}^{-1}$ for the influent and $1.09 \text{ mg}\cdot\text{L}^{-1}$ for the effluent. These low levels became a relatively constant trend throughout the study period. Due to the initial aeration followed by relatively equal concentrations of DO, it is suspected that the established levels are a combination of aeration of the water and an increase in oxygen consuming bacteria, or by development of bio films on the surface of the supernatant within the chambers which would decrease oxygen diffusion from the atmosphere into the water. The DO levels in the influent of the SMBR remained below $1.19 \text{ mg}\cdot\text{L}^{-1}$ throughout the study. These levels were expected as the SMBR was located at the side of the pond and therefore less susceptible to DO fluctuations at the inlet following storm events.

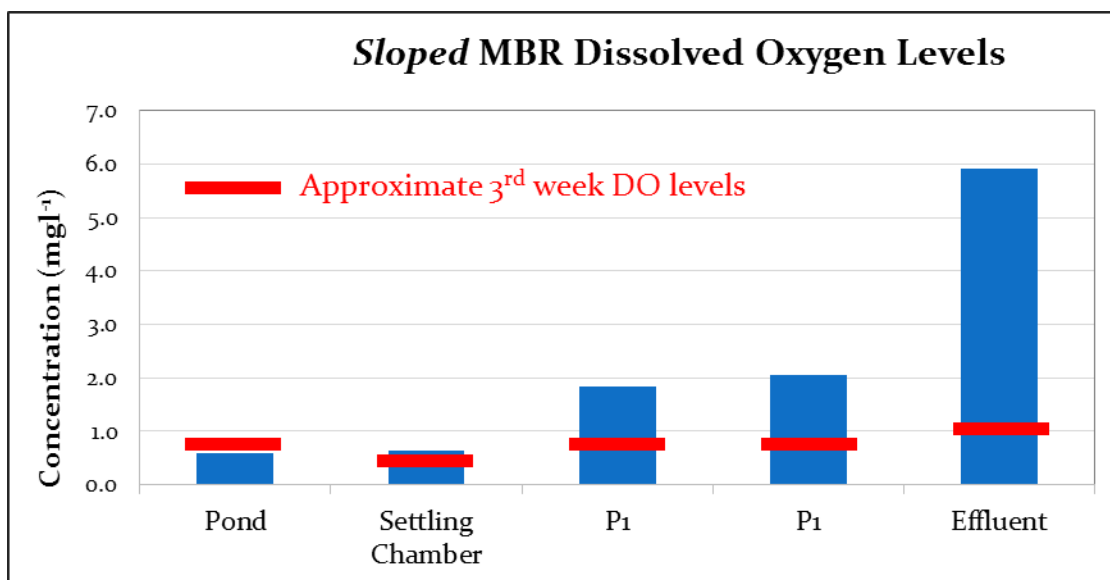


Figure 2-8 Drop in DO levels comparing the first week (blue columns) to the third week of operation (red bars). An initial aerating throughout the chamber occurs which gradually

Examination of influent and effluent chl-*a* concentrations indicates a consistent removal of chl-*a* by the SMBR (Figure 2-9). Also seen in the data is a gradual increase in chl-*a* concentrations in the influent. This trend is suspected to coincide with increases in sunlight with the advance of summer months. The effluent chl-*a* concentrations from the SMBR effluent remained at low levels, which were found to be independent of changes in influent concentrations (R-squared = 0.37). Turbidity measurements for the influent and effluent sides of the SMBR are displayed in Figure 2-10. A drop in turbidity was measured for the first sample, taken on 4/18/2014, following which all following measurements display a drop in turbidity. The initial increase is likely due to an initial flushing phase of the media, which contains small amounts of silt which were observed in the effluent stream following initial run of the SMBR. Further graphs of additional parameters for the SMBR and Zolfo Pond are presented in Appendix A and Appendix B of this report, respectively.

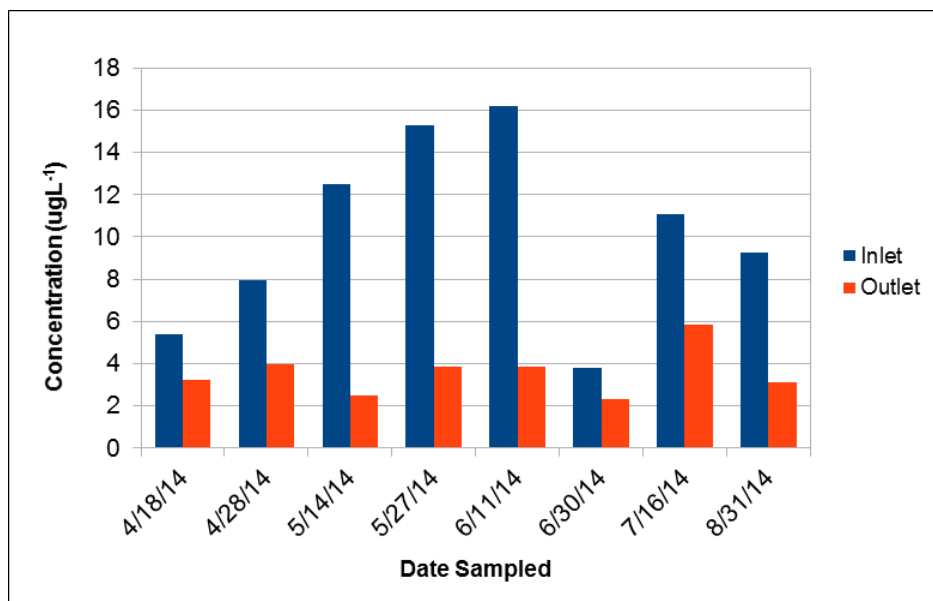


Figure 2-9 Chl-*a* concentrations through the SMBR between influent and effluent sampling locations.

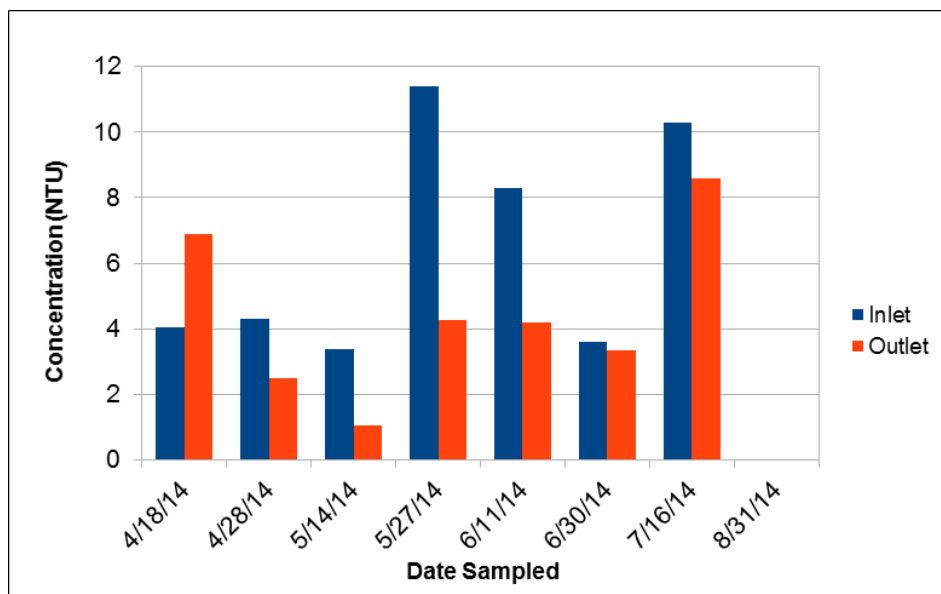


Figure 2-10 Turbidity measurements comparing influent and effluent concentrations measured in the SMBR.

2.3.3 *HMBR Field Performance*

The HMBR was found to reduce mean concentrations of TP, TN, NO_x, Org-N, Turbidity and chl-*a* fairly consistently throughout the study, as displayed in Table 2-9. A one tailed t-test ($\alpha=0.05$) concluded that there was a decrease between the means of the influent and effluent concentrations for TN ($p=0.0240$), Org-N ($p=0.0242$), and Turbidity ($p=0.002$) when tested at the 95% confidence interval and assuming normality and equal variance. Table 2-10 provides a summary of mean concentrations as measured at the influent and effluent of the SMBR and respective standard deviations.

Table 2-9 HMBR Mean Removal Efficiencies

HMBR Average Removal Efficiencies					
TP	TN	No _x	Org. N	Turb	Chl-a
8.9%	26.3%	63.0%	31.3%	55.9%	26.7%

Table 2-10 HMBR Mean Removal Efficiencies

Parameter	Inlet		Outlet	
	Mean	Std Dev	Mean	Std Dev
Total P, µg/L-1	38	10	35	14
Total N, µg/L-1	381	76	281	96
N to P molar ratio	21	NA	23	NA
Nitrates + Nitrites, µg/L-1	39	42	25	26
Organic Nitrogen, µg/L-1	298	57	205	99
Chlorophyll <i>a</i>, µg/L-1	0.9	0.3	0.6	0.3
Turbidity, NTU	3.5	1.5	1.5	0.9

Due to the close proximity of the HMBR to the inlet of the pond, DO levels as measured in the influent were much more varied as compared with the SMBR. The HMBR underwent an initial aeration phase, similar to that witnessed in the SMBR, immediately following the run of the HMBR. DO levels were measured to highly fluctuate following storm events. Figure 2-11 displays two separate events comparing the DO levels shortly following the initial run of the

HMBR and to those shortly following a storm. Fluctuations such as these could theoretically effect the biological activity of bacteria, however it is not clear to what extent these fluctuations have on MBR performance due to a lack of data. Further work examining MBR performance with consistent DO measurements under controlled conditions would be merited to further analyze the relationship.

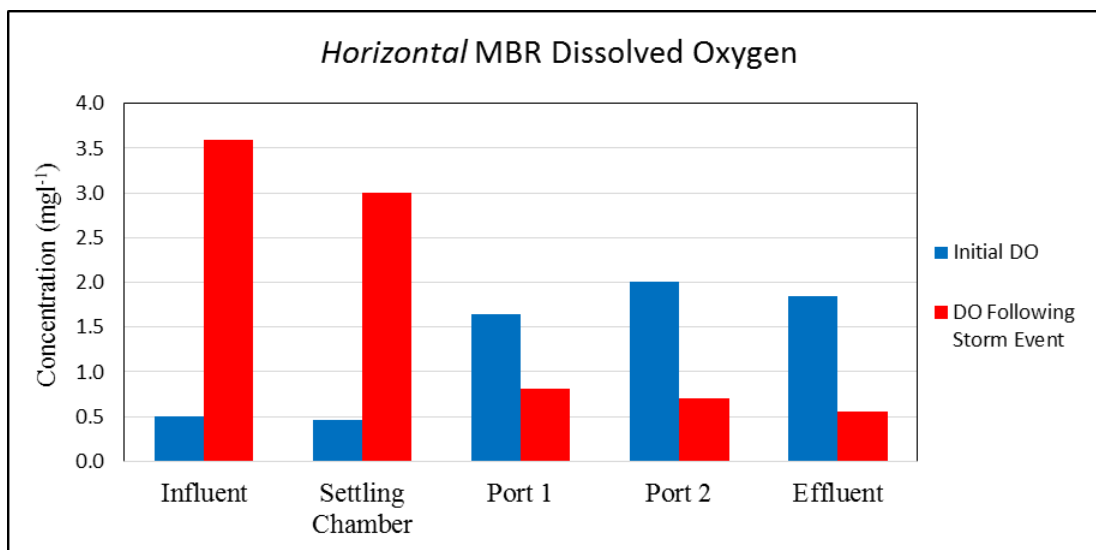


Figure 2-11 DO concentrations in the HMBR one day following the initial run of the HMBR and shortly following a storm event.

Initial measurements showed a negligible decrease in SRP concentrations indicating that the media does not go through a sorption phase such as Media Mix #2 in the SMBR. It is suspected that this is due to there being less surface area per volume for the media as compared to Media Mix #2, and therefore less available sorption sites for SRP to bond to. Additionally this may also be due to there being a weak affinity of SRP to 5/8ths expanded clay and tire chunk. However the HMBR appeared to have good performance in TN and Org-N reductions with respect to time, as displayed in Figure 2-12.

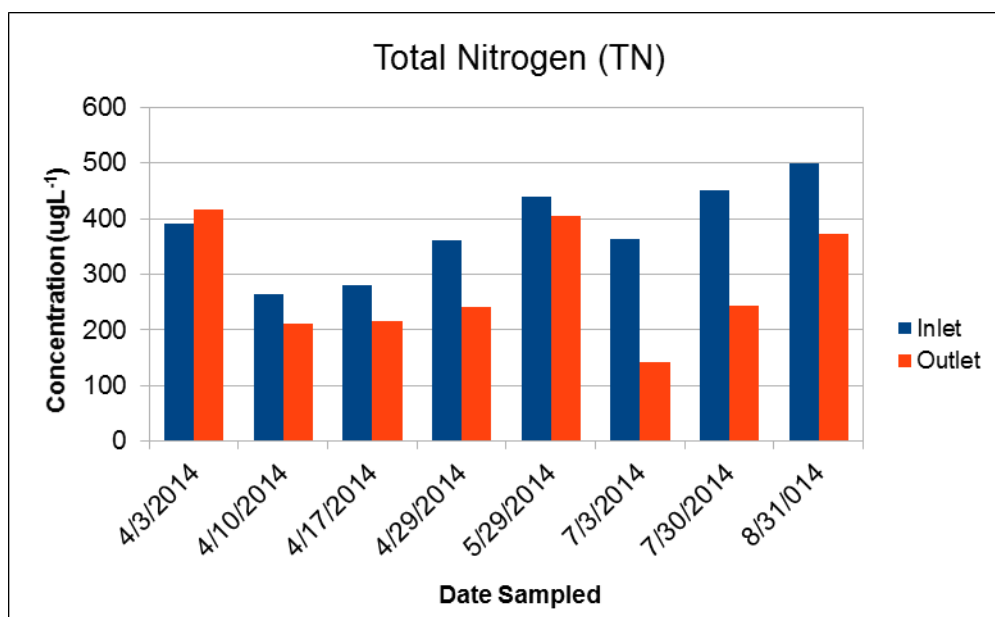


Figure 2-12 TN comparison between influent and effluent sampling locations on the HMBR.

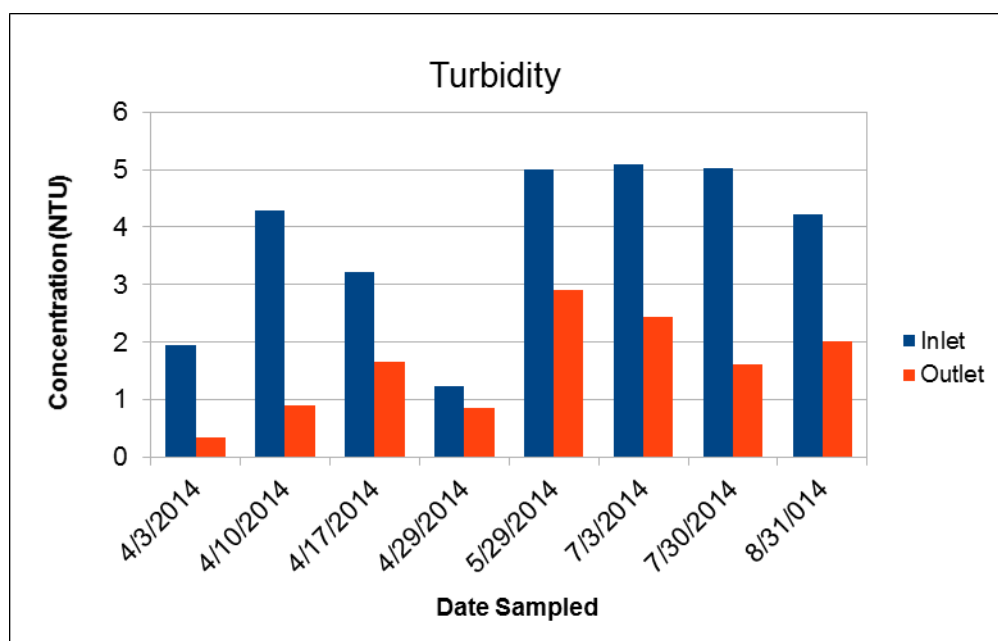


Figure 2-13 Turbidity comparison between influent and effluent sampling locations on the HMBR.

As seen, there is a consistent decrease in TN concentrations ranging from 8% to 61% throughout the sampling duration, with the exception of the first sample taken shortly after the initial run of the HMBR. An average reduction of 26.3% was recorded for TN. Turbidity reductions were found to perform well during the study with consistent decreases in turbidity across the media bed ranging from 31% to 82%, with an overall average of 52.8%. Turbidity concentrations with respect to time is displayed in Figure 2-13.

2.3.4 Hydraulics

Understanding the hydraulic behavior through the media bed is crucial for maintaining operability and effective performance of the MBRs. As mentioned earlier the initial run of the SMBR with Media Mix #2 resulted in clogging of the first chamber and a bypass of the chamber. This is partially due to two reasons, one the close proximity of the HMBR to the inlet pipe of the pond resulted in turbid waters following storm events, and secondly coincidental road construction activities during the first few weeks of operation where influent turbidity levels increased above 20 NTU. However as the SMBR experienced similar clogging issues when only Media Mix #2 was utilized there appears to be a limitation to using Media Mix #2 as the first media contacted with influent water. However, in both cases the MBRs operated well when larger diameter media was included at influent turbidity concentrations <5NTU; a roughing media in the case of the SMBR consisting of 3/8ths expanded clay, and a complete replacement with a 50% 3/8ths expanded clay and 50% tire chunk mix, resulting in both cases in head loss across the media bed remaining less than 2 cm. In either case, analysis of the source water is important prior to installation of a MBR.

2.4 Final Remarks

Use of MBRs in stormwater retention ponds were shown to effectively operate in the field. It was established that for turbidity ranges around 5 NTU premature clogging of Media Mix #2 occurs. This was overcome however by the inclusion of a roughing filter or replacement with a larger diameter media. The SMBR was found to reduce mean values of TP, SRP, TN, NH₄, NO_x, Org-N, turbidity and chl-*a* during a 6-month study period, however only Turbidity and chl-*a* had confirmed statistical reductions in the means when tested at an α value of 0.05 using a one-tailed t-test. TP reductions were found statistically significant at an α value of 0.15. The HMBR was found to reduce mean concentrations of TP, TN, NO_x, Org-N, turbidity and chl-*a*, while TN, Org-N, and chl-*a* were found to have statistical decreases in mean concentrations at an α value of 0.05 using a one-tailed t-test. Both devices were found to be effective technologies for providing inter-event treatment of retention ponds to reduce nutrient concentrations. It should be noted the MBRs are prototype scale and further work is merited on establishing the effects the effluent water has on overall pond water quality on larger scales.

2.5 References

- Bertrand-Krajewski, J., Chebbo, G., Saget, A., 1998. Distribution of pollutant mass vs volume in stormwater discharges and the first flush phenomenon, *Water Resources* (32) 2341-2356.
- Chojnacka, Katarzyna. 2010. Biosorption and bioaccumulation – the prospects for practical applications: Elsevier, April 2010, *Environment International*, Vol. 36, pp. 299-307.
- Cullum, M.G., 1984. Evaluation of the Water Management System at a Single-Family Residential Site: Water Quality Analysis for Selected Storm Events at Timbercreek

- Subdivision in Boca Raton, Florida. South Florida Water Management District, Technical Publication No 84-11, Volume 11, West Palm Beach, FL, 116 pages.
- Deletic, A., 1998. The first flush load of urban surface runoff, *Water Resources* (32) 2462-2470.
- Harper, H.H., and Herr, J.L., 1993. Treatment Efficiency of Detention with Filtration Systems. Final Report Submitted to St. Johns River Water Management District, Project No. 90B103.
- Harper, H.H., 1995. Treatment Efficiencies for Typical Stormwater Management Systems in Florida. Environmental Research & Design, Inc., Orlando, FL.
- Hartigan, J.P., 1988. Basis design of wet detention basin BMPs. Design of Urban Runoff Quality Control, American Society of Engineers 1988.
- Lee, J.H., Bang, K.W., Ketchum L.H., Choe J.S., Yu M.J., 2001. First flush analysis of urban storm runoff, *The Science of the Total Environment* (293) 163-175.
- Martin, E.H., Smoot J.L., 1986. Constituent-load changes in urban stormwater runoff routed through a detention pond-wetlands system in Central Florida: US Geological Survey, Water-Resources Investigations Report 85-4310.
- Schueler, T.R., 1992. A Current Assessment of Urban Best Management Practices. Metropolitan Washington Council of Governments.
- Wanielista, M.P., 1978. Stormwater Management: Quantity and Quality, Ann Arbor, MI: Ann Arbor Science.
- Winer, R., 2000. National pollutant removal performance database for stormwater treatment practices: US Geological Survey: Center for Watershed Protection.

Yousef, Y.A., Wanielista, M.P., Harper H.H., Hvitved-Jacobsen, T., 1986. Best management practices: effectiveness of retention/detention ponds for control of contaminants in highway runoff. Florida Department of Transportation, Bureau of Environment – Environmental Research. Report No. FL-ER-34-86.

CHAPTER 3: STORMWATER NUTRIENT REDUCTION USING UPFLOW FLOATING MEDIA BED REACTOR

3.1 Introduction

Pollutant loading from stormwater runoff of urbanized areas to surface water bodies has been a growing issue in Florida. Wet retention ponds are perhaps the most common Best Management Practice (BMP) to capture and transform pollutants through settling, biological and chemical processes prior to discharges to lakes, rivers and oceans (USEPA, 1999). According to current regulation, a stormwater pond shall achieve an 80% average annual load reduction of pollutants from the influent stormwater (F.A.C. Chapter 62-40). Although the current law pertains to solids removal only, research has indicated that nutrients are the most significant parameters linked to water quality impairment within the State of Florida today (Harper and Baker, 2007). According to a summary of ten studies evaluating wet retention pond performance conducted from 1982 to 2005, ponds in Florida were found to remove a mean value of 37% Total Nitrogen (TN) and 69% of Total Phosphorus (TP), both being below an 80% target range (Harper and Baker, 2007). Clearly there is an acute need to increase the removal capacity of ponds by integrating additional BMPs in order to achieve higher removal efficiencies.

The Lower St Johns River has witnessed water quality degradation due to an increase in urbanization. In a total maximum daily load (TMDL) report prepared by the Florida Department of Environmental Protection (FDEP), 11 of the 15 segments of the river were verified as impaired by nutrients based on annual chlorophyll *a* concentrations (FDEP, 2008). The report estimates contributing loading rates as 46,357 kg·yr⁻¹ TP and 236,695 kg·yr⁻¹ TN for point sources, and 453,968 kg·yr⁻¹ TP and 8,334,868 kg·yr⁻¹ TN from non-point sources. In order to

reach TMDL goals a recommended TP and TN loading rate reduction of 99,285 kg·yr⁻¹ and 1,543,989 kg·yr⁻¹, respectively, are recommended (LSJREC, 2008). Achieving such a goal will require loading reductions for non-point sources by implementation of BMPs designed for the capture of TN and TP species in urban stormwater runoff systems.

The use of filtration/sorption media, such as sand, compost, or wood chips for the capture of nutrients in stormwater runoff has been increasingly studied during the last decade, typically using column studies (Kim et al, 2000; Hossain et al, 2009; Jones et al, 2014). Such sorption media is commonly used in infiltration or exfiltration applications and has been included in commercial applications. Sorption media has been incorporated into upflow filter configurations and found to effectively operate in nutrient reductions in stormwater systems. Khambhammettu et al. (2006) found that a field upflow filter achieved 18% reduction in phosphorus, 70% reduction in suspended solids, and 65% reduction in turbidity. While Ryan et al. (2010) recorded a 29% reduction in TP and a 47% reduction in TN for an upflow filter installed near the outlet of a pond. Although upflow filters show promising signs for nutrient removal, they have the limitation of being storm event-driven technology and only treat stormwater when hydraulic gradients develop across the filter, occurring during and shortly following storm events. As a result, filter surface areas must be increased to account for such relatively short duration times in order to treat significant volumes of water while keeping hydraulic loading rates within a reasonable range. One technique to overcome this deficiency is the incorporation of pumps, enabling the filter to run continuously. Figure 3-1 graphically displays this advantage in which a theoretical comparison of flow rates through a gravity and pump controlled filter is shown for a one week duration with one major storm event. As seen, the continuous flow filter is capable of much larger treated volumes, especially during dry inter-event periods.

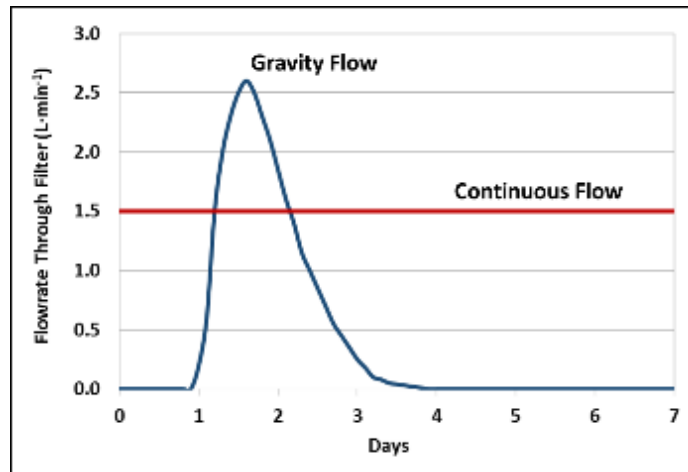


Figure 3-1 Theoretical flow rate comparison of gravity vs. pump filters for one week duration with one major storm event.

This paper presents the use of a Floating Media Bed Reactor (FMBR) filled with a green sorption media to increase the removal capacity of a retention pond for TP and TN species. The FMBR is arranged in a floating upflow filtration design and incorporates a solar powered submersible pump to continuously cycle water through the media bed. Specifically, the study aims to (1) establish the removal capacity of the FMBR for TP and TN species, (2) establish the operability of the FMBR, especially with regard to change in head loss, and (3) supplement the limited database on field performance of stormwater green technology using sorption media in an upflow configuration. To the knowledge of the authors few work has examined the use of continuously cycling upflow filters for inter-event treatment of a stormwater retention pond using sorption media.

Science Questions: To what degree will a FMBR operate in field environments using continuous cycled filtration run at 1 hour hydraulic residence time with respect to adsorption, physical straining and biological removal of nutrient species? To what degree will head loss increase with respect to time?

3.1.1 Chapter Objectives

- Identify the long-term performance of the FMBR's in order to establish recommended replacement frequencies.
- Quantify the total removal of TN, TP, SRP, NO_x, NH₄, turbidity and chl-*a* with respect to time. Analyze the data for correlations with predicted adsorption rates based on laboratory studies.
- Determine maintenance or operation concerns.

3.2 Methodology

3.2.1 Location

The FMBR was installed in a small retention pond located in the city of East Palatka, Florida. The pond receives stormwater runoff primarily from impervious highway, parking, and commercial areas totalling 1.19 acres. The pond directly discharges to a small tributary creek connected to the Lower St. John's River (water body ID 2213M), currently identified as nutrient impaired (FDEP, 2008). The pond has a total wet pool coverage of 0.12 acres and storage volume of 305 m³.

Table 3-1. Field Site Identification Numbers and Geographic Coordinates.

Pond Site	Pond Size (acre)	Pond ID	Coordinates
East Palatka	0.12	209965-1-52-01-P001	29.646012°, -81.594925°

Table 3-2. Field Site Basin and Pond Characteristics.

Basin No.	Total Area (AC)	Imper. Area (AC)	% Imperv	Pond Area (AC)
SR 207	1.19	1.19	100	0.12

3.2.2 Source Water Quality

Background concentrations in the pond were analyzed during a pre-BMP campaign. For the Palatka Pond samples were collected from the inlet, center and outlet of the pond on October 3rd, 2012 and May 29th, 2013. As depicted in below in Table 3-3, the Palatka Pond had relative poor removal efficiencies for all parameters except SRP and NH₄.

Table 3-3. Palatka Pre-BMP Nutrient Concentrations

Parameter	Location	10/3/2012	5/29/2013	Average	SD	95% CI
TP ($\mu\text{g}\cdot\text{L}^{-1}$)	Inlet	170	83	127	44	60
	Center	630	345	488	143	197
	Outlet	180	529	355	175	242
TN ($\mu\text{g}\cdot\text{L}^{-1}$)	Inlet	606	1268	937	331	459
	Center	1305	2975	2140	835	1157
	Outlet	589	3862	2226	1637	2268
SRP ($\mu\text{g}\cdot\text{L}^{-1}$)	Inlet	11	22	17	5.5	7.6
	Center	10	5	7.5	2.5	3.5
	Outlet	10	7	8.5	1.5	2.1
NH ₄ ($\mu\text{g}\cdot\text{L}^{-1}$)	Inlet	2	156	79	77	107
	Center	17	1.5	9.3	7.8	10.7
	Outlet	4	1.5	2.8	1.3	1.7
NO _x ($\mu\text{g}\cdot\text{L}^{-1}$)	Inlet	71	86	79	8	10
	Center	77	67	72	5.0	6.9
	Outlet	75	452	264	189	261

Identified characteristics pertaining to the Palatka pond included; overgrown nearby forest and parking lot and highway runoff. The FMBR was installed near the center of the pond with two cynder block anchors placed on either side of the pond to keep the top mounted solar panels in a southernly facing direction. A floating mat constructed with a foam injected, interwoven, fiber was used to keep the filter bouyant. A wooden cover was placed over the filter to block light from entering the filter to prevent algae growth. Figure 3-2 displays the pond area and location of the FMBR.

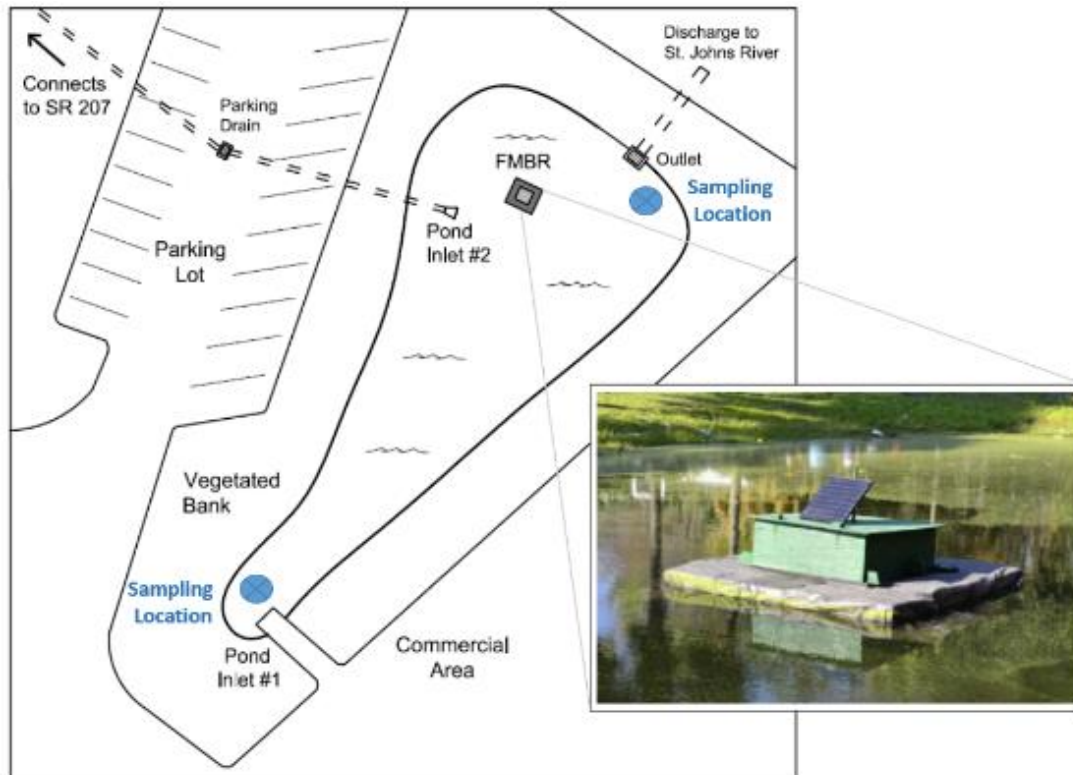


Figure 3-2 Palatka pond site layout with FMBR placement and photo.

3.2.3 Floating Media Bed Reactor Design

The FMBR was filled with a green engineered sorption media comprised of 50% fine sand, 20% recycled tire crumb, 20% fine expanded clay, and 10% limestone. The mix was chosen due its affordability, low impact recyclability, and findings based on previous laboratory column studies examining nutrient removal efficiencies of the media by adsorptive and biological processes (Jones et al, 2014). The filter container was made of a starboard plastic structure, although fiberglass is also optional, and contained a media chamber and settling chamber (Figure 3-3). Further design specifications pertaining to the FMBR may be found in Table 3-4.

Table 3-4. FMBR design specifications

Items	Parameter	Value
Hydraulics	Bed Volume (L)	340
	Maximum Headloss (cm)	25
	Loading Rate ($\text{lpm}\cdot\text{m}^{-2}$)	2.9
	Flow Rate ($\text{L}\cdot\text{min}^{-1}$)	1.5
	HRT (hr)	1
Media	Porosity	0.27
	Surface Area $\text{m}^2\cdot\text{g}^{-1}$	0.446
	% Fine Sand	50%
	% Fine Expanded Clay	20%
	% Recycled Tire Crumb	20%
	% Limestone	10%
Electrical	Battery Type	Deep Cycle
	Pump Current (A)	0.23
	Solar Panel Wattage (W)	30
Treatment	Treated Volume ($\text{L}\cdot\text{yr}^{-1}$)	788,400
	Pond Volume (L)	302,000
	Pond Cycles ($\text{cycle}\cdot\text{yr}^{-1}$)	2.6

Pond water initially is routed through a screened intake via a small 12V DC submersible pump (rated flow $4 \text{ L}\cdot\text{min}^{-1}$) and through a 1/4-inch polyvinyl tubing to the settling chamber whereby heavier particles may settle out. From the settling chamber water flows down a 2-inch PVC pipe and into a connection of perforated PVC piping at the base of the media bed. Water then flows up through a $5/8^{\text{th}}$ diameter expanded clay “roughing filter” and then through a 25 cm layer of sorption media. Treated water then collects in a 4 cm deep supernatant layer prior to flowing down a 2-inch PVC effluent pipe. A valve was attached to the inlet tube to adjust flow rates to match a one hour hydraulic residence time based on flow, media volume, and porosity measurements.

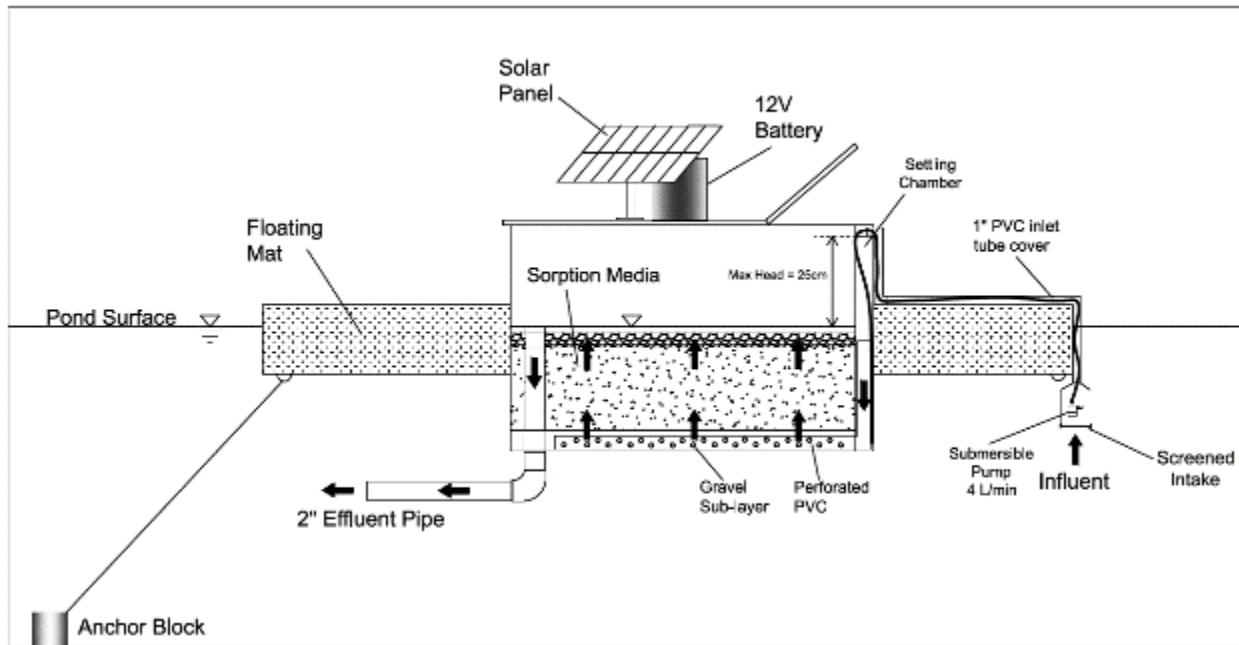


Figure 3-3 Design layout of a FMBR including solar powered submersible recycling pump. Pond water initially is routed into a settling chamber before advancing through the upflow filter filled with sorption Media Mix #2.

3.2.4 Nutrient Removal

Both pre- and post-FMBR monitoring of TP and TN were performed on the Palatka pond. A total of two non-storm samples (October 12th, 2013 and May 29th, 2013) were collected from the inlet and outlet of the pond prior to the FMBR installation. A total of six pond samples (three storm and three non-storm) were collected following installation. FMBR performance was studied for a six month duration starting February 12th 2014 to August 21st, 2014. A total of ten FMBR samples were collected, representing five non-storm and five storm. FMBR inlet samples were collected directly from the influent tube, whereas outlet samples were collected just prior to the effluent overflow pipe within the media bed. All samples were analyzed at Environmental Design and Research Laboratories.

Percent reductions were measured to quantify effective removal of TP and TN by the FMBR and reductions across the pond as measured from sampling locations. Concentration reduction percentage was calculated using the following equation:

$$\text{CRP} = \frac{C_{\text{Inflow}} - C_{\text{Outflow}}}{C_{\text{Inflow}}} \cdot (100) \quad (10)$$

Where:

CRP = concentration reduction percentage (%)

C_{Inflow} = influent concentration ($\mu\text{g} \cdot \text{L}^{-1}$), and

C_{Outflow} = concentration of the outflow sample ($\mu\text{g} \cdot \text{L}^{-1}$)

3.2.5 Hydraulics

In order to test the hydraulic behavior of Media Mix #2 in an upflow configuration laboratory testing was conducted on an upflow filter. The filter was constructed of two sections of HDPE piping with a downflow effluent pipe placed in the center of the filter. The total surface area of the media equaled 0.061m^2 , measured 560 cm in media depth and contained 0.034 m^3 of Media Mix #2 with a 10cm gravel under layer. A total of four constant head tests were conducted on the filter to establish correlation relationships between head and hydraulic loading rates. The media was left within the filter to examine changes in head loss with respect to time.

3.3 Results and Discussion

Concentrations and standard deviations comparing measurements of influent and effluent parameters are presented in Table 3-6. The FMBR was found to effectively reduce concentrations of TP consistently throughout the study, as graphically displayed in Figure 3-4. When tested at a 95% confidence interval the mean reduction measured $52\% \pm 8.6\%$ (standard

deviation equal to 14.3%). A two tailed t-test ($\alpha=0.05$) concluded that there was a difference between the means of the influent and effluent concentrations ($p=0.017$). The minimum and maximum removal of TP measured 25% and 69%, respectively. TN concentrations did not display the same consistency as TP reduction, however mean concentrations were reduced by 10.4% \pm 31.3% when tested at the 95% confidence interval (standard deviation equal to 50.4%). However it could not be concluded that the means differed for TN when tested at an α value equal to 0.05.

Table 3-5. Mean Reduction of Tested Parameters by the FMBR

FMBR Average Removal Efficiencies							
TP	SRP	TN	NH ₃	No _x	Org. N	Turb	Chl-a
43.1%	37.1%	10.4%	-25.5%	25.2%	14.6%	-13.7%	73.4%

Table 3-6. Concentration Comparison between Influent and Effluent Concentrations of the FMBR

Parameter	Inlet		Outlet	
	Mean	Std Dev	Mean	Std Dev
Total P, $\mu\text{g L}^{-1}$	38	24	19	10
Total N, $\mu\text{g L}^{-1}$	475	227	432	127
N to P molar ratio	26	NA	48	NA
Phosphate, $\mu\text{g L}^{-1}$	7.8	7.8	4.9	3.7
Ammonia, $\mu\text{g L}^{-1}$	70	70	88	41
Nitrates + Nitrites, $\mu\text{g L}^{-1}$	18	23	13	14
Organic Nitrogen, $\mu\text{g L}^{-1}$	387	171	330	113
Chlorophyll <i>a</i> , $\mu\text{g L}^{-1}$	5.9	4.7	1.6	0.8
Turbidity, NTU	4.5	2.9	4.2	2.1

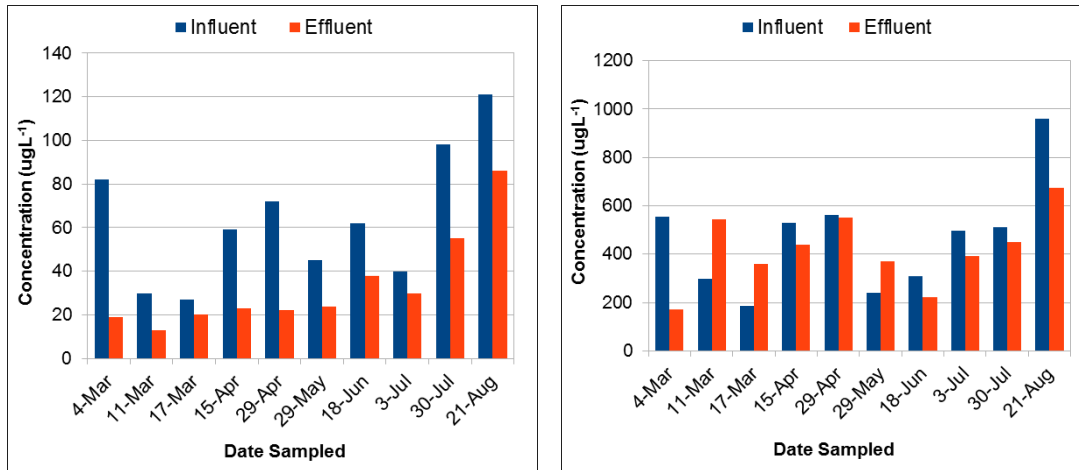


Figure 3-4 TP (*left*) and TN (*right*) concentrations taken at the influent and effluent sampling locations within the FMBR.

Measurements of pond TP and TN concentrations are presented in Figure 3-5. As seen the pond appeared to increase nutrient concentrations from inlet to outlet an average of -180% for TP and -138% for TN prior to FMBR installation. Following installation of the FMBR the pond performance improved with mean TP reductions measuring $19.1\% \pm 14.3\%$ and TN reductions measuring $16.7\% \pm 28.4\%$. As both pre-FMBR samples were taken during non-storm events a comparison was made only to post-FMBR non-storm samples to see if a negative performance correlation exists, but results still indicated a $10.9\% \pm 14.3\%$ reduction in TP and $30.6\% \pm 41.2\%$ reduction in TN. However, it should be noted only two pre-FMBR samples were gathered and therefore pre- and post-FMBR comparisons cannot be concluded at a statistically significant level.

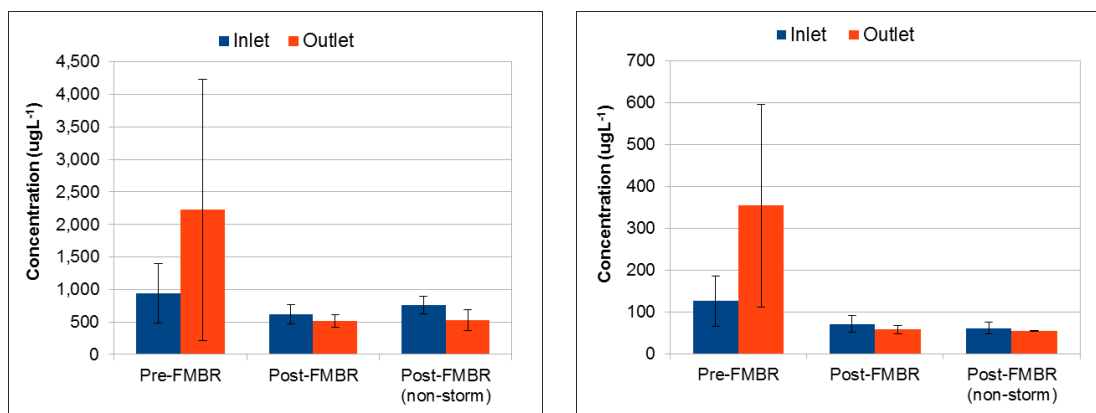


Figure 3-5 TP (left) and TN (right) measurements taken at the inlet and outlet sampling locations of the Palatka pond prior and after FMBR installation.

Using the mean reduction values and a set $1.5 \text{ L} \cdot \text{min}^{-1}$ flow rate, the total loading reduction for TP and TN achieved across the FMBR was calculated as $14.8 \text{ g} \cdot \text{yr}^{-1}$ and $25.3 \text{ g} \cdot \text{yr}^{-1}$, respectively. Although these values are low in comparison to the basin plan reduction, this value represents a relatively small pond in a system of hundreds. It should also be noted that treated water was recycled back to the pond and not directed as a direct discharge, determining the full effects of the recycling process on pond discharge quality would merit further detailed work, however theoretically the effluent from the FMBR could be redirected as a direct discharge from the pond.

Throughout the study period the head loss, as measured between the water levels between the settling chamber and the media bed supernatant layer, remained below 2 cm indicating that a significant buildup of head loss does not occur within the media. Turbidity samples at the FMBR influent measured a mean of 3.9 NTU with a maximum and minimum values of 10.1 and 1.37, respectively. It is suspected that the combination of the screened intake, roughing media at the bottom of the media bed and the cover to block sunlight were critical in keeping the head loss at minimal levels. These results indicate that the FMBR may be operated for long-term durations for influent mean turbidity conditions $<4 \text{ NTU}$, however higher values may be possible.

Additionally the battery voltage was found to remain above 12 volts throughout the study. The remainder of parameters analyzed for the FMBR may be found in Appendix A of this report. The remainder of pond parameters analyzed may be found in Appendix B.

Laboratory testing of an upflow filter containing Media Mix #2 are presented in Figure 3-6. All of the constant head tests resulted in high R-squared power or linear relations. Clearly there is an increase in head loss per hydraulic loading rate with respect to time. As an example a hydraulic loading rate of $10 \text{ L} \cdot \text{min}^{-1} \cdot \text{m}^{-2}$ resulted in approximately 10.0, 10.2, 20.2 and 24.0 cm of head loss for April 5th, May 8th, September 26th, and October 17th, respectively, representing almost a doubling in head loss in a 6-month period. The cause of the increase is likely due to a natural compaction of the media, or possibly biological growth within the media. It should be noted that the filter was only run four times and does not reflect field conditions, however does give some interesting insights into the media behavior.

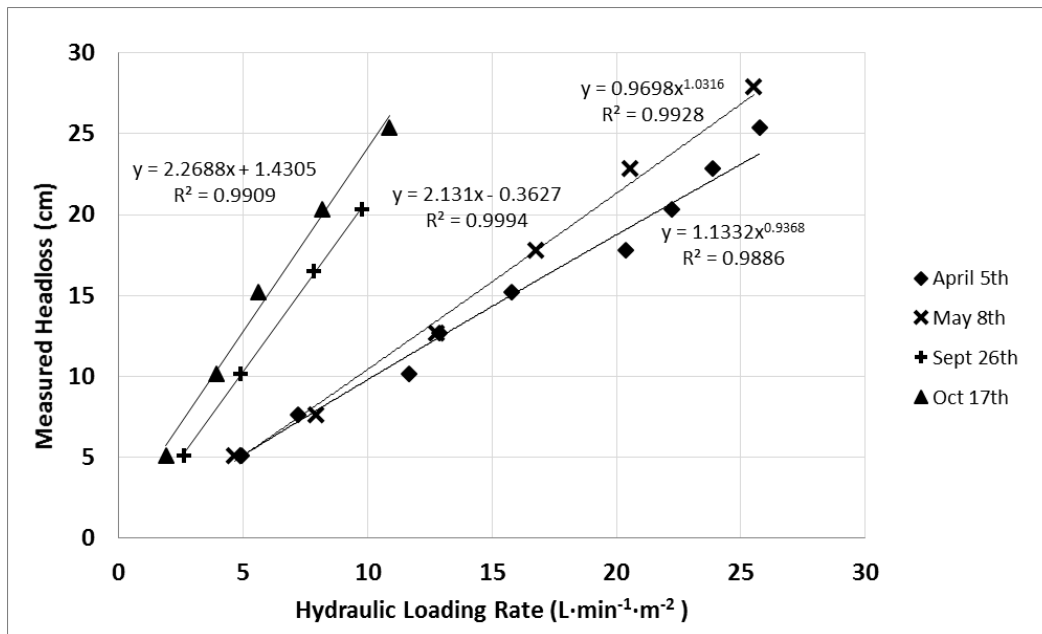


Figure 3-6 Laboratory head loss testing of Media Mix #2 in an upflow filter. Results display the increase in head loss measured over four runs conducted over a six month period.

3.4 Final Remarks

This study provides a unique contribution to supplement the limited scientific data on the use of sorption media in upflow field scenarios for stormwater nutrient treatment. Furthermore, this work introduces a new form of “green technology” inter-event treatment of retention ponds to promote sustainable development of stormwater BMPs. The FMBR was found to reduce TP by 52% \pm 8.6% and TN by 10.4% \pm 31.3% while operating at a one hour hydraulic retention time and surface loading rate of 2.9 L·min⁻¹·m⁻². Removal efficiency of the retention pond was found to increase following installation of the FMBR, however limited pre-FMBR data was available to make a statistically significant conclusion. Headloss across the filter was found to remain below 2 cm during a six month duration period when mean influent turbidity measured 3.9 NTU. A total loading reduction for TP and TN, as measured across the filter, was calculated as 14.8 g·yr⁻¹ and 25.3 g·yr⁻¹, respectively, for a 1.5 L·min⁻¹ flow rate. This study focused on recycling of FMBR effluent to the pond, however further work could be conducted on routing effluent directly to downstream sources.

3.5 References

- Cullum, M.G., 1984. Evaluation of the Water Management System at a Single-Family Residential Site: Water Quality Analysis for Seleted Storm Events at Timbercreek Subdivision in Boca Raton, Florida. South Florida Water Management District, Technical Publication No 84-11, Volume 11, West Palm Beach, FL, 116 pages.
- Harper, H.H., 1995. Treatment Efficiencies for Typical Stormwater Management Systems in Florida. Environmental Research & Design, Inc., Orlando, FL.

- Harper, H., Baker, D., 2007. Evaluation of current stormwater design criteria within the state of Florida. Environmental Research & Design, Inc.
- Hossain, F., Chang, N., Wanielista, M., 2009. Modeling kinetics and isotherms of functionalized filter media for nutrient removal from stormwater dry ponds. Environmental Progress & Sustainable Energy Vol 29 (3) pp 319-333.
- Jones, J., Chang, N., Wanielista, M., 2014. Reliability analysis of nutrient removal from stormwater runoff with green sorption media under varying influent conditions. Science of the Total Environment, 502 (2015) 434-447.
- Khambhammettu, U., Pitt, R., Andoh, R., 2006. Upflow filtration for the treatment of stormwater. Proceedings of the 2nd Biennial Stormwater Management Research Symposium, Orlando, Fl, May 4-6, pp. 223-243.
- Kim, H., Seagren, E.A., Davis, A.P., 2000. Engineering bioretention for removal of nitrate from stormwater runoff, in WEFTEC 2000 Conference Proceedings on CDROM research symposium, nitrogen removal, session 19, Anaheim CA, October, 2000.
- Lower St. Johns River TMDL Executive Committee, 2008. Basin management action plan for the implementation of total maximum daily loads for nutrients adopted by the Florida Department of Environmental Protection.
- Magley, W., Joyner, D., 2008. TMDL report: total maximum daily load for nutrients for the Lower St. Johns River. Tallahassee, Florida Department of Environmental Protection.
- Martin, E.H., Smoot J.L, 1986. Constituent-load changes in urban stormwater runoff routed through a detention pond-wetlands system in Central Florida: US Geological Survey, Water-Resources Investigations Report 85-4310.

- Ryan, P., Wanielista, M., Chang, N., 2010. Nutrient reduction in stormwater pond discharge using a chamber upflow filter and skimmer (CUFS). *Water Air and Soil Pollutants* 208:385-399.
- Schueler, T.R., 1992. A Current Assessment of Urban Best Management Practices. Metropolitan Washington Council of Governments.
- United States Environmental Protection Agency. (1999). Stormwater technology fact sheet: wet detention ponds. Washington: Office of Water, United States Environmental Protection Agency.
- Wanielista, M.P., 1978. Stormwater Management: Quantity and Quality, Ann Arbor, MI: Ann Arbor Science.

CHAPTER 4: EROSION CONTROL MONITORING USING INTEGRATED SOIL MOISTURE AND GROUNDWATER VELOCIMETER SYSTEM

4.1 Introduction

Knowledge of the movement and direction of groundwater flow is critical in understanding phenomena such as the fate and transport of pollutants in subaqueous groundwater environments (Hemond and Fechner-Levy, 2000) and hyporheic zones (Lautz and Siegel, 2006), water flux rates through soil containment barriers (Gavaskar, 1999) and bank stability (Fox et al, 2007; Wilson et al, 2007). Traditional techniques for obtaining velocity measurements by use of the natural hydraulic gradient with velocity estimations using Darcy's Law may only give reasonably accurate measurements due to the reliance of hydraulic conductivity coefficients for velocity calculations, which may be difficult to measure (Hemond and Fechner-Levy, 2000) and vary on greatly on small spatial scales. Furthermore gradient derived techniques involve the drilling of several wells which may be both time consuming and expensive. Due to these limitations, methods of direct *in situ* measurements are required to advance the field and adapt to meet field characteristics needs (Devlin et al., 2012). Several probes have been developed to measure groundwater velocities within a single well including, Heat Pulse Flow Meters (Kerfoot and Massard, 1985), Point Velocity Probe Meters (Labaky, 2007; Devlin et al., 2012) and In Situ Permeable Flow Sensors (Ballard, 1996). These probes are capable of measurements at centimeter spatial scales, which may be useful in applications where generalized measurements derived from the hydraulic gradient lacks resolution, including determining; hydraulic residence times of flow through permeable reactive barriers (PRBs), seepage rates through heterogeneous river banks with varying hydraulic conductivities (Fox et al, 2007; Wilson et al; 2007).

The hydraulic conductivity (K) of groundwater is a measure of the ability of water to flow through a porous medium and is important in both knowledge of and prediction of groundwater flow. The hydraulic conductivity is commonly measured using a permeameter test whereby a soil sample is tested in a laboratory and calculated using Darcy's Law or tested *in-situ* by use of a pumping test or slug test. However pumping tests and slug tests involve the drilling of wells and typically do not provide extremely accurate results (*Sudicky, 1986; Mas-Pla et al., 1997; Gierczak et al., 2006*) and may only agree to within an order of magnitude factor of 10 (*Hemond H. F. and Fechner-Levy E. J., 2000*). However, as the velocity is typically calculated using Darcy's Law and K , any errors in the measurement of K will carry over to the calculation of the velocity. By direct measurement of the velocity using probes, these errors may be reduced, potentially giving more accurate measurements of the sub-aqueous environment at finer spatial resolutions. Furthermore coupling the velocity measurement with porosity and the hydraulic gradient, direct calculations of the hydraulic conductivity may be achieved.

Direct measurements of velocity and K may be quite beneficial for use with groundwater modeling applications. Field measurements may be used for calibration and verification of values generated within groundwater flow models such as MODFLOW, SVFlux and FEHM. Measured velocity and K values may serve to both verify the accuracy inputs chosen for the model, as well as provide additional confirmation of calculated velocity values based on natural hydraulic gradients and K calculations performed on core samples.

The objective of this research demonstrated here is to test a new single well groundwater probe in an integrated wireless field station for collection of erosion control measurements to quantify correlations between hydrological factors with groundwater velocity and erosion concerns due to bank stability. The work also supplements the limited database on groundwater

velocity behavior within a pond bank. The study supplements the need for affordable groundwater velocity sensors capable of accurate measurements of groundwater velocity magnitude and direction on a small scale via wireless remote control.

Additionally the chapter examines the performance of Tri-Lock Blocks, a concrete block erosion measure installed around two inlets which were experiencing periodic erosion at the sides and around the inlet pipes. Observational data examined the degree of erosion before and after installation of the Tri-Locks as well as re-vegetation following installation.

Science Questions What are

4.1.1 Chapter Objectives

- Identify which factors are effecting the bank erosion.
- Develop long term soil moisture monitoring.
- Develop cost-effective technique for monitoring of groundwater velocity.

4.2 Methodology

One representative wet retention pond located in West Palm Beach was examined for this chapter of work. The pond, named the Royal Palm Estates pond, was installed in 2004 and receives mainly highway runoff from Southern Blvd. The cause of initial erosion around the two inlets is unknown however some highway expansion work in 2008 may have added additional volumetric loading to the pond, causing the erosion to occur. From discussions with FDOT staff it was known that the erosion around the inlets was a re-occurring event. Typically FDOT staff would re-stabilize the pond bank with fine grained soil every year, filling in areas where previous soil had eroded away, which eventually itself would require replacement. This cyclical process however may introduce detrimental impacts to downstream waterways as eroded soil will add

TSS loading to the pond. In addition each re-stabilization added a cost to FDOT. Table 4-1 below lists details on the pond.

Table 4-1 Field Site Identification Numbers and Geographic Coordinates.

Pond Site	Pond ID	Coordinates
Royal Palm Estates	209965-1-52-01-P001	29.404433°, -80.070147°

Table 4-2 Field Site Pond Characteristics.

Basin No.	Total Area (AC)	Imper. Area (AC)	% Imperv	Pond Area (AC)
SR80	20.52	14.03	68	2.07

Figure 4-1, Figure 4-2, Figure 4-3, and Figure 4-4 display historical pictures taken at the site prior to implementation of the TriLock Blocks. Figure 4-2 depicts the slopes by Inlet #2 taken on June 2nd, 2012. As seen, large sections of the bank to the sides and behind the inlet pipe headwall had eroded into the pond. It is believed that the causes of erosion were caused both by saturation and desaturation of the bank during pond stages fluctuations, as well as overland flow during storm events. Figure 4-2 depicts the inlet sometime after re-stabilization of the bank, taken March 1st, 2014. As seen, the initial erosional patterns had begun eroding around the side of the headwall. Curiously there are no obvious signs of overland flow erosion and the majority appears to be erosion at the water level interface with the bank. Figure 4-3 displays Inlet #2 immediately following a second re-stabilization which occurred on March 25th, 2014, however only three months following there appears to be obvious signs of bank erosion occurring around the sides of the headwall as shown in Figure 4-4. The current practice of re-filling, followed by erosion presents two issues, firstly an addition of TSS to the pond from the erosion of the fill, and secondly the reoccurring cost of re-filling the bank.



Figure 4-1 Inlet #2 displaying erosion occurring around support wall, picture taken June 2nd, 2012.



Figure 4-2 Inlet #2 displaying erosion occurring around support wall following refilling of the bank, picture taken March 1st, 2014.



Figure 4-3 Inlet #2 shortly following re-filling of the bank, picture taken March 25th, 2014.



Figure 4-4 Inlet #2 erosion re-occurring around support wall three months following re-filling, picture taken March 17th, 2014.

TriLock Blocks were chosen for bank stabilization of the two inlets. These BMPs provide a “hard armor” option for erosion control by incorporation of interlocking concrete blocks, placed one at a time on top of the banks. This solution is anticipated to not require any re-fill, saving FDOT time and money and minimize erosion of TSS into the pond. Prior to installation portions of the banks had to be slightly graded in order to maintain a 2:1 maximum slope as per specifications. Figure 4-5 displays the placement specifications for the Tri-Locks. For the design, a 10 foot coverage extending from the headwalls of the inlets for placement of the blocks was chosen. The top portion of the blocks were placed into an anchor trench which was dug into the ground at approximately 1-foot depth and covered with soil as per specifications (Figure 4-6). A geotextile fabric was laid on the ground prior to paying the blocks. The installation took approximately two days to complete and included FDOT and UCF staff.

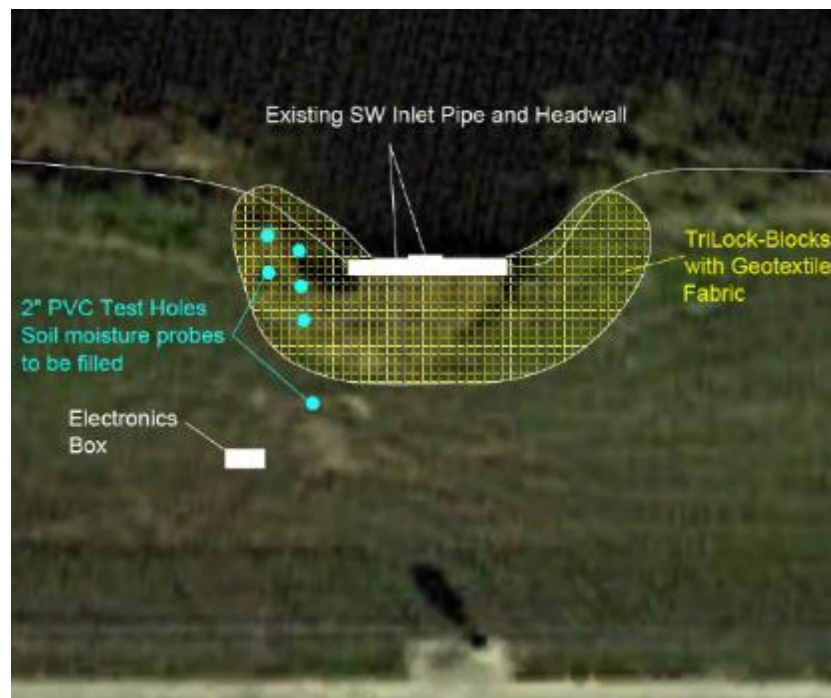


Figure 4-5 Area placement of Tri-Lock Blocks around Inlet #2. Also depicted are locations of test holes for pressure transducers, soil moisture probes and GVP installation.

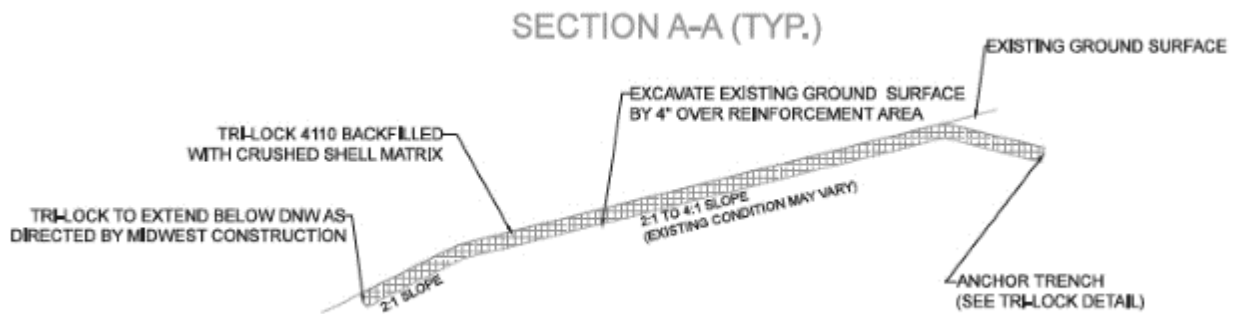


Figure 4-6 Typical slope placement specifications for Tri-Lock Blocks.

4.2.1 Volumetric Water Content

Volumetric Water Content (VWC) measurements were conducted using EC-5 VWC probes produced by Decagon Devices. The EC-5s operate by measuring the dielectric constant of the surrounding media using capacitance frequency domain technology with a two pronged design. The devices have a factory accuracy of at least $0.03\text{m}^3\text{m}^{-3}$ with a resolution of $0.001\text{m}^3\text{m}^{-3}$. For installation three wells, each with two probes, were dug down to 3 foot depth. One probe was vertically inserted into the bottom of the well whereas the second probes was horizontally inserted into the side of the well. The well was then backfilled with the excavated soil. The EC-5s were attached to a Campbell Scientific CR1000 data logger located on the surface into a high-end, ground and excitation channel. SCWin (ShortCut) software was used to program the probes to conduct VWC measurements once per minute. Figure 4-7 below displays the electronics enclosure used for the study. The enclosure included the CR1000 data logger,

Multiplexer, Raven XTV cellular modem solar charge regulator, and GL500 data logger (not shown).

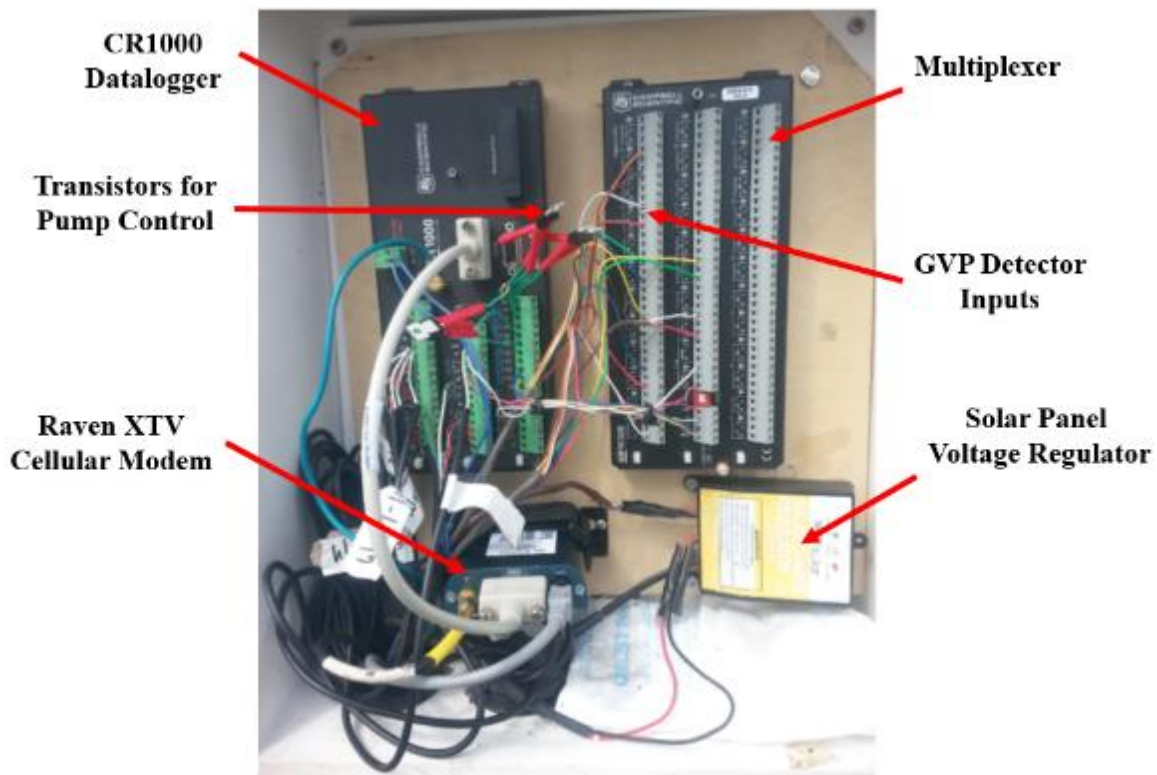


Figure 4-7 Electronics enclosure casing for field station control of GVP, soil moisture probes and pumps for water sample collection.

4.3 GVP Theory

4.3.1 Directional Calculations

Detectors are arranged radially around the injection port to establish the flow direction. As the saline pulse passes nearer to a detector a lowering of the resistance between the detector wires occurs, equivalent to an increase in the resistance ratio as denoted by Δr (Figure 4-8). By using the relative strength of the change in resistance between detectors, a directional component

is derived. The result is then compared with the expected directional angle, as physically measured by the placement of the probe.

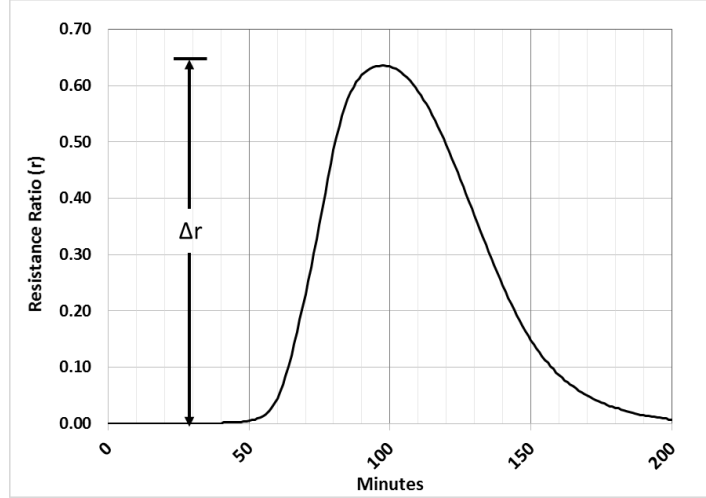


Figure 4-8 Example of a tracer response curve. The peak change in the resistance ratio is denoted by Δr .

The directional angle of the groundwater velocity is calculated using two steps. First the Δr value for each detector is resolved and summed to x and y components to form a combined directional vector. The angle from the x-axis (θ) of the combined vector is solved by:

$$\theta = \tan^{-1} \frac{\sum y}{\sum x} \quad (11)$$

or

$$\theta = \tan^{-1} \frac{(D_0(0) + \frac{D_{45}}{\sqrt{2}} + D_{90} + \frac{D_{135}}{\sqrt{2}} + D_{180}(0) - \frac{D_{225}}{\sqrt{2}} - D_{270} - \frac{D_{315}}{\sqrt{2}})}{(D_0 + \frac{D_{45}}{\sqrt{2}} + D_{90}(0) - \frac{D_{135}}{\sqrt{2}} - D_{180} - \frac{D_{225}}{\sqrt{2}} + D_{270}(0) + \frac{D_{315}}{\sqrt{2}})} \quad (12)$$

Where:

θ = degrees from x-axis

$D_0 = \Delta r$ for the 0° detector

$D_{45} = \Delta r$ for the 45° detector

$D_{90} = \Delta r$ for the 90° detector

$D_{135} = \Delta r$ for the 135° detector

$D_{180} = \Delta r$ for the 180° detector

$D_{225} = \Delta r$ for the 225° detector

$D_{315} = \Delta r$ for the 315° detector

In the second step the final directional angle is calculated using an “if/and” function, depending on which quadrant the final vector lies:

- Quadrant 1: IF $\Sigma x > 0$ AND $\Sigma y > 0$, THEN $\text{Direction}^{(0)} = \theta$
- Quadrant 2: IF $\Sigma x < 0$ AND $\Sigma y > 0$, THEN $\text{Direction}^{(0)} = \theta + 180^\circ$
- Quadrant 3: IF $\Sigma x < 0$ AND $\Sigma y < 0$, THEN $\text{Direction}^{(0)} = \theta + 180^\circ$
- Quadrant 4: IF $\Sigma x > 0$ AND $\Sigma y < 0$, THEN $\text{Direction}^{(0)} = \theta + 360^\circ$

4.3.2 Velocity Magnitude and Dispersion Coefficient

Velocity measurements made by the GVP (hereby denoted as V_{GVP}) were compared to expected velocity measurements ($V_{EXPECTED}$) assuming uniform flow conditions through the flume. $V_{EXPECTED}$ measurements were made based on the flow rate through the flume (Q), the cross sectional area (A) of wetted sand by the probe, and the porosity (n), as shown in eq below:

$$V_{EXPECTED} = \frac{Q}{An} \quad (13)$$

A statistical moment analysis technique was utilized to derive the transport behavior of the saline tracer from the response curve. Similar methods have been used in estimating the pore-water velocity and dispersion coefficients for break-through data sets in laboratory column experiments, especially for conservative tracers (Maloszewski et al., 1994; Pang et al., 1998; Yu et al., 1999). The method assumes a conservative tracer with no retardation effects. The moments method implores the use of the i -th temporal moment of tracer concentration distribution at a distance of x (measured from the center of the injection point to the detector) as defined by (Valocchi, 1985):

$$M_i = \int_0^\infty t^i c(x, t) dt \quad (14)$$

The i -th normalized moment of the distribution is then calculated as:

$$\mu_i = \frac{M_i}{M_0} = \frac{\int_0^\infty t^i c(x, t) dt}{\int_0^\infty c(x, t) dt} \quad (15)$$

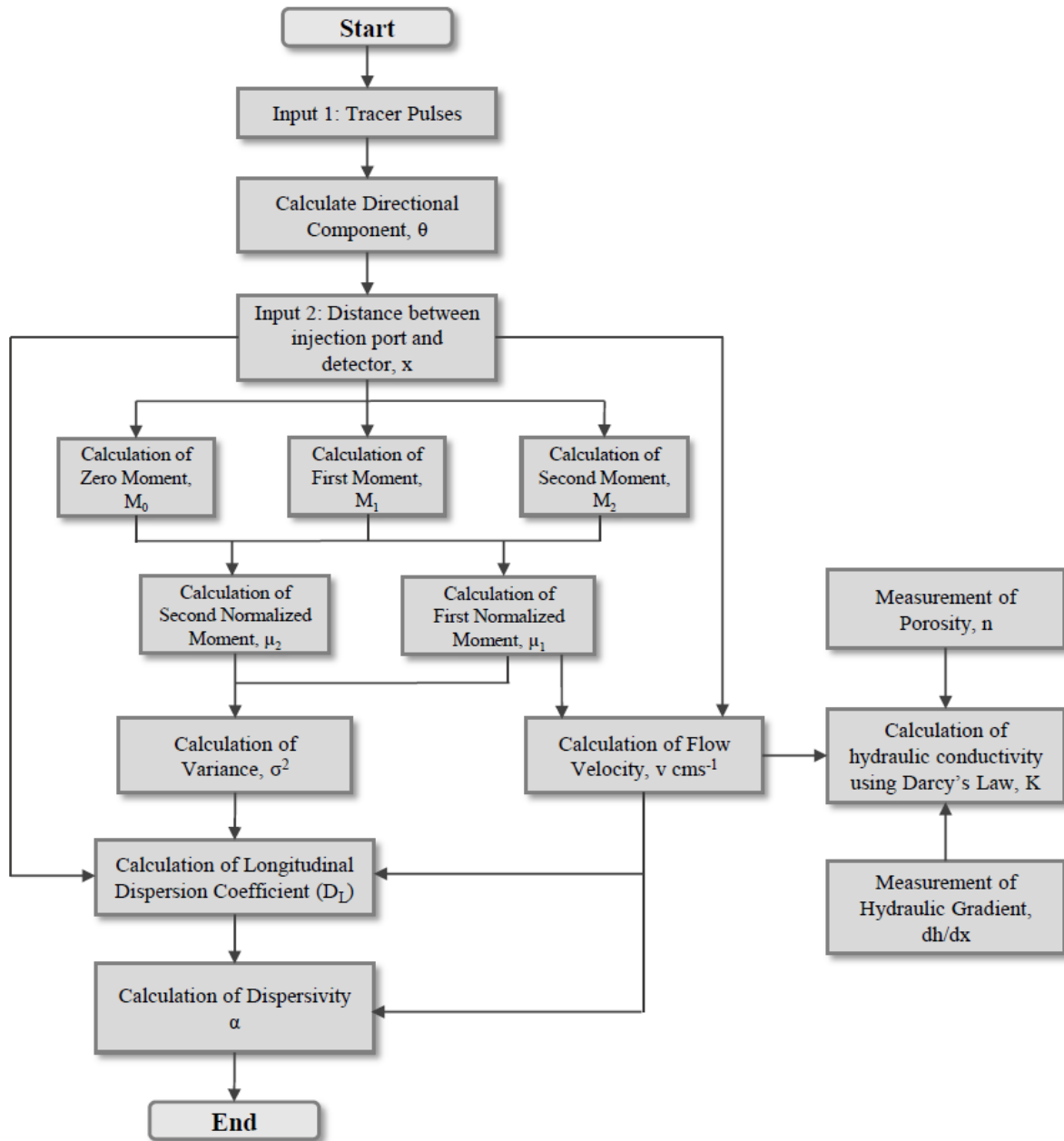


Figure 4-9 Flow diagram for calculation procedure of flow direction, velocity, dispersion coefficient and dispersivity from tracer curves for $P_e > 1$.

Two normalized time moments were used to determine the transport parameters of velocity (v) and the dispersion coefficient (D). First, a normalized time moment, μ_1 , was used to identify the central tendency of the tracer curve. The second central moment, or the variance σ_t^2 , is then used

to describe the spreading of the tracer pulse which can be calculated using the first and second normalized moments $\sigma_t^2 = \mu_2 - \mu_1^2$. The first and second moments are related to tracer transport parameters v and D . This relation may be explained as follows (July and Roth, 1990 and L Weihermüller, 2011):

$$v = x / \mu_1 \quad (16)$$

$$D = \frac{v^3}{2x} \sigma_t^2 \quad (17)$$

A flow diagram of the calculation procedure is displayed in Figure It should be noted that the above mentioned methods are valid when spreading of the tracer is dominated by mechanical dispersion and molecular diffusion of the tracer is negligible. The Peclet number may be used to determine which regime dominated by comparing the degree of mechanical dispersion to the degree of molecular diffusion by the following equation:

$$P_e = \frac{v_x d}{D_d} \quad (18)$$

Where:

P_e = Peclet number
 V_x = horizontal velocity in the direction of flow
 d = mechanical dispersion coefficient
 D_d = molecular diffusion coefficient

Typically mechanical dispersion dominates at $P_e > 0.6$, both occur at $0.2 > P_e > 0.6$ and molecular diffusion dominates at $P_e < 0.2$. The critical velocity below which the moments velocity methods are invalid is calculated by rearrangement of eq (18) to eq (19). Below a velocity of critical value an observational method may be employed to obtain general low velocity movement trends of the pulse.

$$v_{crit} = \frac{P_e D_d}{d} \quad (19)$$

4.3.3 Hydraulic Conductivity

The hydraulic conductivity (K) is a measure of the ability of water to pass through a porous medium and is commonly used in the velocity calculations using Darcy's Law:

$$v = \frac{K \Delta h}{n \Delta x} \quad (20)$$

where v is the groundwater velocity, K is the hydraulic conductivity, n is the porosity, h is the elevation (z) plus the pressure head (ψ), and x is the distance between the two observations of the hydraulic head. With the velocity variable measured by use of the GVP, and the hydraulic gradient ($\Delta h/\Delta x$) known across the sample location, the hydraulic conductivity (K) of the soil may be determined by rearrangement of eq (19).

$$K = \frac{vn\Delta l}{\Delta h} \quad (21)$$

For laboratory measurements Δh was physically measured at the influent and effluent open water chambers. For field measurements Δh was digitally measured by installation of two pressure transducer wells at a distance of 1.8m and 1m of the GVP well, placed laterally to the pond bank (Figure 4-12).

4.4 Methodology

4.4.1 Operation and Laboratory Set-up

The GVP operates by producing a tracer curve from the passing of a small injection of saline solution using continual conductivity measurements. The saline solution is injected via a small peristaltic pump which travels through a tube to an injection port comprised of a cylindrical diffuser stone. The sides of the diffuser stone are sealed with a silicone sealant so the

tracer solely injects vertically downwards through the bottom of the stone (diameter of 0.9cm). The injection port is surrounded by eight conductivity detectors spaced 2.5cm away at 45 degree increments as pictured in Figure 4-10. Each detector is comprised of a pair of parallel 18 gauge stripped copper wires set 0.75cm apart. The detectors are routed to the surface and connected to a data logger. Conductivity measurements are made using half bridge connections, whereby one wire is routed to a single ended channel and the other to ground. A parallel connection with a fixed 1,000 ohm resistor is made between the single end channel and an excitation port. A reverse excitation voltage is applied to the detector and the ratio of the resistance between the detector wires and the fixed resistor is measured. By conducting measurements every one minute, a tracer curve of the resistance ratio is developed from the migration of the saline pulse. The tracer curve is then used to derive the velocity of the pulse. The support frame on which the injection port and detectors are mounted was created using AutoCAD 3D 2014 and printed on a Stratasys Dimension Elite 3D printer using ABS high density plastic (Stratasys blend P430).

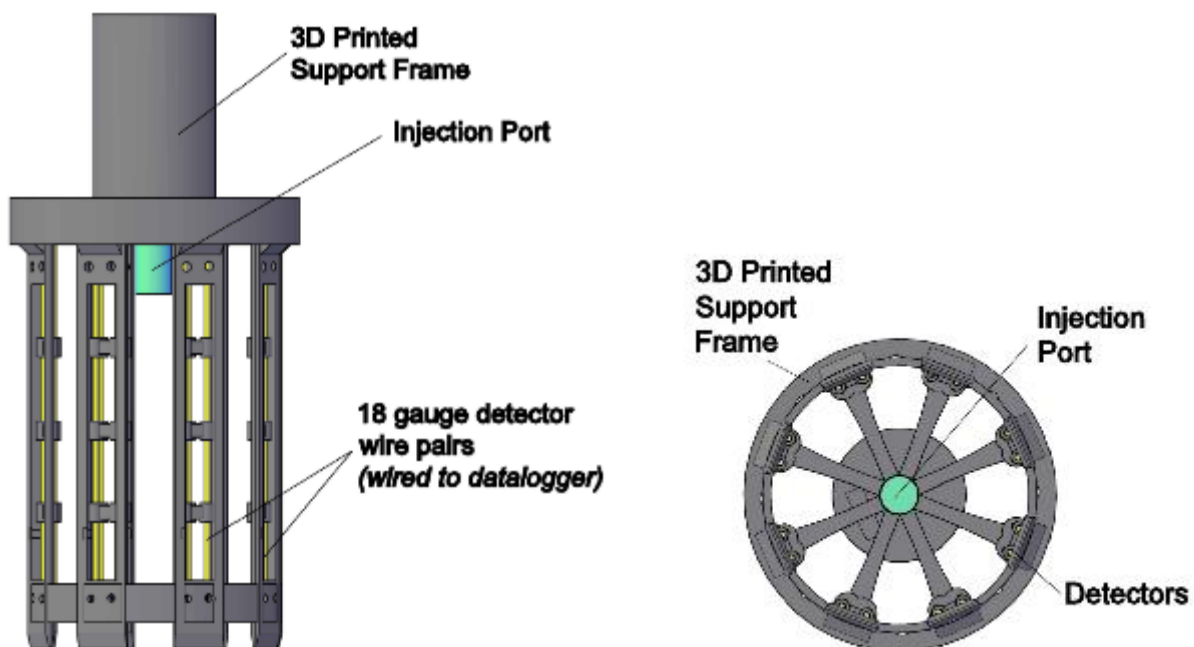


Figure 4-10 Front- and bottom-view schematic of a 6cm diameter GVP. Detectors are comprised of eight sets of 18 gauge copper wires (with an 8.5cm portion stripped) built upon a 3D printed support frame.

The GVP is designed for attachment to a 2-inch PVC coupling to be extended into deeper wells. Injections were made from the surface using a high torque 12V DC peristaltic pump (*Adafruit* product code: RB-Ada-91) and controlled via 5 volt signals from programmable control ports of a *Campbell Scientific* CR1000 data logger. 0.5-inch PVC vinyl tubing was routed from the peristaltic pumps down the interior of the PVC encasing to an injection port. The injections were programmed to a 0.5 second duration, resulting in a total of 1.3 ± 0.5 ml per injection. Both the lab and field tests used a concentration of 15mgL^{-1} NaCl. A connection diagram of the GVP station including pressure transducers and soil moisture probes is displayed in Fig 2.

The hydraulic flume used for laboratory testing was made from glass and measured 66cm in length, 25cm in width and 30cm in height (Figure 4-11). Retaining walls made of plastic starboard with 0.7cm diameter perforations at 2.5cm spacing were placed at either end of the flume to create open water chambers at the influent and effluent sides of the flume. Such arrangement was utilized to produce lateral, uniform, flow conditions. A *Watson Marlow 323* peristaltic pump was used to cycle water through the flume at varying rates. The flume was filled with non-cohesive sand with a measured porosity of 0.253. All laboratory measurements were conducted at 25°C . For laboratory testing, the GVP was tested over an expected velocity range of 26 to 459cm d^{-1} . A total of six velocity increments were conducted, with four to five injections averaged per increment. The volume of the injected pulses were measured prior to the experiment. The GVP was manually inserted into the sand by hand.

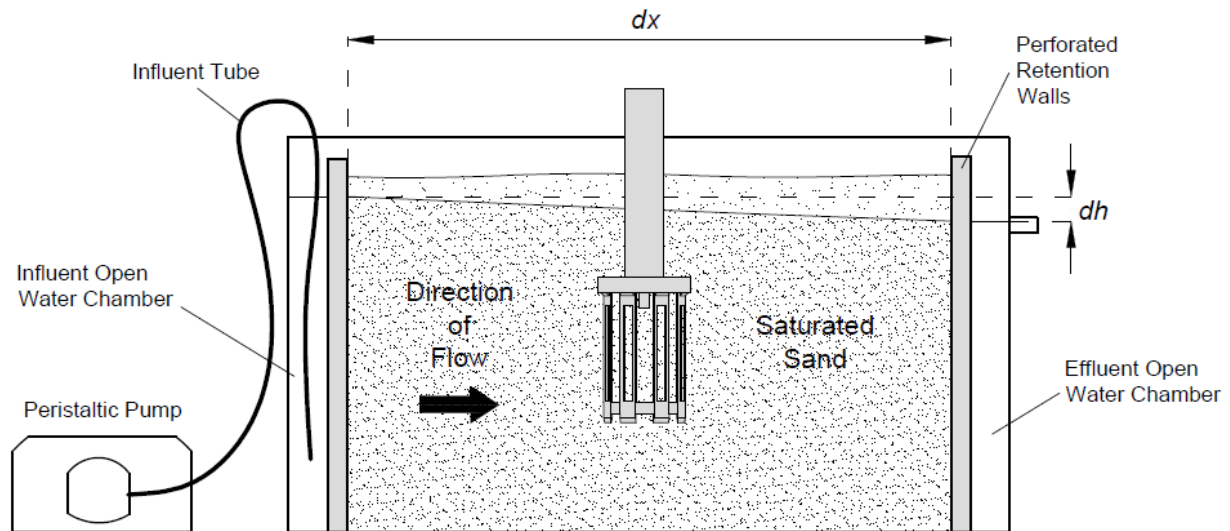


Figure 4-11 GVP set up in a hydraulic flume for laboratory testing. Sand is contained between two perforated retention walls to produce uniform, lateral, flow across the flume. The hydraulic gradient is measured by dh/dx .

4.4.2 Field Measurements

A field network station including one GVP well, two pressure transducers wells and six EC-50 soil moisture probes was installed on the bank of a wet detention pond located in West Palm Bach, Florida to investigate reoccurring bank erosion around the pond inlet structure. The contributing watershed was comprised mostly of highway stormwater runoff. The station was powered by a 12 volt deep cycle marine battery and 4 watt solar panel. All wells were constructed using a 3-inch diameter handheld auger. The GVP was placed at a depth of 1.5 m below the land surface. The soil moisture probes were installed in three locations (SM-A, SM-B and SM-C) with probes placed at 0.5m and 1.0m below the land surface. A CR1000 data logger was connected to the soil moisture probes and an AM 36/64 multiplexer was used for GVP measurements. Two pressure transducers were used and connected to a GL500-2-1 data logger.

Measurements were made between PT-W1 and PT-Pond locations from 6/17/2014 to 8/20/2014 to obtain comparative data between the open pond water and the groundwater elevations, and measurements were made between PT-W1 and PT-W2 from 8/31/2014 to 9/16/2014 to obtain hydraulic gradient measurements within the bank to compare to GVP data. The PT-W1 measured 3.0 m from PT-W2 and 5.2 m from PT-Pond.

A Raven XTV cellular modem was connected to the CR1000 data logger. Combined with the use of *Campbell Scientific LoggerNet* software, this allowed remote data retrieval and full wireless control of the GVP station from anywhere with an internet connection. Both data retrieval as well as alteration to program settings were made remotely. The Raven was connected to an 800MHz 0dBd half wave, whip dipole, cellular antenna and transmitted across a 3G CDMA cellular network. A diagram displaying the field installation of the GVP station is displayed in Figure 4-12 below. Precipitation data was obtained from a South Florida Water Management rain gauge located 1.8 kilometers to the northeast, reported as daily totals.

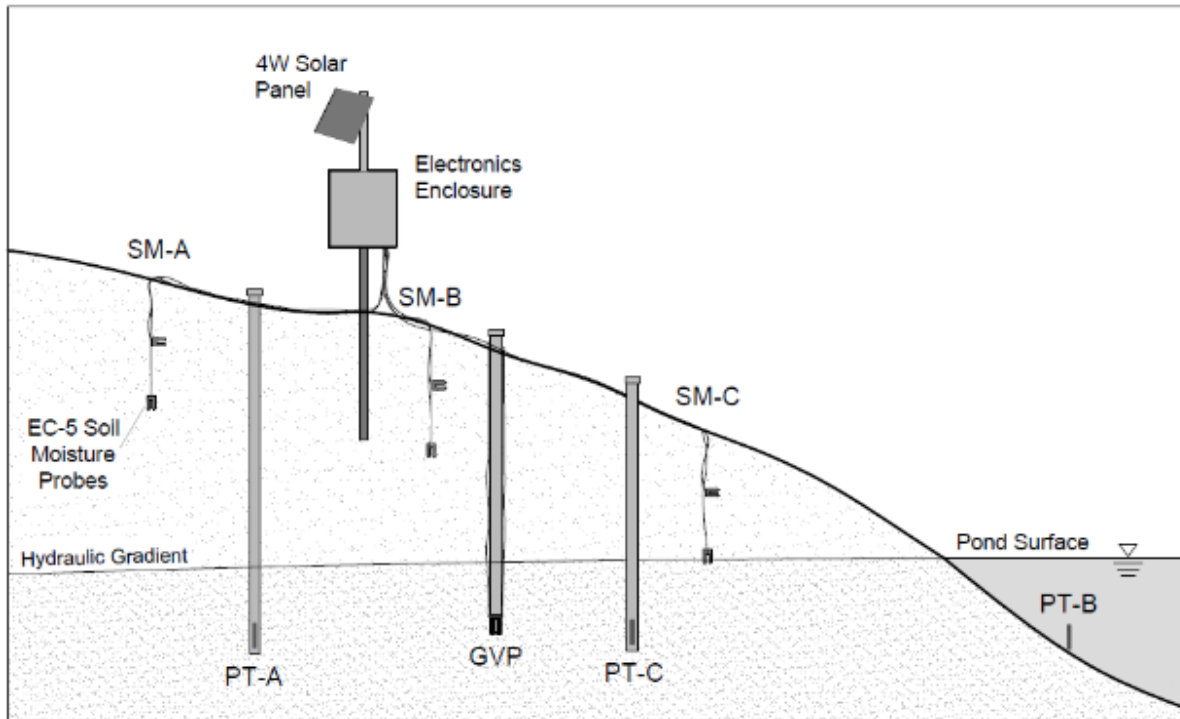


Figure 4-12 GVP field station installation on a pond bank including a GVP probe, pressure transducer wells and EC-5 soil moisture probes.

4.5 Results

4.5.1 Laboratory Testing

During laboratory testing, pulses were detected at all of the velocity increments. Furthermore, testing of the GVP showed consistent tracer response curves for all velocity increments, indicating little variation between individual measurements. This consistency is shown graphically in Figure 4-13 which displays the overlay of five consecutive pulses measured at the same velocity. A statistical summary of measured GVP velocities is presented in Table 4-3. As seen in the table, the largest standard deviation relative to the mean was measured as 6.8 cmday^{-1} for a mean velocity of 111.1 cmday^{-1} . Values for hydraulic conductivity as calculated by (11) were found to have close agreement of GVP (0.0269 to 0.0312 cms^{-1}) to laboratory measurements conducted using permeability tests (0.0329 and 0.0333 cms^{-1}).

Table 4-3 Statistical summary of v_{GVP} and K measurements as compared with the expected values.

Mean $v_{EXPECTED}$ (cmd^{-1})	26	45	89	179	270	360	459
Mean v_{GVP} (cmd^{-1})	23	57	111	240	331	412	526
Standard Deviation	3.8	2.4	6.8	4.1	1.9	2.0	7.7
Sample size	3	4	5	5	5	5	5
95% C.I.	± 4.3	± 2.3	± 6.0	± 3.6	± 1.7	± 1.7	± 6.8
Standard Error	2.19	1.20	3.06	1.85	0.87	0.89	3.45
dh (cm)	0.15	0.28	0.50	1.20	1.70	2.10	3.00
K (cms^{-1})	0.031	0.028	0.031	0.026	0.028	0.030	0.027

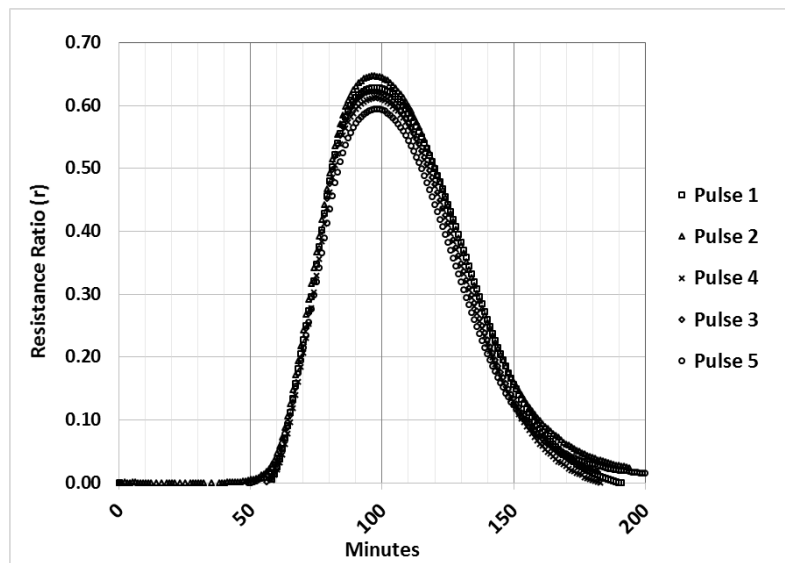


Figure 4-13 Layered response curve for five consecutive pulses at an expected velocity of 80 cmd^{-1} . The overall shape and Δr between each pulse remains similar indicating little variation between pulse measurements.

Figure 4-14 displays correlations between measured V_{GVP} (dependent variable) to $V_{EXPECTED}$ (independent variable) and the head difference measured across the flume (h). As expected, a linear increase occurs with an increase in flow rate ($R\text{-squared} = 0.9921$) as well as with an increase in hydraulic gradient ($R\text{-squared} = 0.9871$). A slight positive bias was measured for v_{GVP} when compared to $v_{EXPECTED}$. It is thought this phenomena may be due to a slight compaction of the sand around the probe which would produce somewhat higher velocities

at due to a decrease in porosity. Another cause could be explained by slight variations in flow within the flume, with higher velocities occurring within the center of the flume. In either case, the bias presents only a minimal degree of error and is not considered significant.

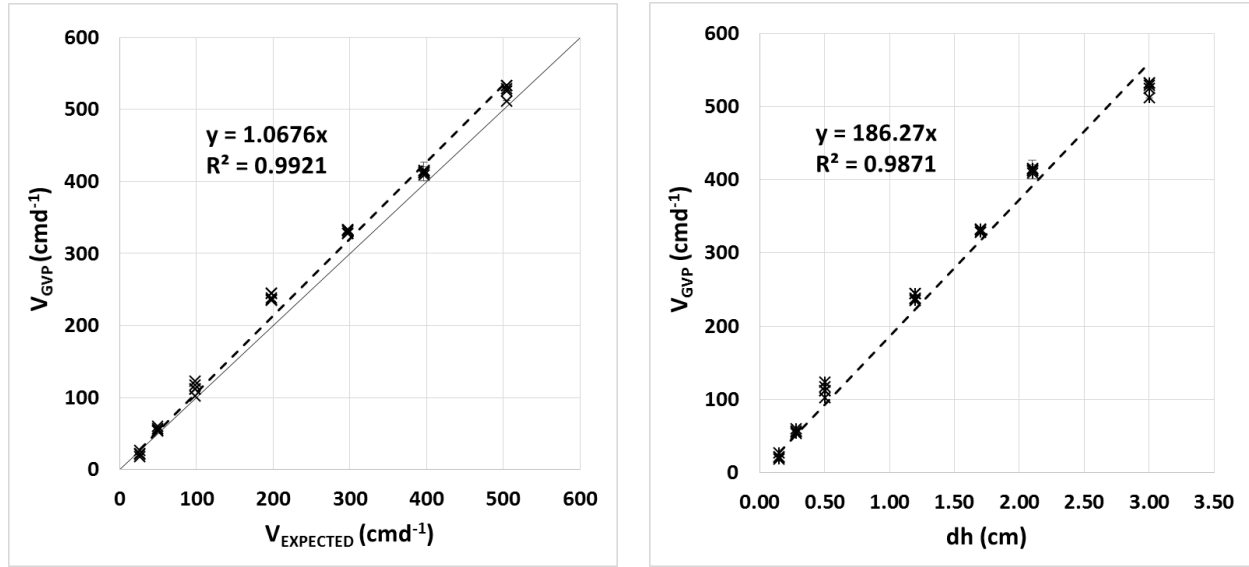


Figure 4-14 *Left* - agreement between $v_{EXPECTED}$ (eq. 1) and v_{GVP} (eq. 4). The expected velocity is used as the independent variable whereas v_{GVP} is used as the dependent variable, the dashed lines represent the linear regression of the v_{GVP} measurements. *Right* – agreement between v_{GVP} and the change in hydraulic head (dh).

The tracer response curves measured by the GVP within the flume for a 270cmd^{-1} velocity and angled flow direction of 45 degrees is graphically displayed in Figure 4-15. As seen, the 45° detector measured the greatest increase in Δr (drop in resistivity), while the 0° and 90° also experienced mediocre increases representative of the plume edge. The increases in the 0° and 90° detectors represents the edge of the plume as it passes by the detectors. Curiously the remaining detectors also experienced slight increases in Δr concurrent with the passing of the pulse by the 45° detector. This is not expected as the salt pulse is not detected on initial injection and migrates away from these detectors with time. Rather it is suspected that these responses are directly related to the drop in resistivity by the 45° detector, although the reason is currently

unknown. Regardless, these responses represent approximately 3% of that measured by the 45° detector and do not significantly contribute to the final directional angle as calculated by eq. 7.

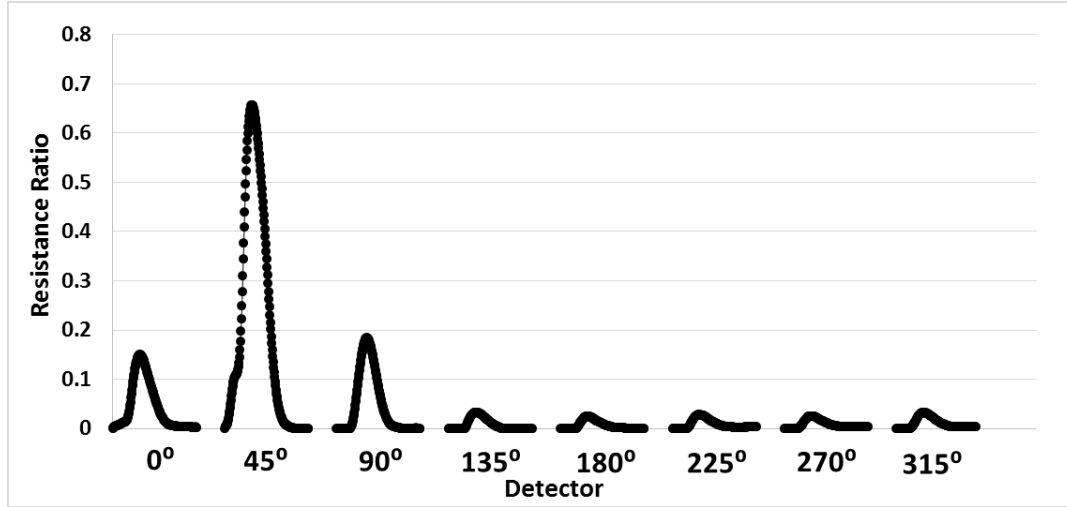


Figure 4-15 Simultaneous plot of all eight tracer response curves measured by each detector for a salt injection with probe set at a 45° angle to the direction of flow and velocity set to 270 cmd⁻¹.

Table 4-4 summarizes all directional measurements made within the flume. The angular flow direction measurements made by the GVP were found to be generally within the range of expected values, the largest discrepancy being 34° when measured at an angle of 80°. The average discrepancy was measured as 14°.

Table 4-4 Statistical summary of GVP velocity directional measurements.

Mean D_{EXPECTED} (°)	0°	35°	45°	80°	113°	180°	200°	315°
Mean D_{GVP} (°)	25°	49°	44°	114°	125°	175°	210°	324°
Percent Difference	7%	4%	0%	9%	3%	-2%	3%	3%
Standard Deviation	1.2	0.7	1.7	0.5	0.2	1.3	1.5	2.0
Sample size	6	8	3	5	7	3	7	5
95% CI	0.96	0.52	1.95	0.46	0.17	1.45	1.09	1.79
Standard Error	0.49	0.26	1.00	0.23	0.09	0.74	0.56	0.91

The longitudinal dispersion coefficient (D_L) of the tracer pulse was calculated from the tracer curves by use of (eq 5). Measurements indicate a slight increase in D_L with respect to an

increase in velocity, however the calculated values for D_L do not approach zero with decreasing velocity, as is expected assuming Fick's first law. The relative high values of D_L with respect to V_{GVP} are likely more representative of turbulent diffusion formed during the injection of the tracer, rather than by tortuous mechanical diffusion caused by the longitudinal transport of the tracer. In order to obtain values which represent the true value of the *in-situ* D_L the turbulence during injection would either need to be minimized, or the distance between the injection port and detector increased so dispersion caused during injection is negligible in relation to the *in-situ* longitudinal dispersion. Regardless, the data obtained gives quantifiable measures of the injection D_L which may be useful in further development of the instrument.

4.5.2 Field Testing

As expected the soil moisture measurements were closely correlated with rainfall events (Fig 10) with sharp increases in soil moisture occurring shortly following rainfall events and a gradual decrease in soil moisture as the pond elevations decreased. As depicted in Figure 4-16 when moisture probes of the same well were both in the vadose zone, probes at the 1m depth experienced sharper increases in soil moisture following rainfall events as compared with probes set at the 0.5m depth. This is clearly seen during the June 8th, 11th, 30th and July 2nd storm events whereby SM-A (1m) measured a sharp increase in moisture content, whereas SM-A (0.5m) measured a relatively minor increase in comparison. This indicates major changes in soil moisture are caused by fluctuations in the groundwater table, rather than by above infiltration of overland runoff.

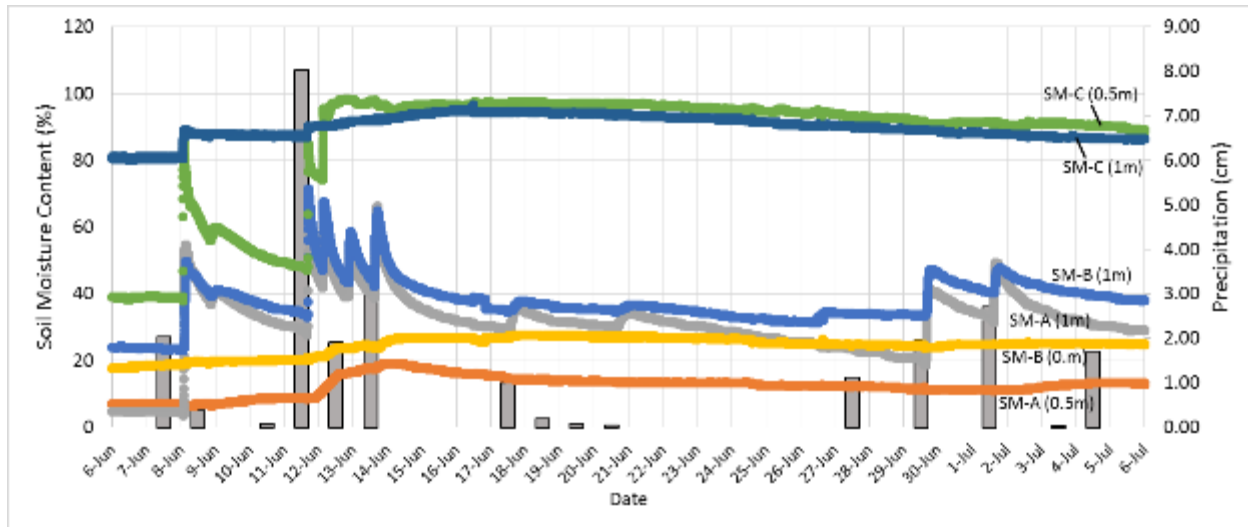


Figure 4-16 Soil moisture readings and precipitation data for the Royal Palm pond bank.

As expected there also exists a close correlation between precipitation and increases in Δh for PT-W1 and PT-Pond locations (Figure 4-17). Typically increases in Δh were only measured following rainfall events $>1\text{cm}$. Furthermore increases in Δh occurred within much shorter time periods for pond stage ($\sim 2\text{ hrs}$) as compared to the bank groundwater stage ($\sim 1\text{ day}$), which created a hydraulic gradient sloping away from the pond. Within approximately one day of the storm event the hydraulic gradient was found to reverse as the pond stage decreased below the bank groundwater stage. It is believed this reversal is explained by two causes, firstly the more rapid decrease in pond elevation due to outflow, evaporative and infiltration processes and secondly the retaining of water within the pond bank via capillary suction. As seen in Fig 12 this gradient appeared to become more pronounced throughout the wet season, as well as when pond elevations rose above the drawdown orifice leading to exponential decreases in pond stage. Conversely a linear decrease in pond elevation was measured at about 1.3cmd^{-1} for both pond and groundwater when stages were below the drawdown orifice, as caused by evaporative and infiltration processes.

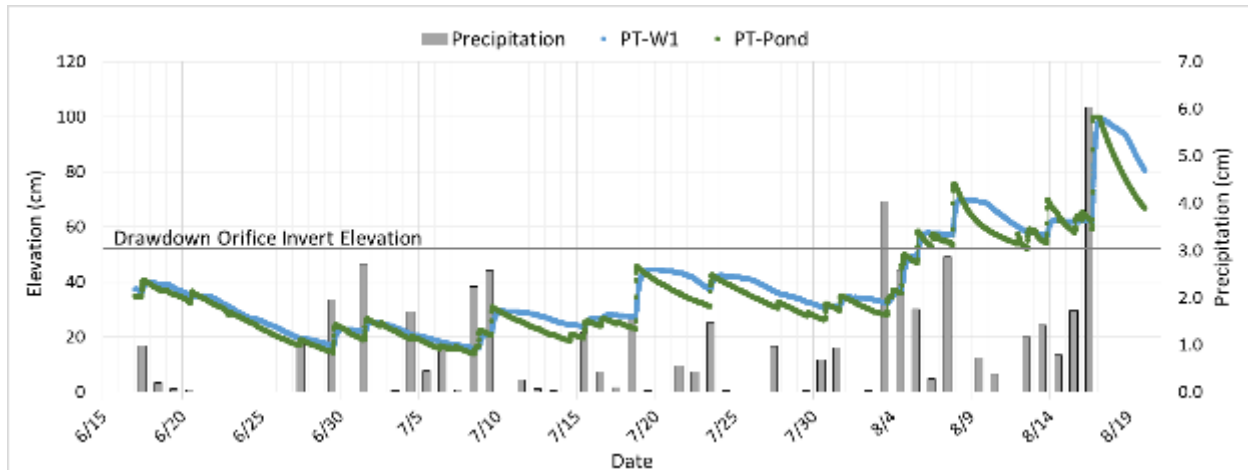


Figure 4-17 Correlation of head differential from pond to PT-W1 measured by pressure transducer (cm) of the pond bank and precipitation data (cm) for the Royal Palm Pond. Water table elevations are in reference to centimeters above the pond outlet drawdown orifice.

Precipitation correlations with elevation measurements within the pond bank (PT-W1 and PT-W2) are presented in Figure 4-18. Measurements of elevations show a similar interaction to pond measurements whereby a negative hydraulic gradient is established shortly following storm events $>1\text{cm}$, followed by a reversal of gradient to positive slope within approximately one day of the storm whereby positive values indicating slope towards the pond and negative values indicated slope away from the pond. PT-W2 displayed slightly more rapid variations in Δh , which may be explained by the pressure transducers closer proximity to the hyporheic zone. The maximum hydraulic gradient measured as 0.024 following the September 17th storm event, the minimum hydraulic gradient of was measured as -0.038 on September 14th following a dry period. Using Darcy's law and a K value measured by core samples in the laboratory of 0.0053 cm s^{-1} , it is expected the bank experiences variable velocity fluctuations in the low range (approximately $< 1\text{ cm d}^{-1}$) during this time frame and GVP measurements should follow an observational methodology, rather than use of the moments method.

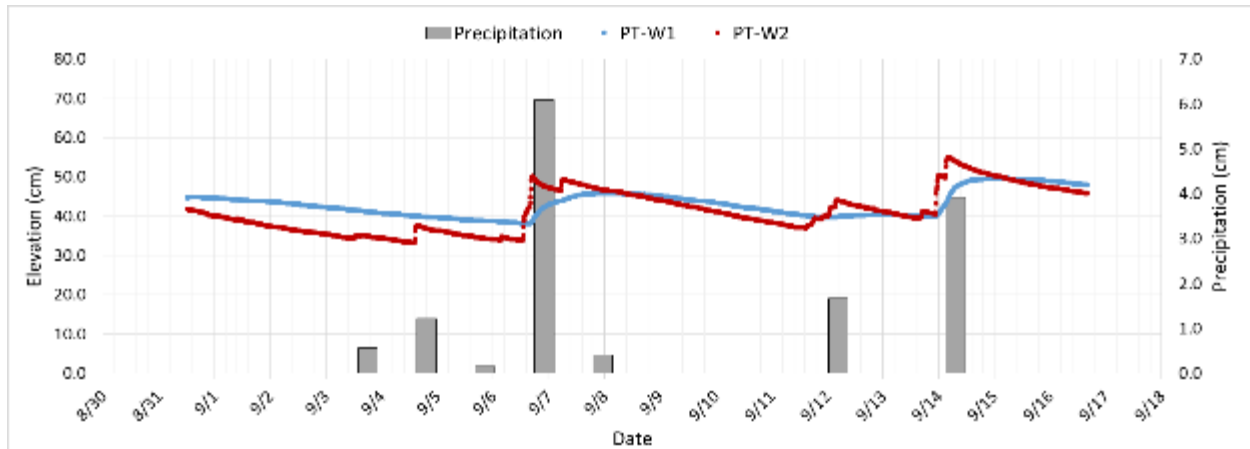


Figure 4-18 Correlation of head differential measured by pressure transducer readings (cm) of the pond bank and precipitation data (cm) for the Royal Palm Pond. Water table elevations are in reference to centimeters above the pond outlet drawdown orifice.

Initial 0.5 second injections were not readily detected by the GVP, indicating a very slow variable velocity regime. Using an observational method, a four second injection was made within the pond bank (Figure 4-19). The GVP detected an initial uniform spreading of the plume which is assumed to be due to molecular diffusion. As depicted in Fig 14 there exists a close correlation of precipitation events and decreases in Δr for the 45° , 90° , 180° , 135° , 225° detectors, followed by an increase in Δr approximately one day later, as especially pronounced by the 180° detector. Figure 4-20 displays the correlation of this phenomena for the 180° detector with hydraulic gradient ($\Delta h/\Delta x$) measurements across PT-W1 and PT-W2. These results indicate that the pulse remains within the general vicinity of the detector during the study period with slight movement away from the 180° detector following storm events and a shifting of velocity approximately one day following the storm event, thus matching hydraulic gradient measurements. Given the small 5.8 cm diameter of the probe, these fluctuations in movement represent very minor values within the range of approximately 1cm, which agrees with theoretical velocity measurements using Darcy's Law. Also of interest are daily fluctuations in Δr by the 90° , 135° , 180° , and 225° detectors. It is expected these fluctuations represent daily

oscillations in molecular diffusion coefficients due to temperature changes, which is most pronounced at the edge of the tracer plume.

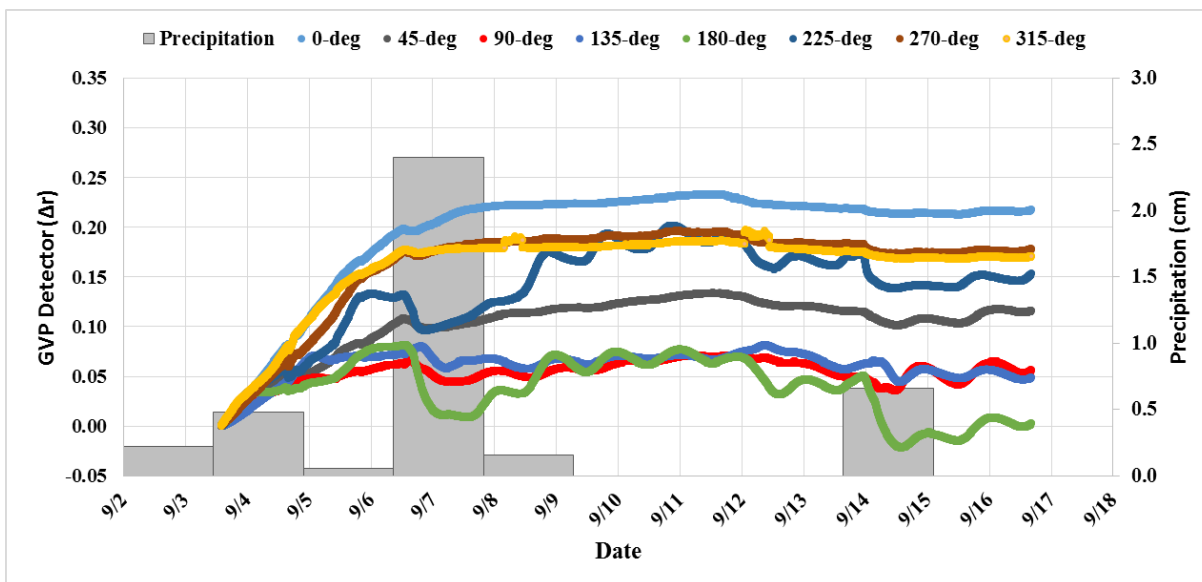


Figure 4-19 GVP measurements following a four second injection (5.2ml) of 15mg l^{-1} NaCl at the Royal Palm pond bank. A general spreading of the tracer is witnessed with close correlation of precipitation events to decreases in Δr by the 135 $^{\circ}$, 180 $^{\circ}$, and 225 $^{\circ}$ detectors, representative of an overall shifting of tracer plume away from these detectors.

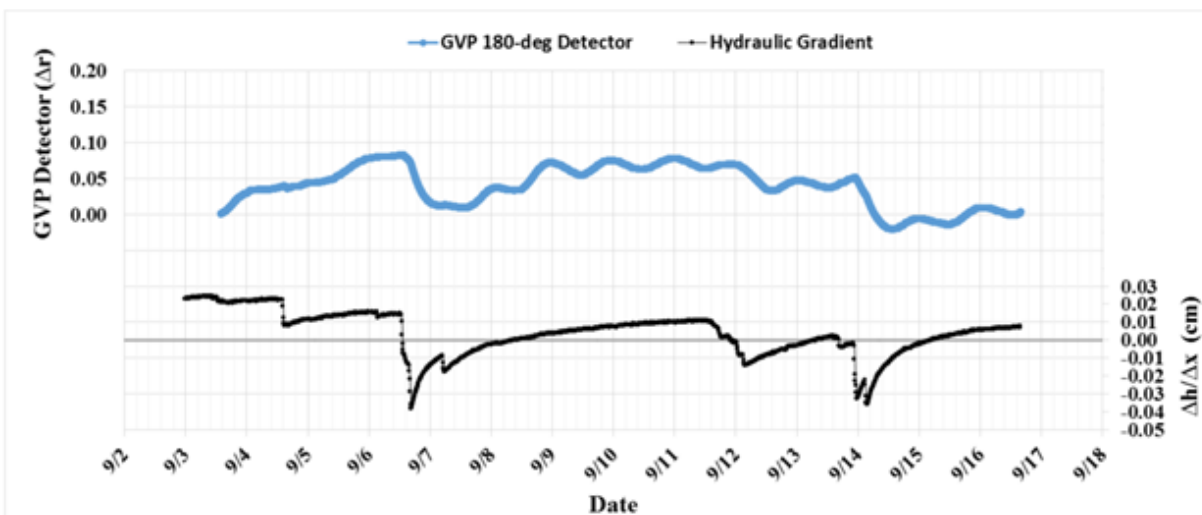


Figure 4-20 Measurement of the tracer plume edge using resistance measurements by the 180 $^{\circ}$ detector correlated with the hydraulic gradient ($\Delta h/\Delta x$). As seen, an increase in $\Delta h/\Delta x$ results in an increase in resistance ratio, relating to the pulse moving away from the pond.

Daily fluctuations in detector readings are believed to be a combined cause of pulse movement and pulse spreading caused by temperature dependent molecular diffusion.

4.5.3 Communications & Sensor Network Design

Integration with remote communications and control expands the ability of the user to collect a variety of real-time data with functionality control of the station. Figure 4-21 displays a communications diagram designed for this study, however a multitude of sensors may be added to expand the versatility of the station including precipitation gauges, soil tensiometers, wind gauge and water quality probes including total organic carbon analyzers, volatile organic carbon analyzers and temperature probes. The station displayed operates using a RavenXTV cellular modem module operating on 3G CDMA networks. Data is transmitted is relayed through a data logger and multiplexer directly to the Raven through RS-232 serial connection and transferred through a SIM card and data plan to static or dynamic IP address(es). Using

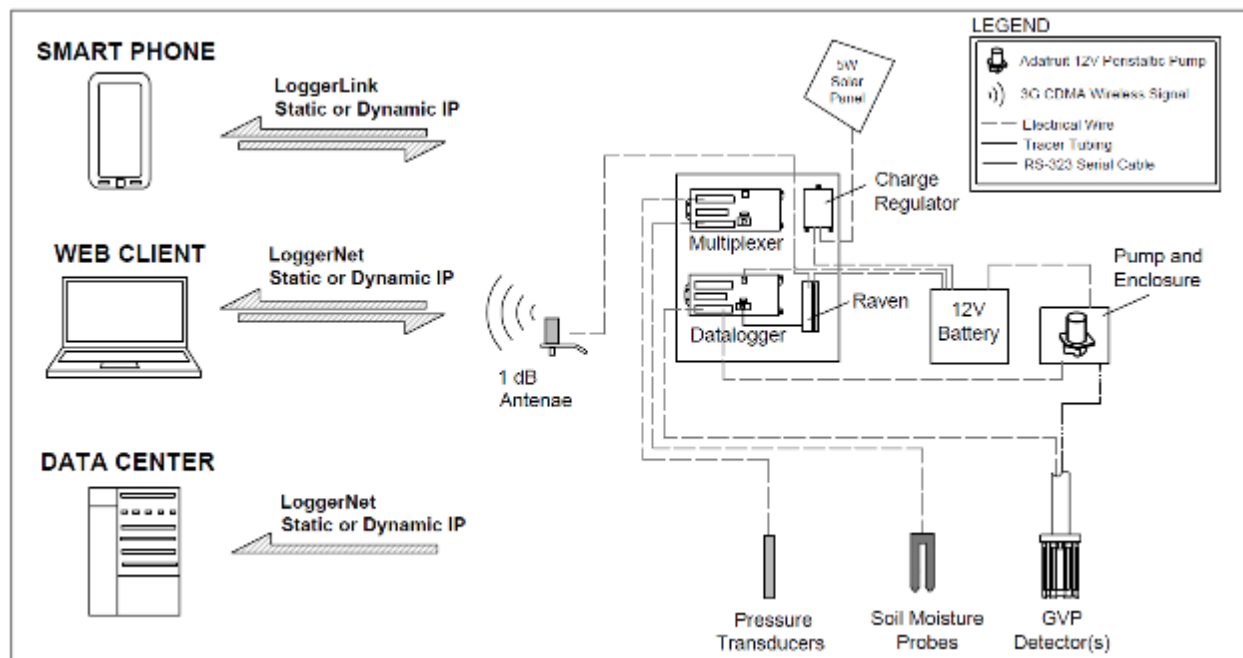


Figure 4-21 GVP communications diagram for a field station including pressure transducers for measurement of upstream and downstream groundwater elevations and soil moisture probes. The station is remotely controllable from anywhere with an internet connection by using a laptop and *LoggerNet* software or 3G network using a smartphone and *LoggerLink* software.

Campbell Scientific LoggerNet for computer applications or LoggerLink for android or iOS operating systems, the station may be fully controlled for; real-time data viewing, data acquisition, station status check or send programs. For GVP measurements in variable flow environments such functionalities enable user control to conduct measurements based on real-time monitoring, ensuring tracer cures have fully developed and will not interfere with additional pulses. Such a station may be expanded to include sub-stations to broaden the spatial range of monitoring, as displayed in Figure 4-22. By operating a station as a master node data may be routed to both collect and send commands to sub-station nodes using antenna and radio transmission frequencies. This could enable the expansion of a network from small to mid-size scales, thus extending the reach of monitoring to the kilometer-scale

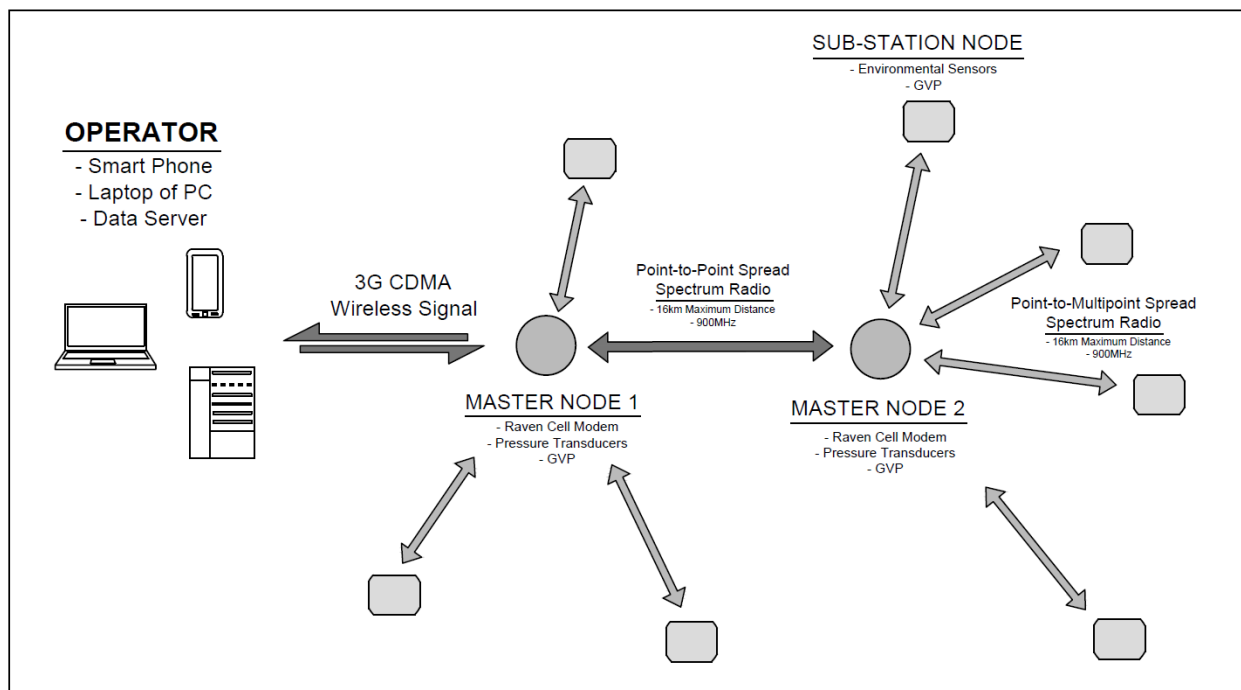


Figure 4-22 GVP sensing network. Two master station nodes communicate via point-to-point spread spectrum radio frequencies, whereas master to substation nodes are operated on point-to-multipoint communications. Final relay is sent via a cell modem and 3G CDMA cellular signals back to the user. All telecommunications are two-way for data retrieval and transmittal.

Such an network enables the user with large spatial analyses of both groundwater velocity and hydraulic conductivity, thus displaying broad scale phenomena such as the directional migration of a pollutant plume to predict future water quality degradation to downstream sources, or the effects of rainfall to the hydraulic characteristics of an aquifer. Coupling of a system to broad range technology such as Electric Resistivity Tomography (ERT) could help to not only verify data but also calibrate ERT equipment.

4.5.4 Tri-Lock Block

Following installation, the Tri-Lock Blocks were found to work effectively in stabilizing the pond banks around the inlet. During the 3-month inspection period following installation several large event storms were recorded occurring in the area including; two (2) storms measuring precipitation amounts $>6.0 \text{ cmd}^{-1}$, six (6) storms measuring $> 1.0 \text{ cmd}^{-1}$, and thirteen (13) storms measuring $>0.5 \text{ cmd}^{-1}$. Figure 4-23 displays Inlet #1 and Figure 4-24 displays Inlet #2, both photographs taken two months following the installation of the blocks.

The majority of the fill soil was found to remain within the interspaces of the blocks, with the exception of the blocks placed at the edges of the retaining wall of inlet #2. In these edge locations the fill soil gradually was washed into the pond leaving gaps between blocks. The loss of fill soil does not appear to negatively impact the structure of the blocks due to their interlocking nature as displayed in Figure 4-25. Where fill soil remained, approximately 40% had signs of vegetative growth within the first two months. In addition the block area perimeter showed signs of vegetation regrowth with minimal overland erosion. Figure 4-26 display vegetative patches developing within the block spaces.



Figure 4-23 Inlet #1 two months following installation of TriLock Blocks, picture taken August 30th, 2014.



Figure 4-24 Inlet #2 two months following installation of TriLock Blocks, picture taken August 30th, 2014.



Figure 4-25 Minor erosion of fill soil between blocks occurring at the headwall edge of Inlet #2. Despite the loss of fill soil the blocks appear to retain their structural integrity.



Figure 4-26 Vegetative regrowth between blocks approximately 2 months following installation.

4.6 Final Remarks

Initial trials of the GVP show promising signs of 2-D velocity magnitude, flow direction, hydraulic conductivity and to some extent lateral dispersion coefficient measurements on the centimeter scale. The GVP was shown to effectively measure the flow velocity using a moments method for non-cohesive sandy soil in a laboratory flume at 25°C from 26 to 459 cm d^{-1} (minimum and maximum values indicating pumping limitations with theoretical detections possible below or above tested ranges). Using a weighted averaging technique directional measurements of flow velocity were shown to be effective to within approximately 14° of expected values with hydraulic conductivity measurements within 1 order of magnitude to core laboratory samples. Dispersion parameters of the salt injection were established across a wide range. Use of the device is beneficial compared to traditional hydraulic gradient methods in establishing small scale spatial variability within aquifers, establishing low-range velocity measurements where pressure transducer resolutions present significant error, and environments with variable directional flow that hydraulic gradient measurements cannot account for. Integration with a wireless field station allowed remote sensing capabilities to the user and real-time retrieval of field data and programmable control of the station. This ability was found to be especially useful for shallow aquifer applications whereby groundwater and surface water interactions dominated, creating variable flow conditions.

Expansion of this technology is discussed into integration into a wireless sensing networks by use of spread spectrum radio frequency antenna operating on point-to-point and point-to-multipoint master and substation nodes. Such methods would broaden the spatial scale of environmental sensing capabilities thus allowing the measurement of large scale aquifer velocity, direction and sub-surface hydraulic conductivity. These methods would be useful in

several groundwater monitoring applications tracking pollutant plumes, analysis of flows through permeable reactive barrier. Furthermore the measurements could help verify and calibrate other broad range sensing technologies such as electrical resistivity tomography. Additionally the technology may be useful in calibration and verification of groundwater models developed with programs such as ModFlow, SVFlux and FEHM.

Testing is limited to sandy non-cohesive shallow depth applications and further work would be merited in use in coarse, cohesive and deep well environments. At present, moment methods for velocity and dispersion calculations are limited to conditions dominated by mechanical dispersion, below which only observational methods are possible. Further work would be useful in establishing new methods for laboratory and field ultralow velocities $<1\text{cm d}^{-1}$ whereby P_e values approach 0.6 and molecular diffusion becomes significant.

4.7 References

- Devlin J. F., G. Tsoflias, M. McGlashan, and P. Schillig, 2009. An inexpensive multilevel array of sensors for direct ground water velocity measurement. *Ground Water Monitoring & Remediation* 29, no. 2, 73-77.
- Devlin J. F., P. C. Schillig, I. Bowen, C. E. Critchley, D. L. Rudolph, N. R. Thomson, G. P. Tsoflias, and J. A. Roberts, 2012. Applications and implications of direct groundwater velocity measurement at the centimetre scale." *Journal of Contaminant Hydrology* 127, no. 1, 3-14.
- Gavaskar, A.R., 1999. Design and construction techniques for permeable reactive barriers. *Journal of Hazardous Waste* 68, 41-71.
- Harbaugh, A.W., E.R. Banta, M.C. Hill, M.G. Macdonald, 2000. MODFLOW-2000, the US Geological Survey modular ground-water models; user guide to modularization concepts and the ground-water flow process. US Geological Survey.

- Hemond F.H., Fechner-Levy E.J., 2000. Chemical Fate and Transport in the Environment. Academic Press, San Diego, California.
- Kerfoot W. B., 1994. Independent verification of heat pulse groundwater flowmeter results through long term observation and tracer tests on superfund sites. *Hydrocarbon Contaminated Soils*, 5, 37-49.
- Kerfoot W. B., V. A. Massard, 1985. Monitoring well influences on direct flowmeter measurements. *Ground Water Monitoring and Remediation*, 5(4), 74-77.
- Labaky W., J. F. Devlin, R. W. Gillham, 2007. Probe for measuring groundwater velocity at the centimeter scale. *Environmental science & technology* 41, no. 24, 8453-8458.
- Labaky W., J. F. Devlin, and R. W. Gillham, 2009. Field comparison of the point velocity probe with other groundwater velocity measurement methods. *Water Resources Research* 45, no. 4.
- Lautz, L.K., and D.I. Siegel, 2006. Modeling surface and ground water mixing in the hyporheic zone using MODFLOW and MT3D. *Advances in Water Resources*, 29, 1618-1633.
- Restrepo, J.I., A.M. Montoya, and J. Obeysekera, 1998. A wetland simulation module for the MODFLOW groundwater model. *Ground Water*, 36(5), 764-770.
- White P. A., 1988. Measurements of ground-water parameters using salt-water injection and surface resistivity. *Ground Water*, 26(2), 179-186.

CHAPTER 5: NUTRIENT FLUX MONITORING USING AUTOSAMPLER WIRELESS NETWORKS

5.1 Introduction

The collection of both spatial and temporal stormwater samples is useful in understanding the fate and transport behavior of aquatic pollutants and nutrient species (Barrenguet et al, 2002). However such samples may be difficult to obtain due to budget constraints, environmental conditions, location or time and labor constraints. Furthermore collection of stormwater grab samples during storm events may pose unwanted environmental hazards to workers. Automated Water Samplers (AWS) have been shown as effective tools for obtaining these often difficult samples in laboratory (Reeburg, W.S., 1967), and stormwater sampling (Hall, et al 1988; Pagotto et al, 2000; Honda et al, 2007). AWS typically operate by pumping water samples through an influent tube and depositing the sample into a bottle(s) located in a storage container. By preprogramming the AWS and including multiple bottles, samples may be collected periodically resulting in temporally spaced data. Following the collection process, a person may then retrieve the samples by hand for further laboratory analysis. A spatial field may be created by installing multiple AWS set to collect from differing locations.

Establishing such a spatial and temporal scheme is useful for pollutant and nutrient analysis and may lead to a better understanding of flux rates as well as fate and transport mechanisms within the pond. This however may be quite costly using current market AWS, especially when applying multiple sampling locations. The goal of this chapter includes creation and field testing of an affordable Wireless Automated Sampling Network (WASN) of auto samplers capable of synchronized sampling at several different spatial locations. For ease of use

the WASN is design for activation by use of cellular text messaging across cellular networks. This chapter will discuss the key points of the WASN including: physical design, network design, remote activation via text messaging, simple electronics, and operability. The WASN provides key benefits to the sampling process by way of the described features.

Science Questions: How effective can an automated water sampler be produced which operates using Arduino microcontrollers, GSM module, XBee transmitters and 3D printed sampling arm? To what degree does dispersion play in the intake tube and what factor of safety needs to be applied to ensure no mixing between samples?

5.1.1 Chapter Objectives

- Develop a cost-effective technique for spatial and temporal collection of water samples during a storm event for identifying the dynamics of nutrient flux entering a wet retention pond.
- Establish the dispersion of sample within intake tubes and develop a factor of safety for flush times.

5.2 Methodology

5.2.1 Location

One wet retention pond was selected for the installation of the WASN located in Gainesville, FL. The pond is located adjacent to a four lane wide road named West Newberry Road. The pond banks are grass vegetated and several trees are located along the banks of the pond. Table 5-1 below presents information regarding the ponds acreage and coordinates.

Table 5-1 Field Site Identification Numbers and Geographic Coordinates.

Pond Site	Pond Size (acre)	Pond ID	Coordinates
Gainesville	0.67	214256-1-72-P001	29.660602°,-82.461857°

5.2.2 Wireless Autosampler Network Development

To make the Automatic Sampling Network function as an integrated unit, a systemic approach is necessary which allows both synchronization of sampling, as well as flexibility to the user based on the often unpredictable nature of precipitation events. In order to accomplish this task, a text activation function was included into the WASN design. By doing so, the user may activate the WASN without limitations on location, assuming a cellular signal is available. Using such a method, the user maintains control on when sampling should begin such as observations of radar precipitation patterns, time of day, or simply convenience. A schematic of the activation communication pathways is displayed below in Figure 5-1.

Cellular transmittal is received by a GSM (*Global System for Mobile Communications*) Cellular Transmitter/Receiver and processed by a built-in microcontroller. From there the signal is passed by direct connection to an Arduino microprocessor with an XBee radio transmitter. The XBee thereby transmits the signal to individual WASN units which are comprised of an XBee receiver and microprocessor. Upon receiving of the activation command, the microprocessor executes a pre-programmed sampling process. By adding multiple WASN units, an integrated network is established. A data plan is required to enable the transmission of texts to the GSM. For this project an AT&T data plan was established. Propagation of this activation command is displayed in Figure 5-1.

An important functionality with regards to establishing nutrient flux concentrations is the collection of time related samples. By integrating the WASN units into one functional, networked, device, all samples are collected at equal time intervals. Using this technique allows direct comparison of samples to show temporal changes in nutrient concentrations. Additionally, pre-programmed time sampling intervals may be altered, allowing the user the ability to change sampling intervals based on the storm events.

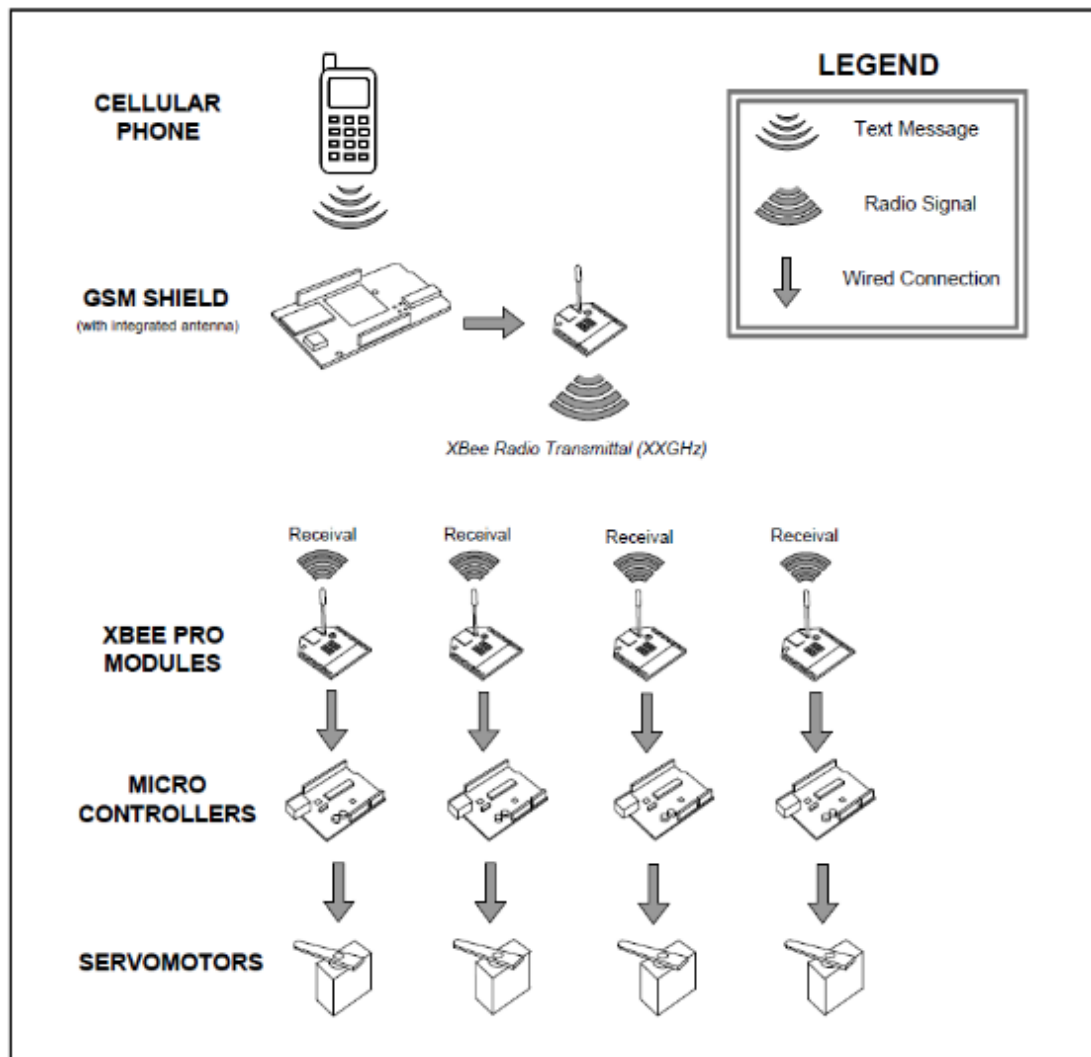


Figure 5-1 Communications diagram for activation of the WASN. Activation may be accomplished anywhere with a working phone signal.

As an example, if a user needed to capture samples throughout an entire storm duration, and a storm of approximately 5 hours was anticipated based on weather patterns or location, then the WASN may be programmed to sample once per 30 minutes. With a total of 12 sampling bottles, this would result in a total sampling duration of six hours allowing for both one pre- and post-storm sample and ten storm samples.

The XBee transmitters are rated at a total radial range of approximately one mile. If the system were to be installed in for maximum coverage than the GSM transmitter would be placed in the center of any other WASN collection units. This would allow a maximum radial range of mile as measured from the GSM. By creating floatable WASN units this technology may be extended to mid-sized lake and coastal applications.

The Autosampler consists of four integrated systems: the XBee radio transmitter/receiver, the microcontroller, the servo rotation arm, and the peristaltic pumps. Upon the GSM passing the activation command forward to the Autosamplers, the XBee radio receivers obtain that signal to confirm that the samplers should in-fact activate. This signal is then transmitted to the microcontroller which then processes the signal to interpret the command. After confirming that the device should activate, the microcontroller signals the servo rotation arm and the two peristaltic pumps to begin the sampling process. Throughout this process, the microcontroller coordinates all of the other systems to allow for efficient operation. A basic circuit connection diagram for the WASN collect unit is depicted in Figure 5-2 below.

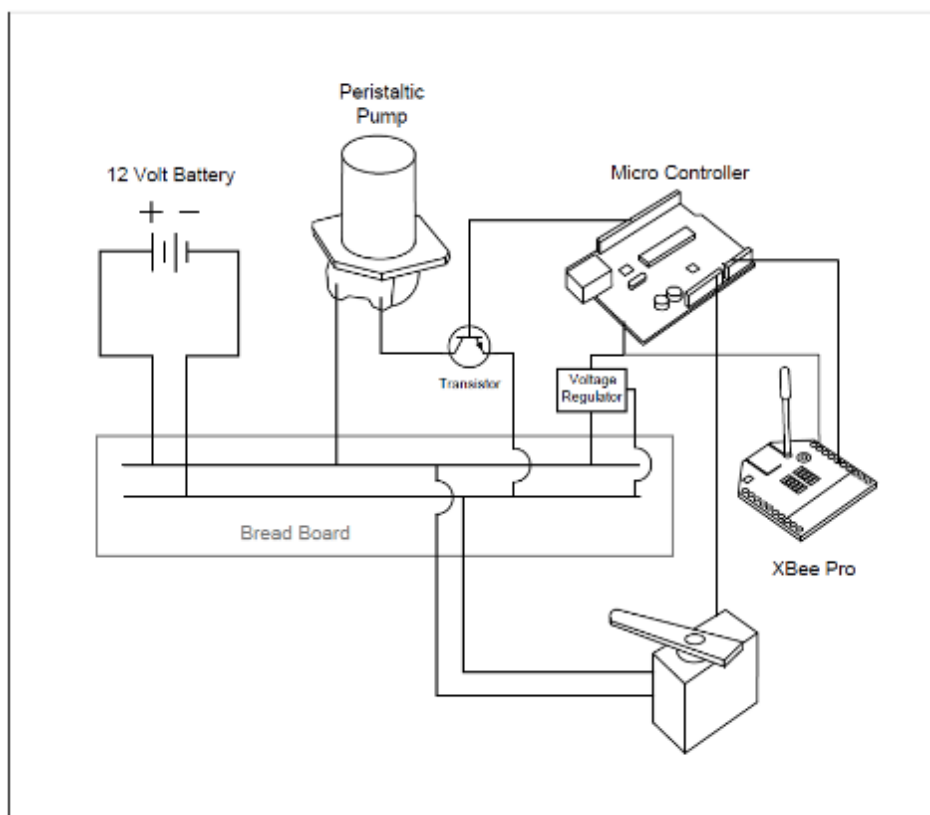


Figure 5-2 Basic circuit diagram for connection of WASN collection units. The microprocessor, XBee, voltage regulator, transistor and bread board are located within the electronics enclosure whereas the battery, peristaltic pumps, and servomotor are located in the main enclosure.

Broadly speaking, the WASN is comprised of two main system components. The first is the GSM enclosure which houses the activation and text processing components including; the GSM module, microprocessor, XBee transmitter, and 12V battery supply. The second is the sampling enclosure which houses the sampling components each comprised of; an XBee, microprocessor, servo motor with sampling arm, sampling tray with bottles, two peristaltic pumps with tubing, and a 12V battery (see Figure 5-2). Each WASN system is comprised of one GSM enclosure and at least one sampling enclosure (one for each sampling location). An itemized description of the individual components is outlined in the following subsections.

A key feature of the WASN is the ability to be remotely activated via text message. An operator can send an SMS text message to the WASN and the system will subsequently be activated. This is done by connecting to the Global System for Mobile Communications (GSM) Network. GSM is a common network used to transmit data between cellular devices around the world. The GSM module that is featured in the WASN was purchased off-the-shelf from Arduino (Figure 5-3). This device connects to an Arduino microcontroller directly by way of vertical mounting. The GSM system is typically operated at a frequency of 1800MHz; this makes for a quick and efficient data transfer speed.

Upon receiving a message from an outside source, the GSM module logs the phone number from which the message originated from. It then parses the incoming message and checks for the activation command. If the activation command is not present in the message, the message is deleted and no action is taken. However, if the command for activation is received, the microcontroller will then instruct the XBee radio transmitter module onboard to broadcast the same activation command to all Autosamplers in the immediate vicinity. This allows for the simultaneous activation of all devices to ensure time accurate water samples.



Figure 5-3 GSM module used for receiving text command and transmittal to XBee Pro.

The enclosure for the Autosampler is a simple Tupperware container to provide easy transportation and basic protection from the outside elements including rain, UV radiation, and moderate wind. The enclosure may not be as strong as other typical AWS units available on the market, but is suitable for most outdoor environments. The advantage of choosing a Tupperware container for the enclosure are that it is affordable, replaceable, and very easy to work with. The cost of this container is approximately \$20 and makes attachment of system components such as the tray easily done with a handheld screwdriver. Due to a build-up of humidity inside the enclosure the electrical components are housed in a small Pelican case located inside the main enclosure. The Pelican case provides an air tight seal to prevent moisture from damaging the electrical components. Additionally, desiccant may be added to the Pelican case to absorb any moisture which may enter.

An important part of the Autosampler is the sampling tray. This component is used to hold all of the sample bottles throughout the duration of the collection process. The sampling tray is designed to collect a total of 12 samples. To achieve this, the system uses two separate peristaltic pumps to simultaneously fill up two concentric semi-circles of sample bottles. These bottles are placed in intervals of 20° aligned with each other along a radial axis with its origin positioned at the center of the servo rotation arm. As seen on the left side of the tray in Figure 5-4 there are two “flush” holes. These holes are used to flush the pumping tubes before every sample is taken. This ensures that each sample is representative of the water in the pond at the time of the sample taken. This is necessary because the time between samples could be anywhere from 5 minutes to 15 or 20 minutes; as the pond water changes, the water in the tubes will remain at constant nutrient levels. Figure 5-5 displays a completed Autosampler tray with attached servo motor and arm.

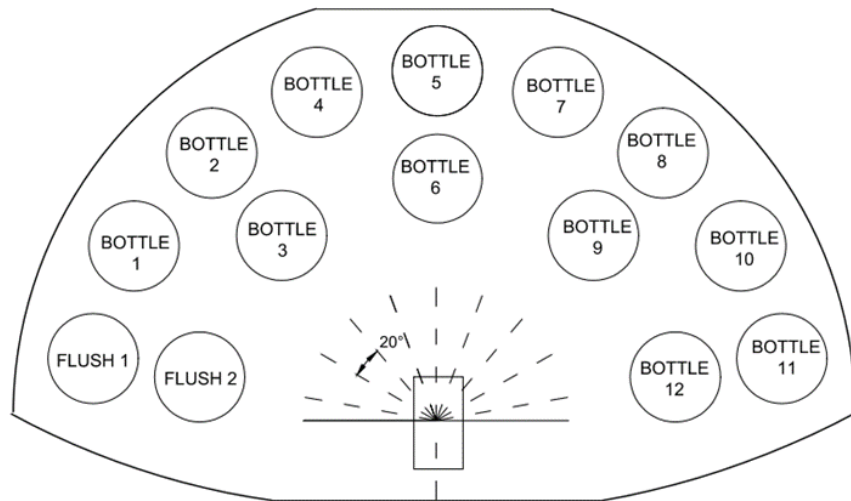


Figure 5-4 AutoCAD layout of the WASN sampling tray. The servo motor sits at the center of the tray and rotates at 20° increments to fill sample bottles via an attached arm. Two flush holes are included to flush the tubes in-between samples.



Figure 5-5 Photograph displaying the WASN sampling tray, servo motor and arm for holding influent tubes. The tray may hold up to 12 bottles (only two are pictured for clarity).

One possible modification of the enclosure and tray is to raise the servo motor to an elevation above the bottles. By doing so the enclosure could be filled with ice which would surround the bottles keeping samples below 4°C. Ice would need to be added prior to activation of the device. Additionally a refrigerant system could be added to the design to keep samples cool, or the WASN collection unit could be placed in a refrigerator for indoor sampling applications.

To achieve the actual sampling of the water, pumps that control the flow of fluids must be used. Since the design of the servo rotation arm is dropping water into the sample bottles, the pumps need to be able to stop the fluid from dropping into the bottles. If any excess water gets into a sample bottle out of turn, that sample can be considered contaminated and would no longer be representative of the nutrients in the pond at the time of actual sampling. Peristaltic pumps have the ability to “grip” the water inside of its tubes. It uses pressure differentials to stop and start the flow of fluids from the pond and into the sample bottles. Below in Figure 5-6, a peristaltic pump is shown.



Figure 5-6 Adafruit high torque peristaltic pumps used for sample collection. Pumps operate on 12volt DC power and are directly powered by a battery.

The XBee radio receiver (Figure 5-7) inside of the Autosampler is designed to transmit and receive radio waves within a 1-mile radius. With a frequency of 2.4GHz, a very large amount of data can be sent in relatively short period of time. The Autosamplers each feature a single XBee module in order to allow for the reception of activation commands from the GSM module. The largest advantage of using XBee modules is that they are low-cost and also low-power. This allows us to deploy a device in the field for an extended period of time with an XBee attached with very little power consumption difference. Another great advantage of using XBees is the fact that they are specifically designed to network with each other. This makes the process of networking the Autosamplers extraordinarily simple.



Figure 5-7 XBee radio transmitter/receiver used for communications between the GSM shield module and the sampling units. Each XBee has a maximum 1-mile transmittal radius.

Inside of the Autosampler device is an array of electronics that allow it to function properly. The core of this component consists of a microcontroller which processes signals from the XBee and controls the peristaltic pumps and servo arm.

After conducting research on common microcontrollers available on the market, the Arduino Uno was chosen to be the best candidate for the Autosampler (Figure 5-8). This device was chosen because of its simplicity and affordability. The Arduino Uno costs only \$25 and has more than enough I/O (*input/output*) pins on-board to suffice for the Autosampler project. This is

the logic board inside of the Autosampler. The Arduino Uno board can only be powered on voltage levels between 7V and 12V. For the field application 12V batteries were used for the Autosampler with the batteries starting out at approximately 12.7V at full charge. To compensate for this, a 12V voltage regulator is used to make sure that the Arduino Uno is not being overpowered. This is a precautionary step to prevent hardware failures. To be able to receive the activation command from the GSM module, the Autosampler needed some way to interact with the radio waves moving through the air.

In order for the Arduino Uno to interact with the pumps, two TIP120 transistors were used. These are rated for high voltages, such as our 12V batteries. The transistors act as switches for the Arduino to have control over the pumps. When the Arduino wants to turn on a pump, it will send a signal to the transistor which will subsequently trigger the pump to activate by providing power.



Figure 5-8 Arduino Uno microprocessor used for programming and control of the WASN collection units and peristaltic pumps.

5.3 Results and Discussion

To test this technology in a field setting a WASN system was installed in a wet retention pond. A total of one (1) GSM module and four (4) WASN collection units were installed as displayed in Figure 5-9 below. The goal of the field application was to test the operability of the system as well as to determine concentrations within the pond during a storm event. WASN units were placed near to the pond bank on stable ground and tubes extended into the pond. Two types of main enclosures were tested, one a small stackable cooler and the other a large Tupperware container. A kayak was required to extend a rope across the width of the pond in order to hold the inlet tubes in place and prevent drifting of the inlet tubes from wind or water movements. The installation took approximately 2 hours to complete.

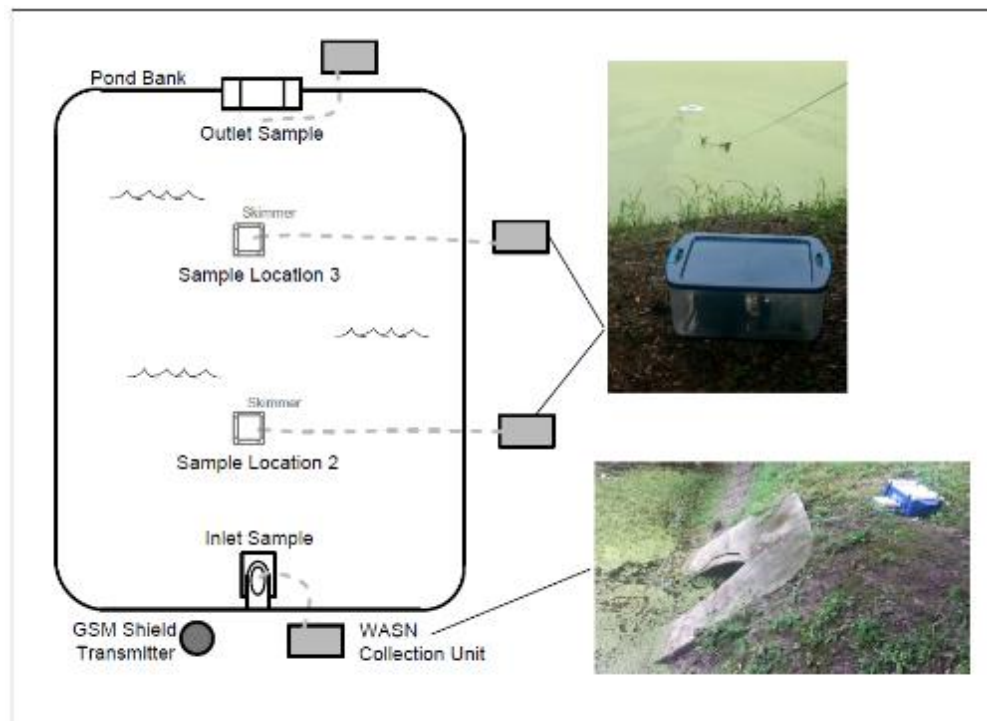


Figure 5-9 Field application of WASN networked system. The GSM unit is comprised of an enclosure case, GSM module, XBee radio transmitter, microprocessor and 12 volt battery; each WASN is comprised of an enclosure case, XBee, microprocessor, sampling tray, one servo motor, two peristaltic pumps, tubing, and 12 volt battery.

Each WAN collection unit was comprised of:

- Main Enclosure & Electronics Pelican Case
- Two (2) Peristaltic Pumps
- Sample Tray with Bottles, Servo and Arm
- Small 12V Battery
- Arduino Uno and XBee Pro

Sample tubes were set at equal distances below the water surface by use of floatable support structures made from 1.5-inch PVC pipes assembled in a square configuration. The tube was attached to the PVC squares and small weights attached to the tube end in order to sink the intake approximately 6-inches below the water surface. An important factor when using tubing is making sure water remaining in the tube from a previous sample is not included in the following sample. Such an oversight would not lead to samples representative of the sampling times. As mentioned earlier a flush between samples is conducted, however dispersion of water within the tube must be considered when applying a flush time.

For this study a tracer test using Rhodamine WT was conducted on a 12-foot section of tubing to establish the degree of spreading which occurs within the during pumping, the results of which are presented in Figure 5-10 below. As seen, a relative large degree of spreading occurs. A MATLAB code using a moments method was used to calculate the longitudinal dispersion coefficient which equaled $0.48 \text{ ft}^2\text{s}^{-1}$. Due to this spreading a safety factor of 3 was applied for field samples.

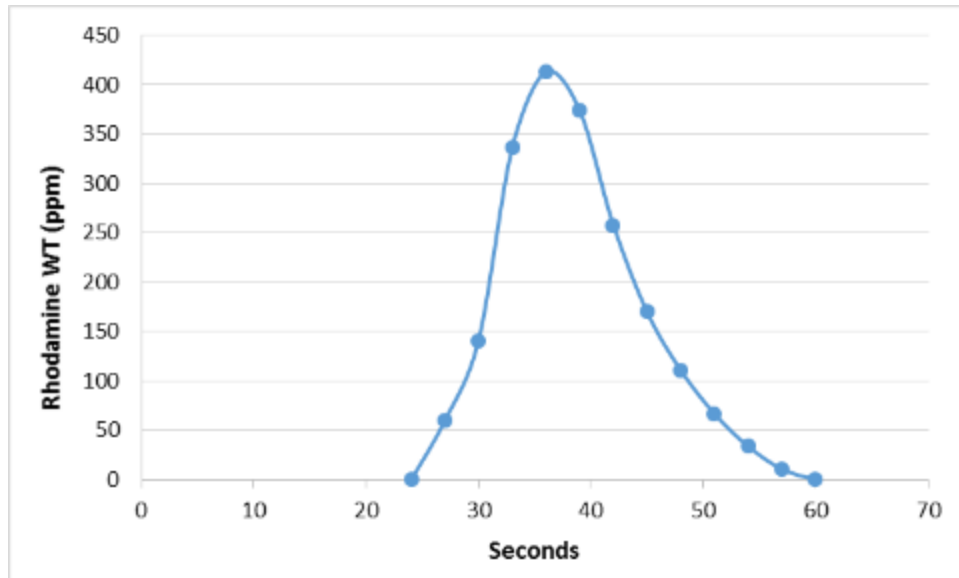


Figure 5-10 Rhodamine WT tracer test conducted for 12' section of tubing to establish the degree of spreading within the intake tubes. As seen a relatively large spread occurs due to frictional forces acting near the walls of the tube.

5.4 Final Remarks

It is concluded that integration of affordable microprocessors including Arduino, XBee and GSM modules combined with 3D printed parts are capable of creating an effectively operating water sampling network. Integration with cellular modem allowed the activation of the networked samplers by use of a text activation command. This allows ease of use for operators and separates the user from the field environment which may minimize hazards to operators. A factor of safety of 2.0 was determined for flush cycles of the tubes in order to prevent any mixing of samples on a temporal scale. The entire system operates effectively in the field at a low cost to users.

5.5 References

Hall, K.J., Anderson, B.C., 1988. The toxicity and chemical composition of urban stormwater runoff. *Journal of Civil Engineering* 15(1) 98-106.

- Honda, M.C., Watanabe, S., 2007. Utility of an automatic water sampler to observe seasonal variability in nutrients and DIC in the northwestern Pacific. *Journal of Oceanography* 63(3) 349-362.
- Kotamaki, N., Thessler, S., Koskiahho, J., Hannukkala, A.O., Huitu, H., Huttula, T., Havento, J., Jarvenpaa, M., 2009. Wireless in-situ sensor network for agriculture and water monitoring on a river basin scale in southern Finland: Evaluation from a data user's perspective. *Sensors* 9, 2862-2883.
- Pagotto, C., Legret, M., Cloirec, P.L., 2000. Comparison of the hydraulic behavior and the quality of highway runoff water according to the type of pavement. *Water Research* 32 (18) 446-4454.
- Reeburgh, W.S., 1967. An improved interstitial water sampler. *Limnology and Oceanography* 12(1) 163-165.
- Rundel, P.W., Graham, E.A., Allen, M.F., Fisher, J.C., Harmon, T.C., 2009. Environmental sensor networks in ecological research. *New Phytologist*, 182(3) 589-607.

CHAPTER 6: MEASURING THE LOW VELOCITY FIELD WITH AN ARC-TYPE AUTOMATIC PULSE TRACER VELOCIMETER IN WETLANDS AND PONDS

6.1 Introduction

Understanding low flow velocities is an important challenge in characterizing the fate and transport of contaminants in wetlands, streams and groundwater environments. By capturing the velocity with the aid of various sensors, progress has been made in calculating drag coefficients, diffusivity, and turbulence (Nepf, 1999) as well as understanding the transport of nutrients (Nixon, 1980; Barko et al, 1991), metals (Orson et al., 1992; Lee et al., 1991), sediments (Philips, 1989), and other contaminants. Furthermore, measuring velocities in heterogeneous field environments such as constructed wetlands with multiple vegetation types helps deepen the knowledge of what affects wind, stage and precipitation may have on the fluid motions of the system, thereby ultimately leading to better system planning, design, and operation to promote pollutant removal efficiency. In many instances these environments are dominated by low range velocities regimes ($<5 \text{ cm}\cdot\text{sec}^{-1}$) characteristic of directionally variable flows and shallow depths ($<15\text{cm}$), making measurements difficult without the use of expensive equipment. The development of techniques that better characterize such local-scale temporal and spatial variations in velocity and direction are particularly valuable.

Currently, few technologies exist capable of measuring the low heterogeneous velocities commonly found in the Stormwater Treatment Areas (STAs). Inexpensive current meters utilizing mechanical propellers have been found useful at higher flow rates, however begin to become infeasible at flows $<6 \text{ cm}\cdot\text{sec}^{-1}$ (Water Survey of Canada, 2006). Acoustic Doppler Velocimeters (ADV) and Acoustic Doppler Current Profilers (ADCP) have found popularity in

wetland applications and have been shown to measure down to 0.02 cmsec^{-1} in the Everglades (Ball, 2000; USGS, 2004; Schaffraneck, 1999; Lee, 1999), however come with inherent drawbacks including depth limitations, single point measurements (ADV), side lobe interference (ADCPs), signal aliasing and high costs ranging from \$10,000 - \$20,000. Specifications on current commercialized velocity meters are presented and summarized in Table 6-1. With few devices available on the market, there exists a need for a cost-effective, reliable alternative for capturing low flow, directionally variable velocities.

Table 6-1 Velocity Meter Specification Comparison

Velocity Meter	Unit	Purchase Cost (US\$)	Min Operating Depth ¹ (cm)	Minimum Velocity (cm/sec)
Pulse Tracer	APTV	\$1,600 - \$6,000 ²	5	0.5
Acoustic Doppler Velocimeters (ADV)	Sontek 3D ARG-ADV	\$10,000	7.5	0.1
	Nortek Vector ADV	\$15,000	20	0.1
	Sontek 2D FlowTracker	\$9,000	7.5	0.1
Acoustic Doppler Current Meters (ADCP)	Sontek ARG-XR 3.0MHz	\$10,000	90	0.1
	Sontek IQ Plus	\$9,000	8	0.1
Laser Doppler Velocimeter (LDV)	PowerSight LDV	\$100,000	<1	0.1
Mechanical	Price AA	\$900	10	6

¹ Represents the approximate minimum depth of water required to capture the velocity at the middle of the water column

² Low range cost represents laboratory APTV, high range cost represents full field-scale APTV network including seven sensors.

In order to capture such flow characteristics, both laboratory flume and field campaign studying the conditions of STAs constructed for phosphorus removal in the northern Everglades were carried out to collect velocity measurements using an ADV to calibrate and validate a new device named the Automatic Pulse Tracer Velocimeter (APTV). The study aimed at capturing centimeter-scale surface water velocities throughout the STA cell to deepen our understanding of correlations among velocity, precipitation, stage, vegetation density, phosphorus removal, and bathymetry. Due to high costs of the ADV, the APTV was designed as a cost-effective and reliable alternative for capturing both low range velocities ($<5\text{cm}\cdot\text{sec}^{-1}$) as well as directional variations commonly found in the heterogeneous nature of the STAs. In this paper a 1st generation lab and field scale Arc-Type APTV was designed, constructed and tested in a hydraulic flume and within one treatment cell (i.e., 3B cell) of the STA 3/4 system. Two types of ADVs, including Sontek Flowtracker ADV and Nortek Vector ADV, were used for calibration and validation of field performance of APTV comparatively to improve the reliability. Additionally the results of lab testing of a 2nd generation APTV with an improved body design and hydrofoil for directional measurements is presented.

6.1.1 Wetland Applications

Wetland and estuary marshes provide an important role for environmental ecosystems. The dense vegetation commonly found in these environments serve to facilitate nutrient cycling, enhance sedimentation of suspended solids, create barriers for storm surge protection, and provide protective habitats for aquatic species. Through hydrodynamic processes, wetlands and marshes have been shown as effective treatment methods in reducing several pollutants from surface waters including phosphorus (Kovacic, 2000), suspended solids (Cliff, 1993) as well as

metals (Scholes, 1998). Several studies have been conducted in these environments to further characterize their fluid motions. Table 6-2 presents a summary of studies used for low velocity measurements in surface water environments.

Table 6-2 Velocity meters used for surface water measurements

Device	Reference	Environment	Velocity Range (cm·sec⁻¹)
Acoustic Doppler Velocimeters (ADV)	Ball and Schaffranek (2000)	Wetland	0.15 to 0.66
	USGS, (2004)	Wetland	0.26 to 2.43
	Schaffranek and Riscassi (2003)	Wetland	0.53 to 0.62
	Lee and Carter (1999)	Wetland	0.2 to 1.2
	Lightbody and Nepf (2006)	Wetland/Estuary	1.2 to 3.7
	Chanson et al. (2008)	Estuary	0 to 28
	Nepf (2000)	Hydraulic Flume	2.2 to 15
	Nepf (1999)	Hydraulic Flume	N/A
	Rehmel (2007)	Streamflow Gauging Stations	13 to 60
Acoustic Doppler Current Meters (ADCP)	Genereux and Slater (1999)	Canal	9 to 40
	USGS (1996)	Sawgrass in Flume	0.61 to 1.42
	Irish et al. (1995)	Tidal Bay	0 to 22
	Vermeyen (2003)	Lake	0.1 to 5
Laser Doppler Velocimeter (LDV)	Nepf (2000)	Hydraulic Flume	2.2 to 15
	Nepf (1999)	Hydraulic Flume	N/A
Propeller Current Meter	Water Survey of Canada (2006)	Creek	6 to 68

Flow velocities in the Florida Everglades have generally been recorded within a 0.0 to 3.5 cm·sec⁻¹ range (Ball and Schaffranek, 2000; Lee and Carter, 1999; Schaffranek and Riscassi, 2003; USGS, 2004), while flow velocities in estuaries have been recorded as ranging from 0 to 28 cm·sec⁻¹ (Lightbody 2006, Chanson 2008). Velocities within wetland and marshes typically

follow a spatially heterogeneous nature which may be explained by several reasons. Lightbody (2006) describes the velocity heterogeneity as being due to both stem-scale dispersive effects caused by velocity depressions just downstream of vegetative stems, as well as depth-scale shear dispersion effects. In addition, with sufficient low velocities and shallow water depths, wind effects may also play a role in velocity direction. Due to these factors, the velocity fields within wetlands and estuaries may vary widely on a temporal, vertical and lateral scale, and any device used to measure them should be able to account for fluctuations in both direction and magnitude. As a result wetlands have been shown to be challenging environments for velocity measurements.

Acoustic Doppler technology has been shown to work effectively in wetlands, however comes with some limitations. Acoustic Doppler meters operate by measuring the Doppler shift produced when an acoustic pulse is reflected off of suspended particles moving in the water. For ADVs, the sampling volume is a “single point” approximately 0.25 cm^3 in volume located about 7cm from the sensor, whereas for ADCPs the sampling volume may measure hundreds of meters in length from the meter. Although the ADV is a robust device capable of high sampling frequencies, several researchers have reported issues with measurements including high levels of noise and spikes in the velocity components (Nikora, 1998; MecLelland, 2000), signal interferences caused by velocity shear and boundary proximity (Chanson, 2007) and disturbances from other Doppler signals or passing boats. Obviously the ADV has a limitation in measuring a single point, making velocity profiling only possible by physically moving the device to height increments. The ADCP is excellent at vertical velocity profiling, however becomes ineffective in shallow waters due to blanking distances and side lobe interferences. The ADCP may also be

used for horizontal profiling, however this application is limited to deeper waters such as canals and lakes.

In addition, some studies have shown difficulties in producing precise measurements for regions of wetlands. In establishing dispersive properties in the Everglades, Huang, et al. (2008) attempted to use an ADV to establish velocity profiles along a 4.8 meter stretch, however concluded the device was insufficient due to lateral changes in the vertical velocity profile. With such heterogeneous natures, clearly single point measurements or single vertical profiles are not sufficient to fully characterize velocity fluid motions in wetlands and estuary environments, and without sufficient data, conclusions can only be made on a broad scale.

6.1.2 Stormwater Pond Applications

The Arc-Type APTV may also be used in a pond or canal setting. For pond configurations with large diameter submerged influent pipes, the APTV may be placed inside of the pipe, allowing measurements of the center of pipe flow. With the velocity known application of known equations to relating velocity to flow given the pipe size, type and roughness may be used to obtain volumetric flow rates. It should be noted that the APTV would only measure the low velocity portion of flow during the beginning and at the tail end of the storm, however in combination with mechanical type meters a full range of velocity could be attained in order to calculate the volumetric loading rate.

Science Questions Can small tracer pulses of NaCl and conductivity detectors be used in a small arc arrangement to measure the velocity of surface water? If so, what velocity range and directional range can an arc-type APTV be capable of measuring? What degree of accuracy is possible compared with high end market devices? Can the device be integrated into a remotely controlled field station capable of wireless automated control?

6.1.3 Chapter Objectives

- Identify velocity and directional ranges of the APTV. Determine any inherent limitations in conducting these measurements.
- Determine the accuracy of velocity and directional measurements as compared to high-end market devices such as acoustic Doppler velocimeters (ADV).
- Determine a total cost for implementation of a wireless controlled automated station in a field setting.

6.2 Methodology

6.2.1 Study Sites

Two study locations were chosen for field application of the Arc-Type APTV. The first site was installed in a constructed wetland located at the headwaters of the Florida Everglades referred to here as “STA 3B”, whereas the second site was located at the inlet to stormwater retention pond within the University of Central Florida campus referred to as the “Arboretum Pond”. Both sites are further described in the following sections.

6.2.2 STA 3B – Everglades, Florida

Although few water quality data exists prior to the 1940s, the Everglades is thought to historically have been an oligotrophic system characteristic of low phosphorus concentrations (Chimney, 2006), as evidenced by low concentrations ($<10 \mu\text{g}\cdot\text{L}^{-1}$) found in some undisturbed locations in the Everglades (Swift, 1987; Scheidt et al., 1989; McCormick et al., 2002), and the low nutrient requirements of native vegetation. During the early 20th century, a large tract of the land south of Lake Okeechobee (2,830 km²) designated the Everglades Agricultural Area (EAA) was drained and developed for agricultural purposes. The run-off from the EAA was routed

through an extensive canal system, which entered at the headwaters of the present day Everglades. Due to human development and agricultural activities such as fertilizer application, high nutrient concentrations became common in the EAA runoff, becoming a major source of anthropogenic phosphorus enrichment of the Everglades ecosystem.

In an effort to reduce nutrient loading to the Everglades, the South Florida Water Management District (SFWMD) constructed a number of Stormwater Treatment Areas (STAs) during the 1990's to intercept and treat run-off from the EAA prior to entering the Everglades. A map displaying the STA locations and surrounding area is displayed in Figure 6-1. The STAs are man-made wetland cells which currently stand as the world's largest constructed wetlands totaling approximately 52,000 acres, STA-3/4 being the largest of these cells totaling over 16,000 acres (SFWMD, 2013). The STAs operate by increasing the deposition rate of phosphorus into the sediment by settling of suspended particles and natural vegetative uptake and decay by vegetation, whereby some of the phosphorus is retained in the dead plant matter. By improving the region's overall hydroperiod and hydropattern, the STAs have been shown to effectively reduce phosphorus loading up to 85% (SFWMD, 2013). However, even with such high removal rates, the STAs are not always capable of meeting low phosphorus discharge concentrations and further understanding of the hydrologic mechanisms within the STA cells are required to enhance their performance.

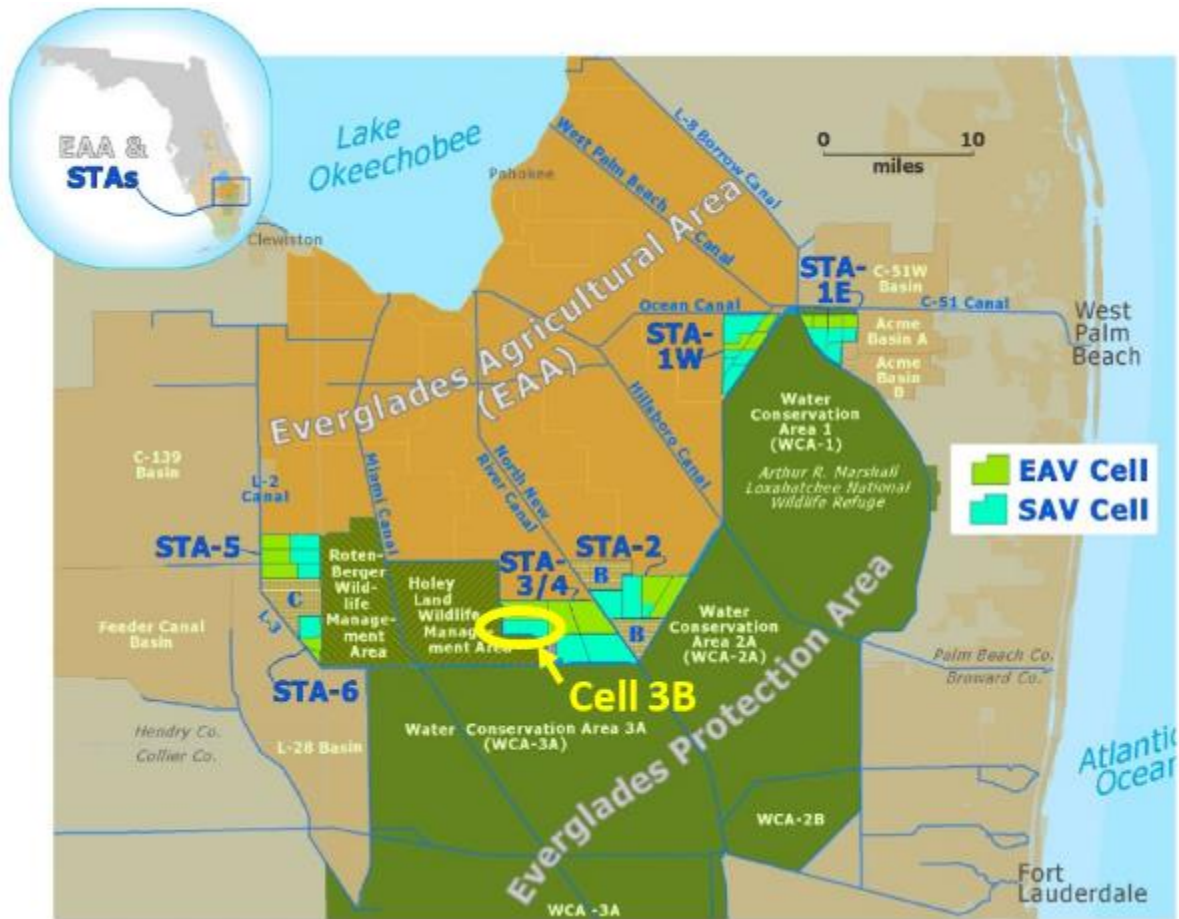


Figure 6-1 Map displaying Lake Okeechobee, the EAA, the STAs and the Northern Everglades. The STAs were strategically located to intercept runoff from the EAA prior to entering the Everglades (Source: SFWMD, 2012).

For this paper, measurements were conducted in Cell 3B of the STA3/4 system as marked in Figure 6-1. Cell 3B, located in the southern portion of STA 3/4, measures approximately 4.8 km in length and 2 km in width. Receiving waters enter the cell through weir structures capable of adjusting the inflow and discharge rates. Two sites were measured within Cell 3B. Both sites were located towards the southern portion of Cell 3B and were spaced approximately 0.23 km away from each other. Prior to construction of the STA, Site 1 contained a farming ditch which resulted in the bathymetry of the site characteristic of relatively deep

waters running in a southern direction. Whereas Site 2 was located in an area more characteristic of the STAs with a relatively dense vegetation and shallower depths. The surrounding vegetation was mainly composed of both submerged aquatic vegetation (SAV) including chara and hydrilla species, as well as emergent aquatic vegetation (EAV) primarily dominated by cattail.

6.2.3 APTV Operation and Laboratory Set-up

The APTV measures flow velocity within the water column by developing a tracer curve from the passing of a small injection of a conductive tracer from an injection port to a set of detectors. For this study, sodium chloride (NaCl) was chosen for the tracer because of the solutions high conductivity and low toxicity. Detections of the tracer pulse were accomplished by building conductivity detectors, comprised of pairs of stripped 18 gauge copper wires set approximately 1.0 cm apart and arranged in an arc pattern. The wires were routed to a *Campbell Scientific* CR1000 data logger whereby a 2.5 volt reverse excitation DC current was applied to the detectors and half bridge measurements taken using fixed 1,000 Ohm resistors. The resistance ratio between the stripped copper wires and the fixed resistors was calculated, normalized, and plotted with time to establish tracer curves. The half bridge measurement frequencies were taken every 0.5 seconds for both the laboratory and field studies to establish tracer curves of suitable resolution.

The APTV support structure was built using 3/4-inch Schedule 40 PVC, whereas the detector support frame was built using a 3D printer. The detector body, detector wires and a portion of the support frame are displayed in Figure 6-2 and Figure 6-3. Five pairs of copper detector wires were arranged in a vertical orientation which formed an arc shape as displayed when viewed from above, Figure 6-4. Each set of copper wires had a 12.7 cm portion stripped and exposed to the water. The injection port was positioned at 7.6 cm horizontal distance away

from each detector and 3.7 cm vertically above the center of the detector. The injection port was composed of a small cylindrical diffuser stone measuring 0.9 cm diameter. The top and vertical surfaces of the diffuser stone were sealed with silicone so the tracer would only inject from the bottom of the stone. A hydrofoil created using a 3D printer was added to the injection port to reduce turbulent eddies from developing behind the diffuser stone during higher velocities regimes ($> 2.0 \text{ cm}\cdot\text{sec}^{-1}$).

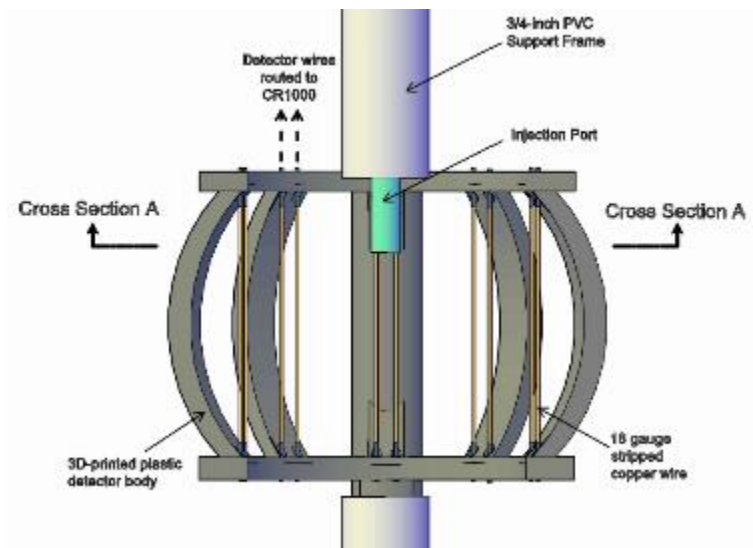


Figure 6-2 Front-view schematic of an APTV cross-type detector. Detectors are comprised of four sets of 18 gauge copper wires (with 5 cm stripped) built upon a 3/4-inch support frame.

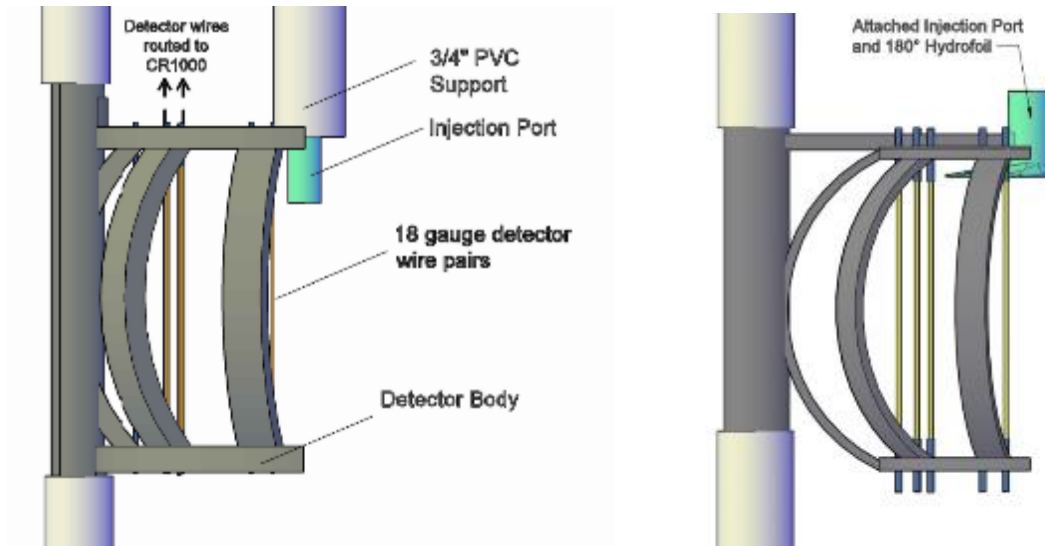


Figure 6-3 Side-view schematic of a 1st generation (left) and 2nd generation (right) APTV arc-type detector. The 2nd generation APTV attaches the injection port physically to the body, includes a slimmer frame, moves the injection port closer to the detectors, and has an improved hydrofoil design.

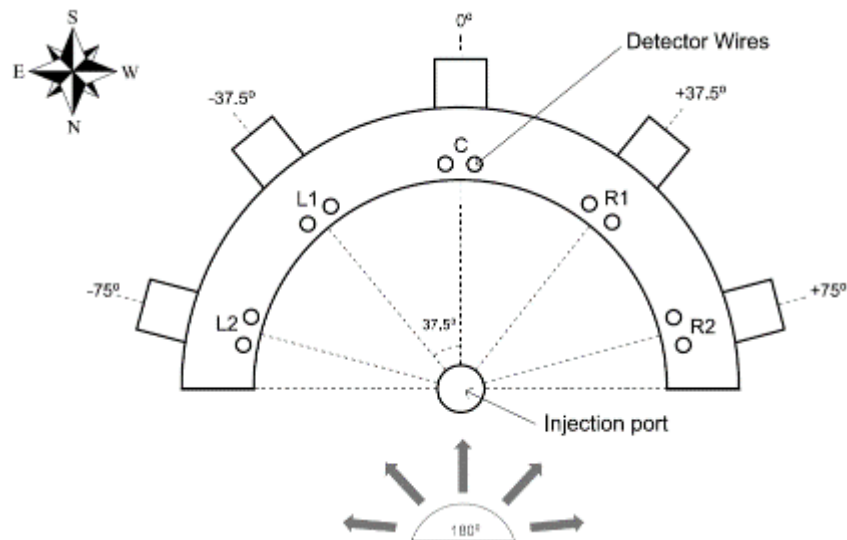


Figure 6-4 Top view (cross section A) of APTV detector body and injection port. Five detector wire pairs are located equidistant from the injection port to allow 180 degree detectable range. The field prototype APTV detector was placed with the center detector wire pair oriented to capture southern flow velocities.

An Engineering Laboratory Design hydraulic flume (model number 14) was used for the laboratory study as displayed in Figure 6-5. The flume measured 4.75 m in length and 0.3 m in width. Water depths recorded in the flume varied from 30.5 cm to 38.0 cm depending on the velocity regime. A stainless steel metal diffuser grid containing 0.30 cm diameter holes was located at the beginning of the flume to dissipate flows entering the flume.

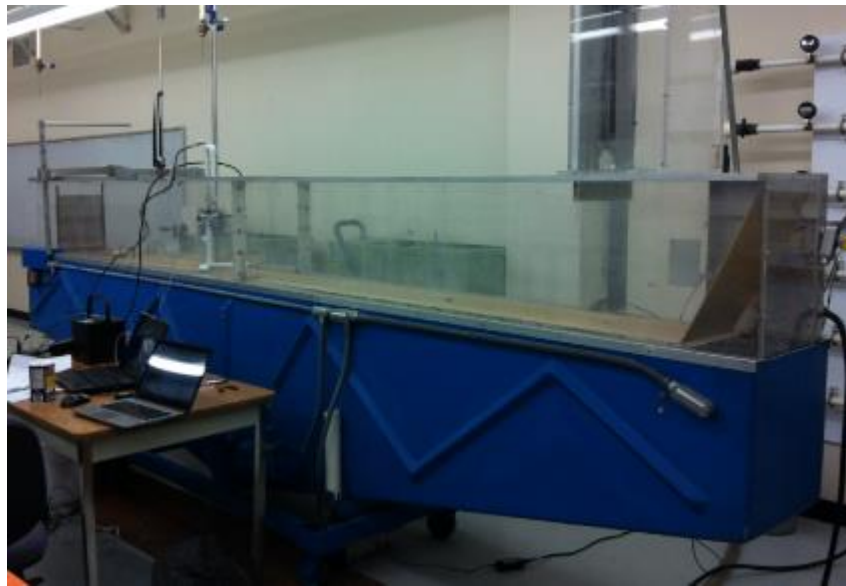


Figure 6-5 Picture of the Engineering Laboratory Design hydraulic flume used for the laboratory study. An APTV detector and Flow Tracker ADV are seen setup approximately three fourths from the beginning of the flume.

Injectors were made using an *Adafruit* peristaltic liquid pump. The pump was powered by a 12V battery and controlled by the data logger by use of programmable 2.5V output signals and a TIP31 transistor. All injections were programmed for a two second injection, which resulted in a tracer injection volume of approximately 1.6 ml.

For calibration testing, direct velocity comparisons were conducted between the APTV and a Sontek Flow Tracker ADV at eight velocity increments, the lowest recording 0.48 cmsec^{-1} and the highest recording $5.3 \text{ cm}\cdot\text{sec}^{-1}$. In order to resolve variations due to turbulence and

velocity shear within the flume, both the APTV and Flow Tracker ADV continuously recorded velocity measurements for 15 minute durations for each velocity increment. These data were then averaged to one velocity measurement per velocity increment. A one minute settling time prior to recording was allowed for flume velocities to equalize between velocity adjustments. Flow Tracker velocities were measured using a 10Hz sampling frequency and 60 second duration time per velocity measurement, conducted every two minutes. The APTV was programmed to inject and measure tracer pulses once per minute. Resistance ratios were continuously measured at a 0.5 sec sampling rate in order to produce tracer curves with sufficient resolution.

During calibration, ADV sampling volumes were located 17.8 cm upstream of the APTV sampling volume. Both ADV and APTV sampling volumes were positioned in the middle of the flume 25.4 cm above the flume bottom. The Flow Tracker ADV was positioned in a side-facing orientation so as to not create interference with the APTV measurements.

6.2.4 APTV Velocity Calculations

A method termed the Δt_{peak} method was developed to obtain velocity components from the tracer curve. The Δt_{peak} method utilizes the time for the peak of the tracer curve to travel from the injection port to the detectors. Velocity measurements were calculated by dividing the horizontal distance of the injection port to the detectors (7.6 cm) by the time from injection to the time of peak detection of the tracer curve (Δt_{peak}). Tracer pulses were injected in a downward orientation, and as a result, create a pulse delay in detection due to the tracer pulse needing to accelerate and equalize with the horizontal velocity. Using a regression analysis, a calibrated APTV velocity equation was generated to account for this delay.

In order to cancel out weak tracer curve pulses from the velocity calculations, a signal-to-noise ratio (SNR) was applied for all APTV velocity measurements based on the strength of the tracer curve. Any pulses which did not register above the SNR were not included in velocity calculations. An example of a pulse tracer curve with SNR ratio setting is displayed in Figure 6-6.

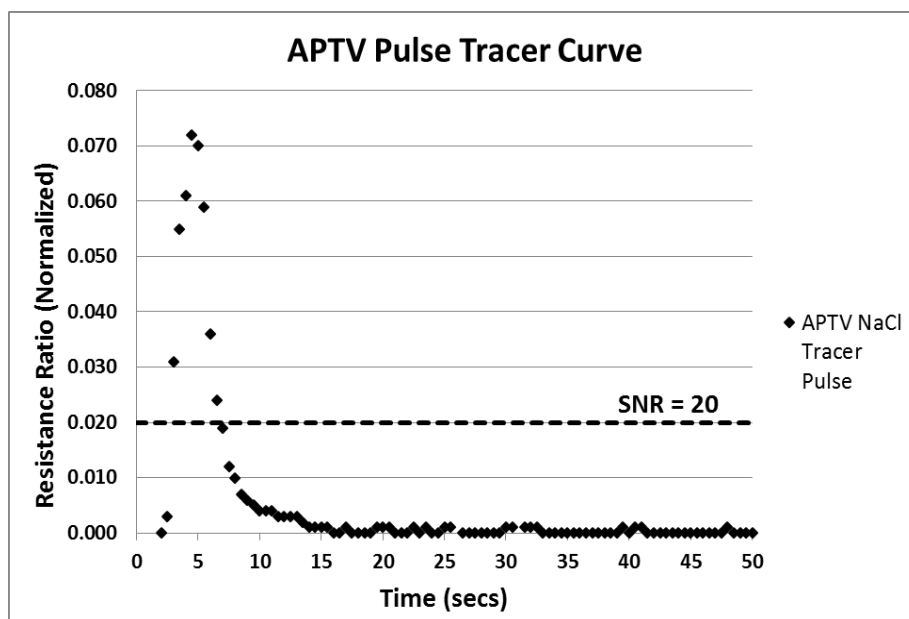


Figure 6-6 Example pulse tracer response curve generated by the APTV in the hydraulic flume. Sodium chloride tracer used at 15gL^{-1} concentration. Injection of the pulse occurred at zero seconds. The correlating peak detection time (Δt_{peak}) was measured at 4.5 seconds.

6.2.5 APTV Field Measurements

An APTV field station was constructed to test the versatility and operation of the device in a wetland condition. The APTV field station was comprised of a wooden support structure, electronics enclosure box, CR1000 data logger, peristaltic pump housing box, multiplexer, Raven XTV cell modem with antenna, 12 volt battery, peristaltic pumps, tracer reservoir with salt water, small solar panel, and a portable satellite APTV cross-detector placed 18 cm directly downstream (south) of the ADV sampling volume. An electronic enclosure box was used to

protect the data logger and cell modem. Data was transmitted via a 3G CDMA cellular network with static IP address back to a centralized computer server for data storage and processing. The Raven was directly connected to the CR1000 data logger by use of a RS-232 serial port and a 1dBd omni-directional antenna was utilized for data transmittal. The use of the multiplexer enables multiple sensors to be connected to one APTV station, thus spatially forming a sensor network. Due to the remote location of the project site, the field station was designed for autonomous control from a home computer. A photograph of the APTV field station and system communications diagram is displayed in Figure 6-7.

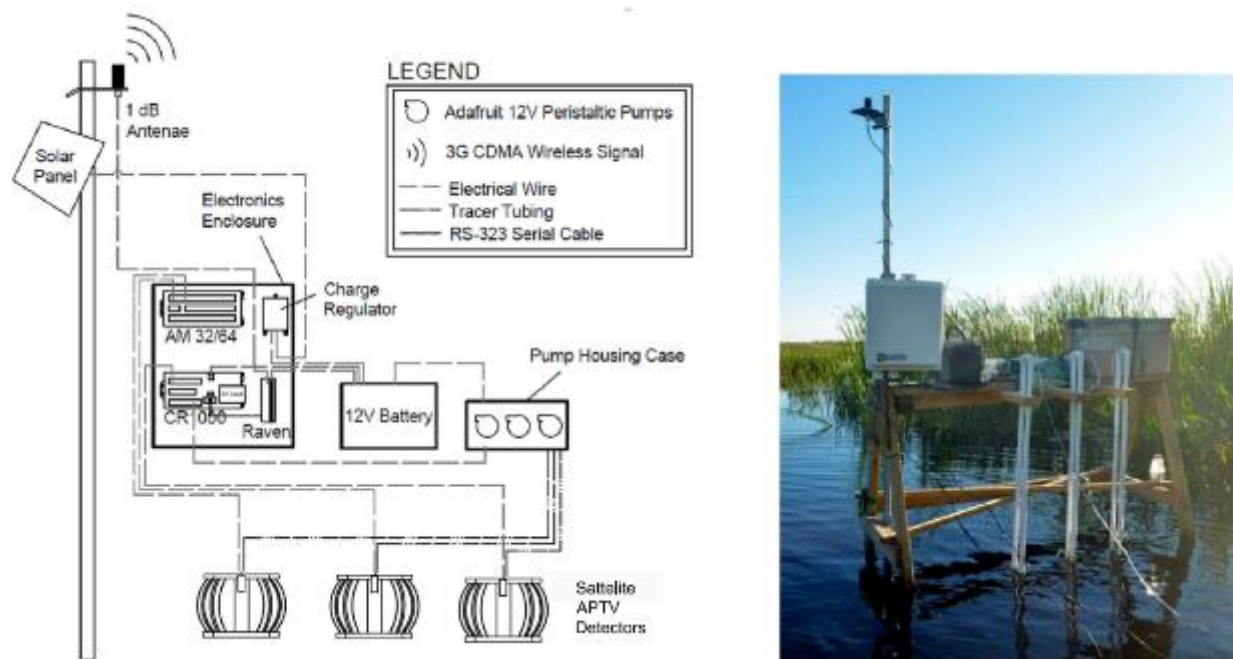


Figure 6-7 APTV field station system communications diagram and photograph displaying support structure, tracer reservoir, electronics enclosure box, cell modem antennae, profiling detectors, 12V battery and pump enclosure box. An additional portable “satellite” detector was set up approximately 4 meters from the station next to a Vector ADV (*not pictured*). Picture was taken at Site 1 facing south.

For Site 1 measurements were conducted for a 3-day duration beginning October 6th and ending October 9th 2013. For Site 2 a 3-day duration beginning October 12th to October 14th was

conducted. Vector ADV velocity measurements were made using an 8Hz sampling frequency with 10 samples being collected and averaged per measurement. Three measurements were taken per hour and averaged to hourly velocity measurements. Both the APTV C detector and the Vector ADV X-axis probe were orientated to the south. Prior to a sampling event a 30 second settling duration occurred to allow measurements of the data logger to equalize. Following this the APTV was programmed to inject 15 mgL⁻¹ NaCl pulses every 30 seconds for two and a half minutes, resulting in a maximum of five possible velocity measurements. The velocity measurements were then averaged to one measurement for the sampling event in order to resolve variations in turbulence.

The directional components for each velocity was calculated by taking the weighted average of the number of pulses detected above the SNR per detector wire pair. The detector wire pairs were designated as L2, L1, C, R1, and R2 pertaining to the -75°, -37.5°, 0°, +37.5°, and 75° offset from the center line of the detector body. For field measurements, the center line of the detector body was aligned in a southern orientation, thus measurements made by the C detector were representative of southern flow while measurements made by the R2 detector are representative of 75° west of the southern axis. The equation for calculating the APTV is given as follows:

$$\text{Direction}^{(0)} = \frac{\sum_{L2=0}^{L2} (-75^{\circ}) + \sum_{L1=0}^{L1} (-37.5^{\circ}) + \sum_{C=0}^C (0^{\circ}) + \sum_{R1=0}^{R1} (37.5^{\circ}) + \sum_{R2=0}^{R2} (75^{\circ})}{n} \quad (22)$$

Where:

- L2 = number of pulses detected above SNR by L2 detector
- L1 = number of pulses detected above SNR by L1 detector
- C = number of pulses detected above SNR by C detector
- R1 = number of pulses detected above SNR by R1 detector
- R2 = number of pulses detected above SNR by R2 detector

n = total number of pulses detected by all detectors

For example, if only the C (0°) detector measured pulses the corresponding direction would calculate as 0° , representative of direct southern flow, whereas if only the R1 ($+37.5^\circ$) detector measured pulses then the direction calculated as 37.5° west of the southern axis. However, if only one pulse was detected on the C detector and four pulses were measured on the R1 detector, the direction is more weighted towards the R1 detector resulting in a calculation of 31° west of the southern axis.

6.3 Results and Discussion

6.3.1 Laboratory Performance

For the laboratory studies of the 2nd Generation APTV pulses were detected from a range of 0.27 to 4.88 cm·sec⁻¹, the latter upper limit representing the maximum velocity attainable in the flume, however peak signals were lowered at this velocity range, indicating that the 4.88 measurements were approaching the maximum detection limit. The APTV showed higher tracer pulse signals and detections for mid-range velocity measurements (0.5 to 4.5 cm·sec⁻¹) whereas weaker pulse strengths were recorded for the lower (<0.5 cmsec⁻¹) and higher (>4.5 cm·sec⁻¹) velocity ranges. This can be explained by the relatively smaller area the tracer pulse contacts on the wires during high and low range flows. During high range flows the tracer has less time to vertically spread, whereas during low range flows the tracer bulk sinks below the bottom of the detector.

A statistical summary of the laboratory testing for the APTV and ADV is presented in Table 1 and 2, respectively. Of the 15 pulses injected per velocity increment, 100% of the pulses

were detected for the 0.73 to 4.43 cmsec⁻¹ range whereas 93% were detected for the 0.27 and 0.36 cmsec⁻¹ velocity increment and 87% detection was recorded at the 4.88 cmsec⁻¹. This indicates that the operational range of the design is approximately 0.5 to 4.5 cmsec⁻¹. The standard deviation is of interest to determine the degree in variation of velocity measurements occurring due to turbulent fluctuations within the flume.

Table 6-3 Statistical summary of velocity magnitude measurements made by the 2nd Generation APTV.

Average Velocity (cms ⁻¹)	APTV Measurements				ADV Measurements		
	Range	Variance	Standard Deviation	Percent Detection	Range	Variance	Standard Deviation
0.27	0.22	0.00	0.06	93%	0.20	0.00	0.06
0.49	0.54	0.02	0.14	93%	0.30	0.01	0.10
0.73	1.31	0.05	0.23	100%	0.20	0.00	0.05
1.01	1.31	0.16	0.40	100%	0.20	0.01	0.07
1.52	0.86	0.10	0.32	100%	0.30	0.01	0.09
2.02	0.95	0.14	0.37	100%	0.20	0.01	0.09
2.71	0.88	0.20	0.45	100%	0.30	0.01	0.10
3.67	1.52	0.39	0.63	100%	0.50	0.02	0.13
4.43	4.52	1.58	1.26	100%	0.60	0.03	0.18
4.88	4.52	3.84	1.96	87%	1.00	0.09	0.30

As seen in Figure 6-8 there is a clear increase in the standard deviation with increasing velocity. This phenomena is expected as the Reynolds number and degree of turbulence should increase with increasing velocity. Furthermore the APTV was found to measure approximately 50% higher standard deviations for velocity ranges <4.0 cmsec⁻¹, however approximately 100% higher standard deviations when the velocity range. This is explained by the nature of the calibration equation which adjusts exponentially more at higher ranges.

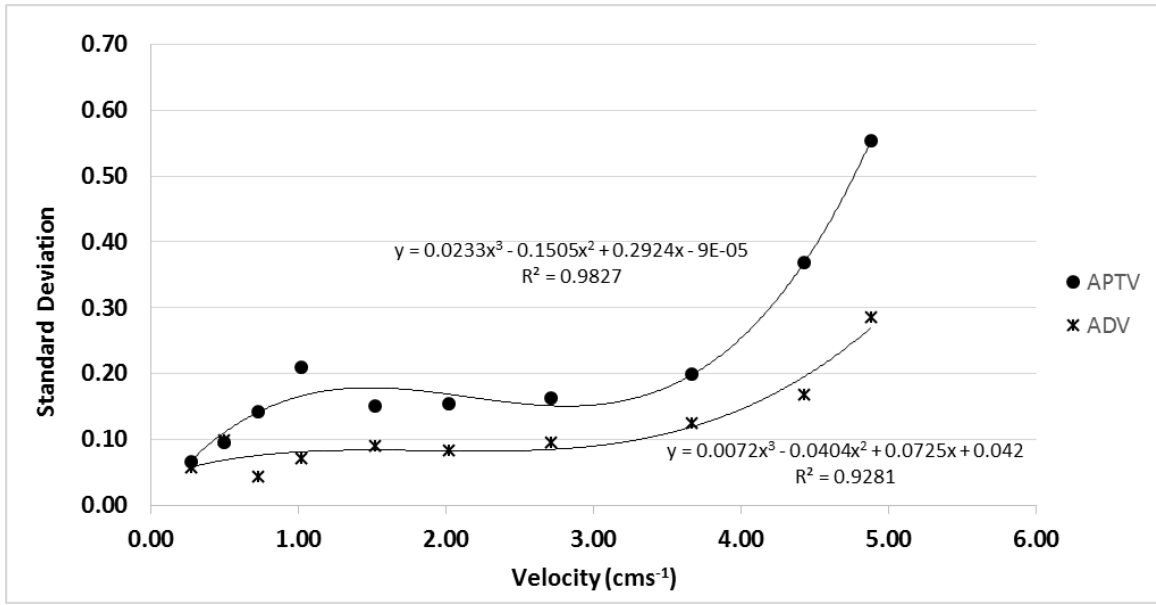


Figure 6-8 Standard deviation values for APTV vs ADV measurements in the flume. The effects of the calibration equation on the standard deviation is seen to increase at velocities $>4.5\text{cm}\cdot\text{s}^{-1}$.

6.3.2 Velocity Comparison

In order to account for the acceleration delay caused by the pulse, an empirical approach was applied to develop calibration equations based on comparative measurements with a Sontek Flow Tracker ADV. Plotting the APTV velocity measurements against Flow Tracker ADV velocities displays a clear division between low velocity ranges ($0 - 1.4 \text{ cm}\cdot\text{sec}^{-1}$) and higher velocity ranges ($> 1.4 \text{ cm}\cdot\text{sec}^{-1}$) is seen for the 1st generation APTV as displayed graphically in Figure 6-9. The 2nd generation APTV shows a clear power function throughout the velocity increments due to the closer proximity of the injection port to the detectors, Figure 6-10. During low velocities the delay in the pulse is largely dampened out by relatively longer travel times. As a result the APTV and ADV measurements approach unity thus creating a linear relation whereby the APTV velocity approximately equals the ADV velocity. However as the velocity increases above $1.4 \text{ cm}\cdot\text{sec}^{-1}$ the delay effect becomes more prominent due to shorter travel times and a power relation develops. By applying a piece-wise regression, with a linear regression in

the lower velocity range and a power regression in the higher velocity range, two calibration equations were formed. The regressions displayed relatively good fits with R-squared values of 0.9238 for the lower linear range and 0.9435 for the higher power range. The calibration equations generated for the two ranges are presented below.

$$APTV_{CAL} = 0.9298(APTV_{MEASURED}) - 0.0368 \quad 1^{st} \text{ Gen Velocities} < 1.4 \text{ cm}\cdot\text{sec}^{-1} \quad (23)$$

$$APTV_{CAL} = 0.5272(APTV_{MEASURED})^{3.5354} \quad 1^{st} \text{ Gen Velocities} > 1.4 \text{ cm}\cdot\text{sec}^{-1} \quad (24)$$

$$APTV_{CAL} = 1.0719(APTV_{MEASURED})^{1.6664} \quad 2^{nd} \text{ Gen All Velocities} \quad (25)$$

Where:

$APTV_{MEASURED}$ = APTV velocity from Δt_{PEAK} method

$APTV_{CAL}$ = calibrated APTV velocity

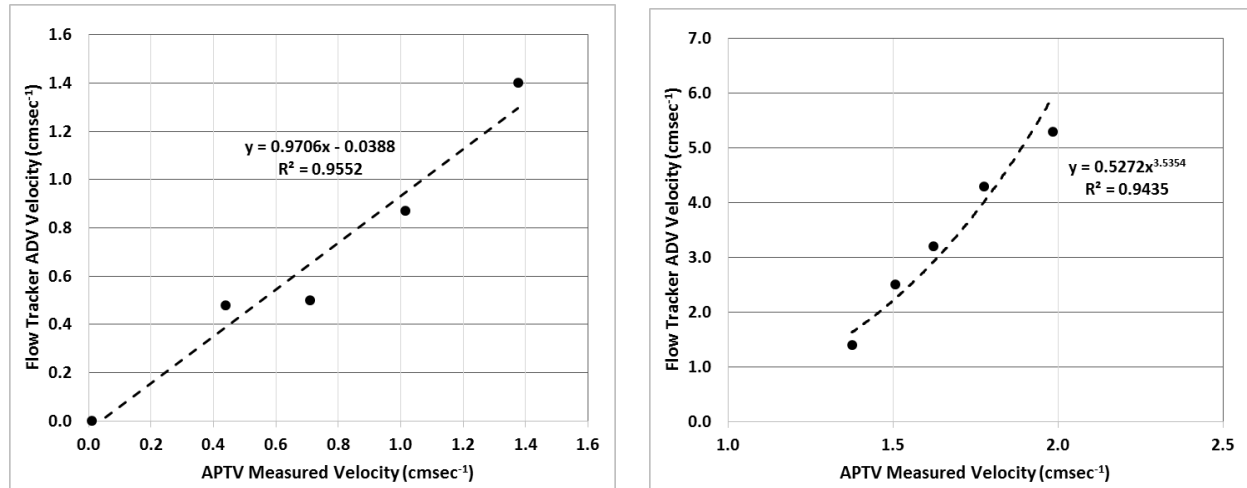


Figure 6-9 Calibration curve developed from direct comparison of APTV raw velocity low regime (left) and high regime (right) data using Δt_{peak} method to Sontek Flow Tracker ADV velocity data for the 1st generation APTV.

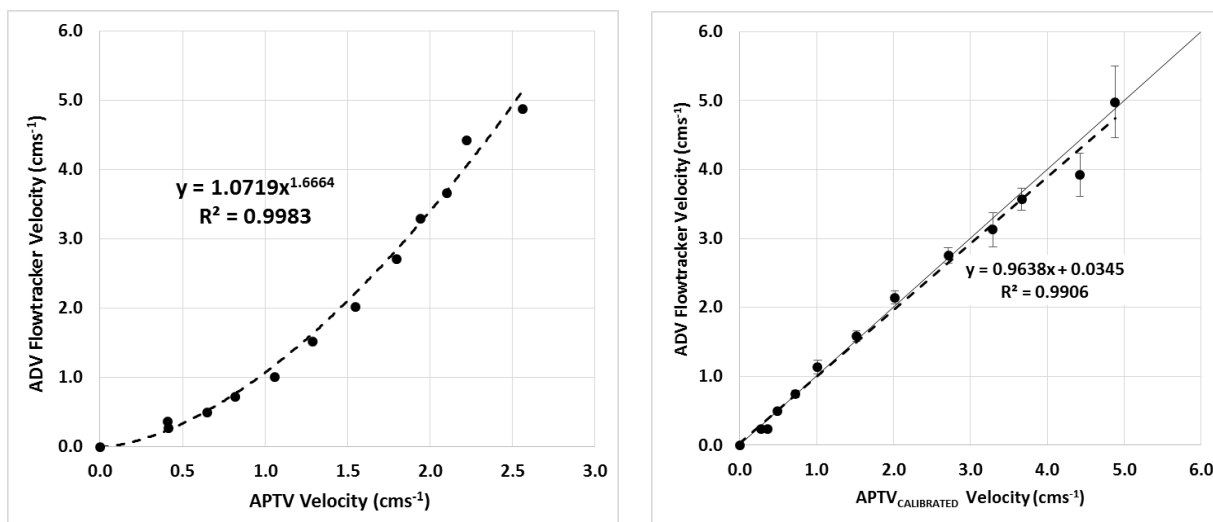


Figure 6-10 Calibration curve developed from direct comparison of APTV raw velocity data using Δt_{peak} method to Sontek Flow Tracker ADV velocity data for the 2nd generation APTV (left) and correlation between APTV calibrated and ADV velocity measurements.

It is important to note how the distance of the injection port effects the calibration equation. If the distance of an injection port is increased the linear range will extend to higher velocities. Conversely if the injection port is moved closer to the detectors the linear range will decrease until a power relationship solely exists as seen with the 2nd generation APTV (Figure 6-10a).

Also of importance is determining how many pulses should be averaged per velocity measurement to attain sufficient accuracy for the specific application setting of the device. Figure 6-11 establishes the relationship between 2nd Generation APTV and ADV velocity measurements for 3, 5, 10 and 15 pulse averaging amounts. As seen there is a clear drop in correlation ($R\text{-squared} = 0.9893$ to 0.9465 for 15 to 3 pulses) as the number of pulses per velocity measurement decreases. As such, at least 15 pulses per velocity measurement is recommended in order to attain higher accuracy for steady flow conditions, however this may not always be possible depending on environmental conditions.

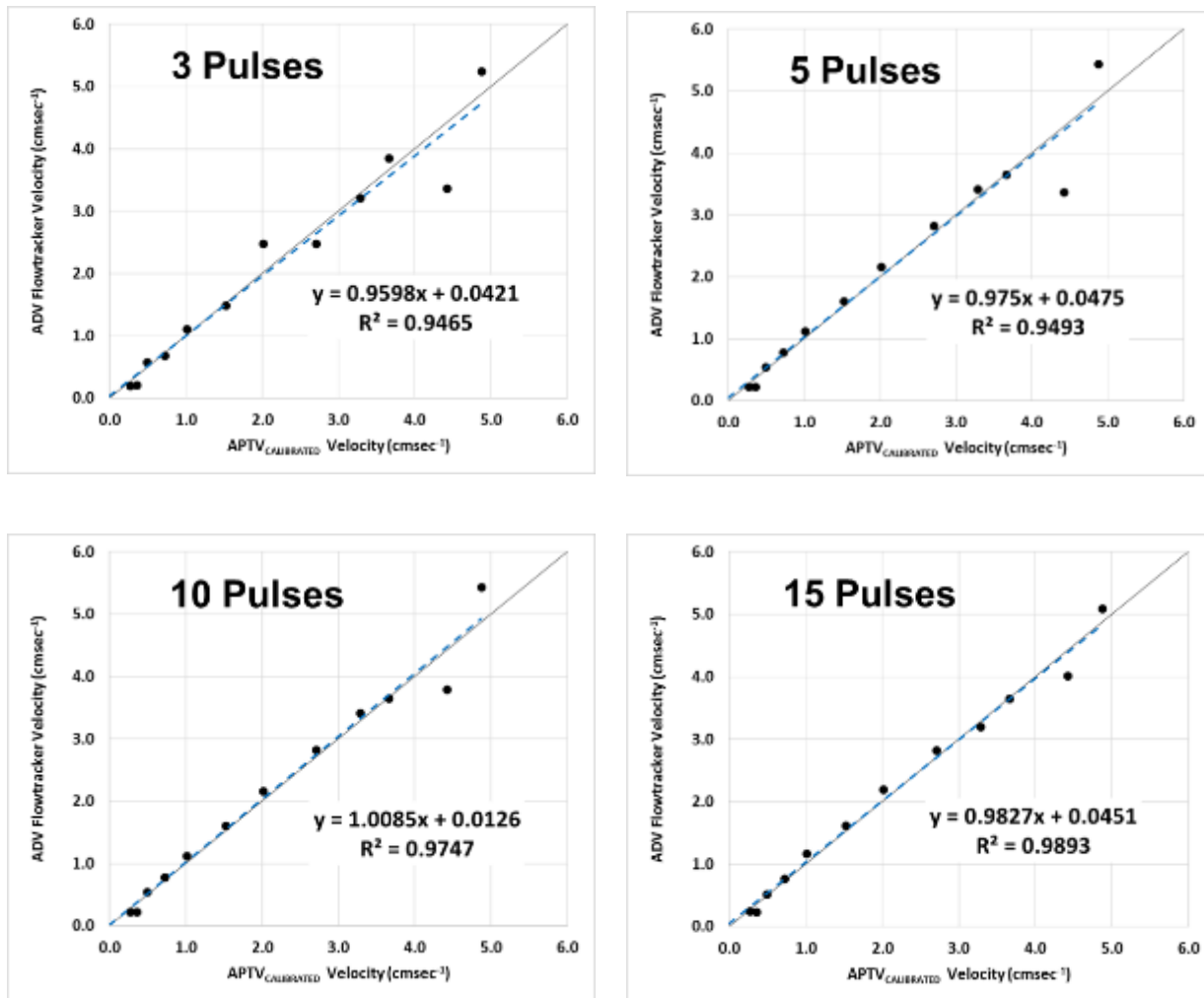


Figure 6-11 Effect of pulse averaging on correlation with ADV velocity measurements for 2nd Generation APTV.

Examples for tracer response curves for directional measurements made by the 3rd Generation APTV for 0°, 56°, and 75° flow directions tested in the hydraulic flume are displayed in Figure 6-12. For the directional measurement calculations a SNR Cut-off of 10 was selected. As seen a clear increase in pulse peaks are witnessed relating to the direction of flow. Table 6-4 summarizes the directional measurements and difference from expected values for the nine different directional angles measured. A maximum difference of -10° was measured for the flow scenario with a flow angle directed 56° to the right of the center detector.

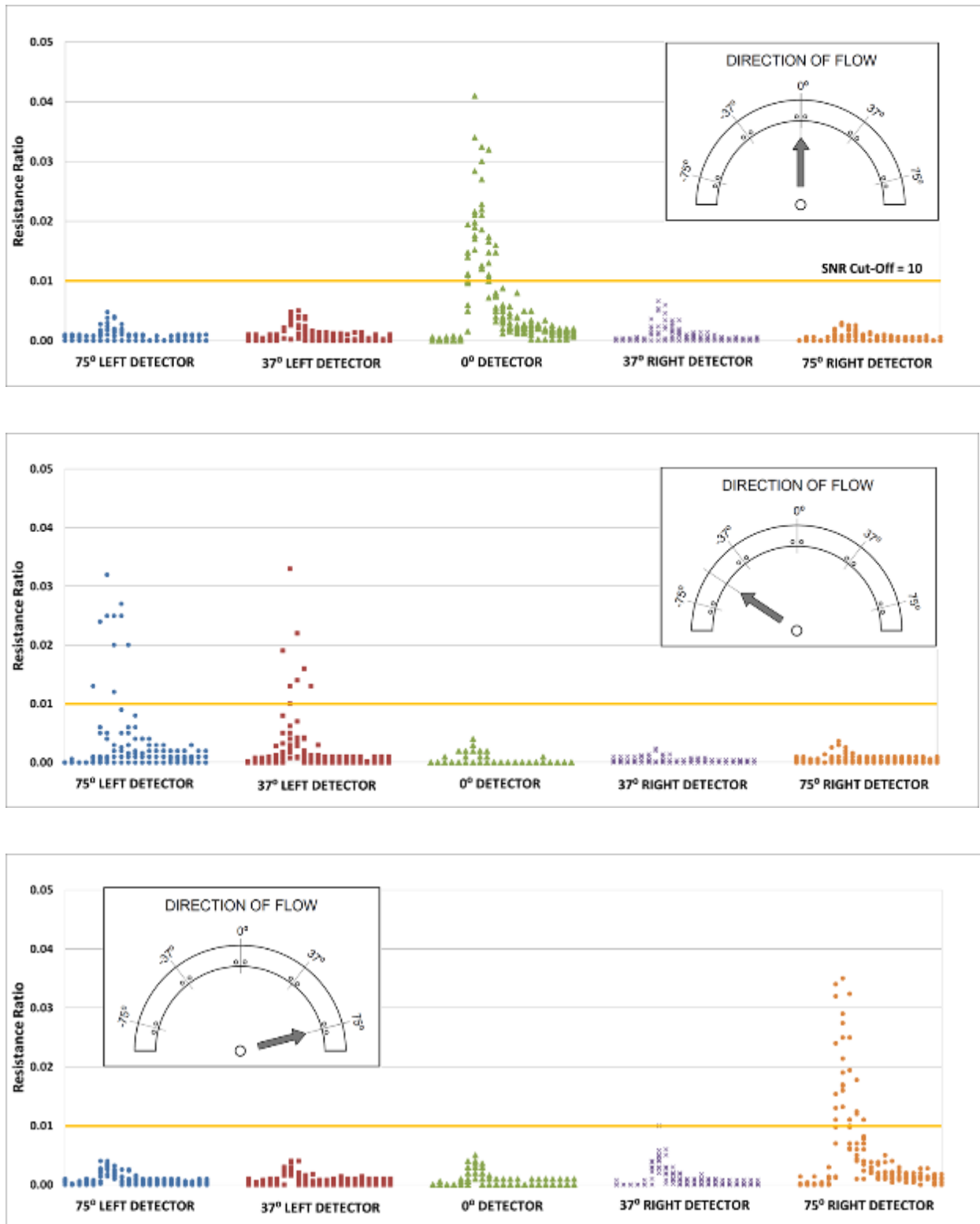


Figure 6-12 Detector response curves conducted in the flume using the 2nd Generation APTV for 0° (top), 56° to the left (middle) and 75° to the right (bottom) flow directions.

Table 6-4 Statistical summary of velocity magnitude measurements made by the 2nd Generation APTV.

APTV Orientation	Expected	Measured	Difference
Left 75 ⁰	-75	-75.00	0 ⁰
Left 56 ⁰	-56	-51.00	+5 ⁰
Left 37 ⁰	-37	-37.00	0 ⁰
Left 18 ⁰	-18	-13.00	+5 ⁰
Center 0 ⁰	0	0.00	0 ⁰
Right 18 ⁰	18	25.00	+7 ⁰
Right 37 ⁰	37	37.00	0 ⁰
Right 56 ⁰	56	46.00	-10 ⁰
Right 75 ⁰	75	75.00	0 ⁰

As mentioned earlier the accuracy of the APTV decreases with a decrease in pulses average per velocity measurement. Ideally multiple pulses should be conducted per measurement, however may not be suitable for environments with highly variable velocity conditions such as those influenced by precipitation events, where only a few pulses may be made per velocity increment. In order to test the functionality of the 2nd generation Arc-Type APTV in variable flow conditions, a flume test was conducted whereby the velocity was quickly incrementally changed on a short time scales. Both the APTV and a Flowtracker ADV were used to take continuous measurements for comparative purposes. An averaging of 3 pulses per measurement was used for APTV measurements. Figure 6-13 compares the velocity magnitude, whereas Figure 6-14 compares the flow direction. As seen there is somewhat of a reduction in correlation (R-squared = 0.855) for such environmental conditions, however overall the APTV has good agreement with the ADV. If these measurements were used for calculating volumetric loading the APTV would be expected to be within an approximate 10% error margin. Figure 6-15 displays the correlation between devices which resulted in an R-squared value of 0.855. As seen the APTV appears to under-estimate velocity measurements $> 4.5\text{cms}^{-1}$ which may be explained by the nature of the power function in the calibration equation.

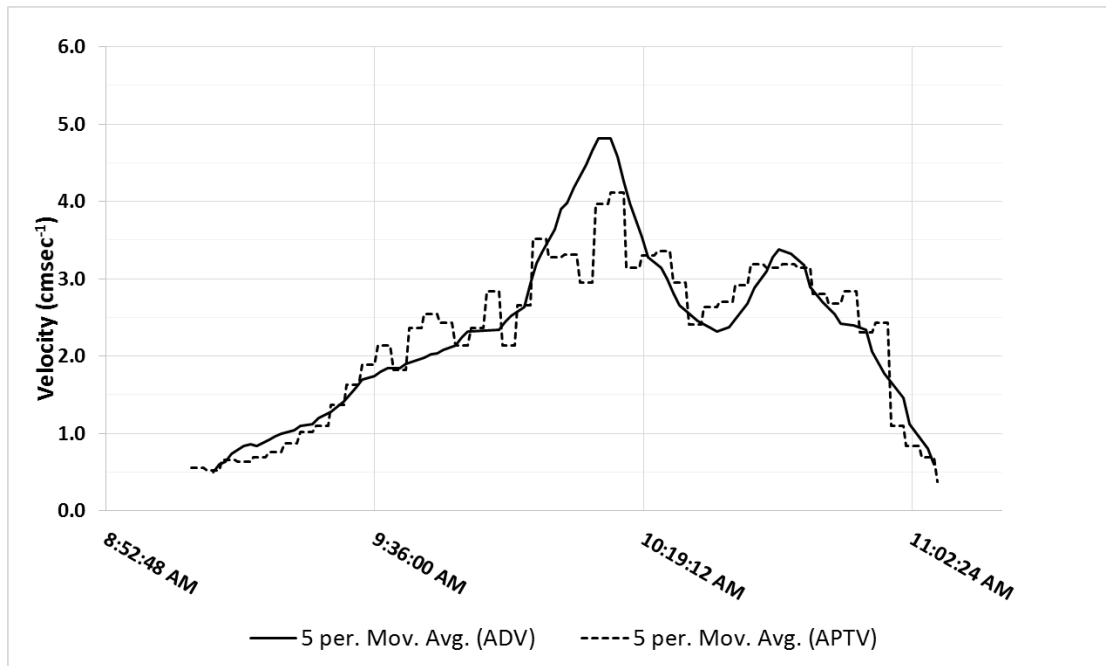


Figure 6-13 Variable velocity flume test comparing ADV with 2nd Generation APTV velocity measurements.

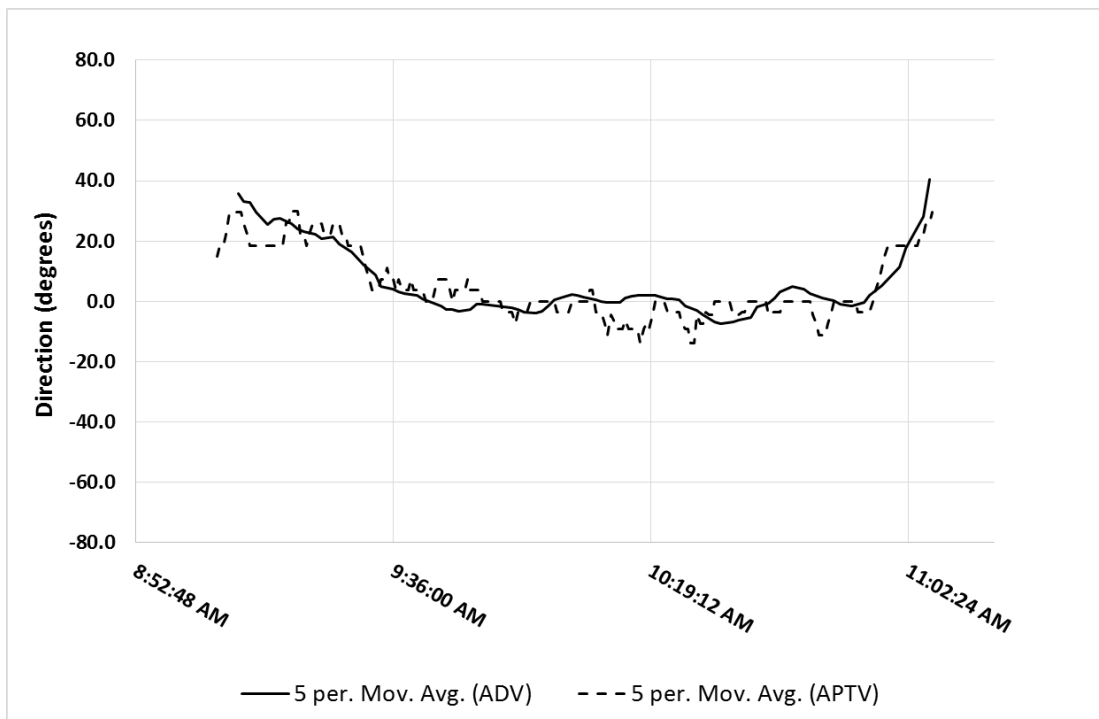


Figure 6-14 Variable velocity flume test comparing ADV with 2nd Generation APTV flow direction measurements.

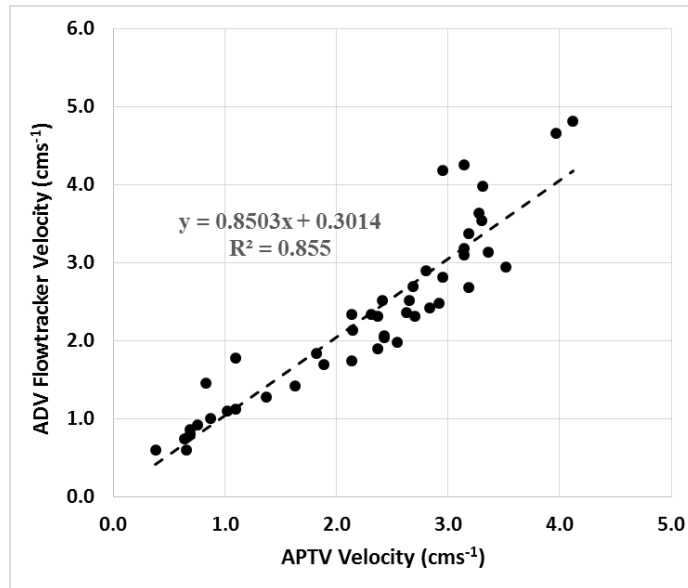


Figure 6-15 Correlation between ADV and 2nd Generation APTV velocity magnitude measurements.

6.3.3 *Field Testing*

Site 1 field velocity data indicate a flow regime dominated by a southerly flow direction by both the Vector ADV and 1st Generation APTV. For comparative purposes, the X-axis (north-south) Vector ADV velocity component was compared against the central detector (0°) for the APTV (orientated to detect southern flow). A 5-hourly moving average was applied to both the APTV and ADV data, as displayed graphically in Figure 6-16. 83 of the total 84 sampling events were measured by the APTV, resulting in a 98.8% detection rate. Five pulses were made per sampling event, of which 0, 1, 2, 3, 4 and 5 of the five pulses were detected 1%, 4%, 20%, 32%, 29% and 14% of the time, respectively. Measured velocities ranged from 1.75 cm·sec⁻¹ to 3.36 cm·sec⁻¹ for southerly flow. Data generally indicates good correlations between the two devices with both the APTV and Vector ADV displaying similar variations in flow. The highest discrepancy between the averaged data occurred on October 8th whereby the APTV measured 0.9 cm·sec⁻¹ less than the ADV, representative of a 59% slower measurement. This discrepancy

could be caused by an insufficient amount of measurements made by the APTV, a slight underestimation due to the calibration equation, or turbulent fluctuations occurring during different sampling events. The directional components of the velocities were derived using the weighted average method and displayed in Figure 6-17. Both the ADV and the APTV show a flow regime highly dominated by southern flows with a maximum difference of 16° .

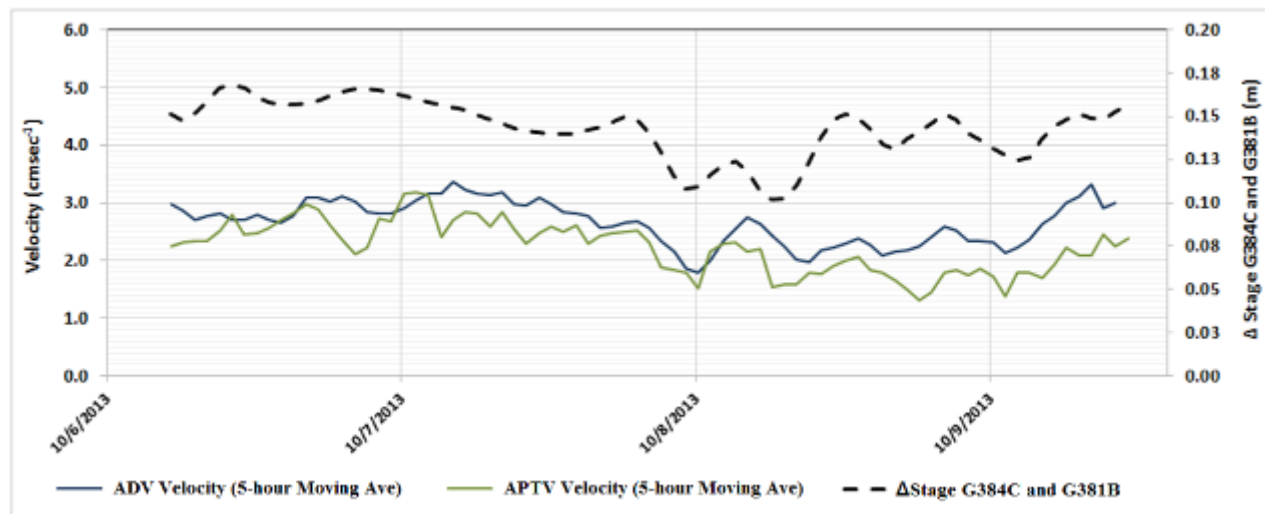


Figure 6-16 Field comparison of Vector ADV and calibrated APTV velocities for Site 1. Field measurements were conducted in Cell 3B of the STA located in the northern portion of the Everglades, FL.

Site 2 presented a more challenging environment for measurements with strong east/west fluctuations, a consistent southerly flow pattern and a low range velocity regime. This is likely due to environmental characteristics such as dense SAV and shallower waters commonly found around the study site. The X-axis (north-south) Vector ADV component was used for comparative analysis against the central detector (0°) for the APTV (which was orientated to detect southern flow), Figure 6-18. A total of 53 sampling events were attempted, of which 49% and 92% were detected by the center and combined detectors, respectively.

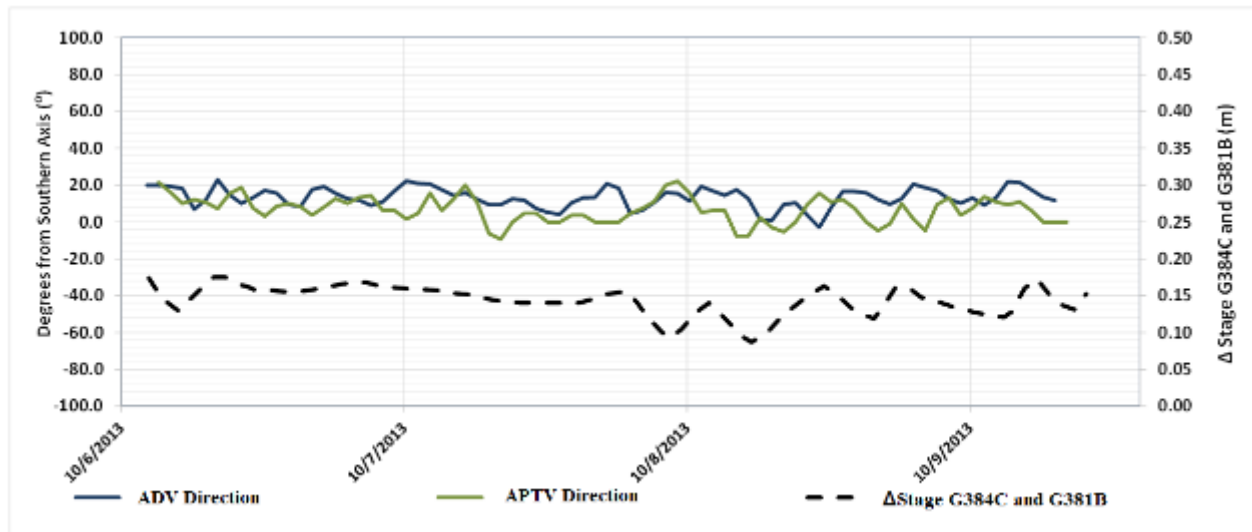


Figure 6-17 Field comparison of Vector ADV and calibrated APTV velocities for Site 1. Field measurements were conducted in Cell 3B of the STA located in the northern portion of the Everglades, FL.

ADV velocities ranged from 0 to $2.3 \text{ cm}\cdot\text{sec}^{-1}$. The APTV velocity measurements ranged from 0.60 to $1.52 \text{ cm}\cdot\text{sec}^{-1}$, whereas the ADV velocity measurements ranged from -0.27 to $2.05 \text{ cm}\cdot\text{sec}^{-1}$. These results confirmed the minimum range of the 1st Generation APTV found in the laboratory of approximately $0.5 \text{ cm}\cdot\text{sec}^{-1}$ (the minimum range limit may theoretically be lowered by decreasing the distance between the injection port and detectors). The east/west fluctuations allowed an opportunity for the directional capabilities of the detector to be tested, as graphically displayed in Figure 6-19. Although the APTV displayed a relatively good tendency in capturing the southern velocity and direction components at Site 2, the velocity measurements for the R2, R1, L1 and L2 (not shown) were not usable due to the hydrofoil design which was initially designed for strait flows. Further design work in producing a hydrofoil suitable for all the detectors is still merited.

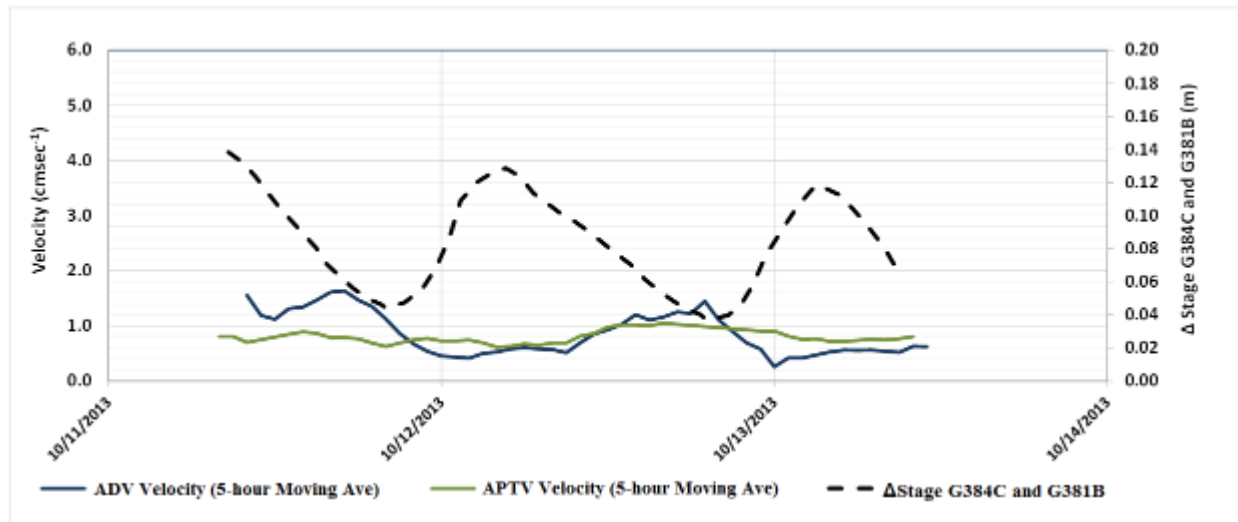


Figure 6-18 Field comparison of Vector ADV and calibrated APTV velocities for Site 2. Field measurements were conducted in Cell 3B of the STA located in the northern portion of the Everglades, FL.

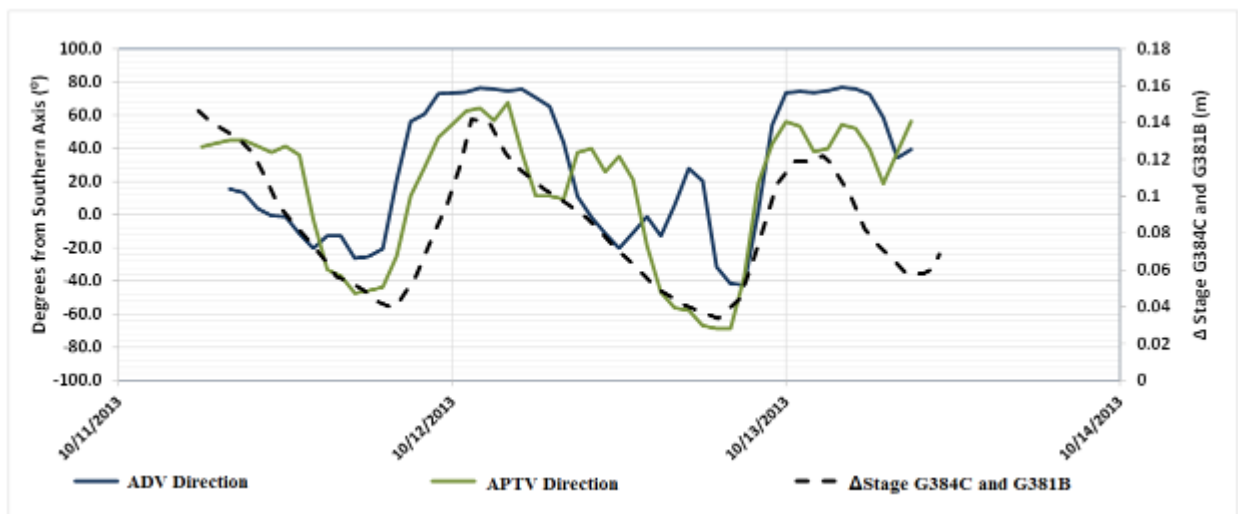


Figure 6-19 Field comparison of Vector ADV and calibrated APTV velocities for Site 2. Field measurements were conducted in Cell 3B of the STA located in the northern portion of the Everglades, FL. Positive results indicate degrees west of southern axis while negative results indicate degrees east of southern axis.

6.4 APTV Sensor Network and Other Potential Applications

The initial trials of the APTV shows promising signs for affordably installing a velocity network for measurements within a wetland system with remote sensing capabilities. Furthermore, the station may serve as a base to which an expanded sensing network system including integrated water quality and environmental sampling may be built. Utilizing the additional ports from the multiplexer, several portable “satellite” APTV detectors could be installed along a horizontal transect to capture the horizontal velocity profile for a given area. Such data would be valuable for determining areas of water “short circuiting” which may occur within wetland systems due to changes in vegetation density, bathymetry or wind effects.

Coupling such a system with water quality sensors would help establish an overall understanding of the treatment performance of a wetland, establish concentration gradients and help planners in decision making for future modifications. Additional sensors may include pressure transducers for depth measurements, turbidity meters, dissolved oxygen (DO) probes, pH probes, oxidation-reduction potential (ORP) probes as well as micro-sensors capable of measuring phosphate, ammonia, nitrate and nitrite. Additional environmental sensors may also be added such as wind gauges, precipitation gauges and solar radiation gauges. Integrating Campbell Scientific’s *LoggerNet* software, coupled with a cellular modem, allows the user the versatility to completely control the system from a laptop anywhere with an internet connection. This includes programming of pulse injection intervals, injection duration as well as satellite station operation. This could be beneficial to the user by increasing pulse frequency to obtain more accurate results during turbulent conditions, or conversely turning off pulses when measurements are not required to preserve the tracer reservoir.

Figure 6-20 displays a theoretical communications system designed to capture the horizontal velocity field using portable “satellite” APTV sensors with a master station fitted with water quality probes, solar power, data logger, multiplexer and cellular modem. Spacing of the satellite probes would only be limited to wire length, a maximum 50 meter spacing is assumed in the design, however a broader spacing is theoretically possible but has yet to be tested. Figure 6-21 displays an aerial view of the sensor network system. As seen, the surrounding area is comprised of a density variation in both SAV and EAV, as well as variations in water depths. Such an environment would prove difficult to conduct horizontal velocity field measurements with traditional velocity meters. By installing a master APTV station and multiple satellite APTV stations, a horizontal field is created to capture the flows representative of shallow dense EAV, dense SAV, and clear “channelized” flow. By utilizing such a configuration, short circuiting effects and vegetative effects on the hydrodynamics of the area may be better quantified.

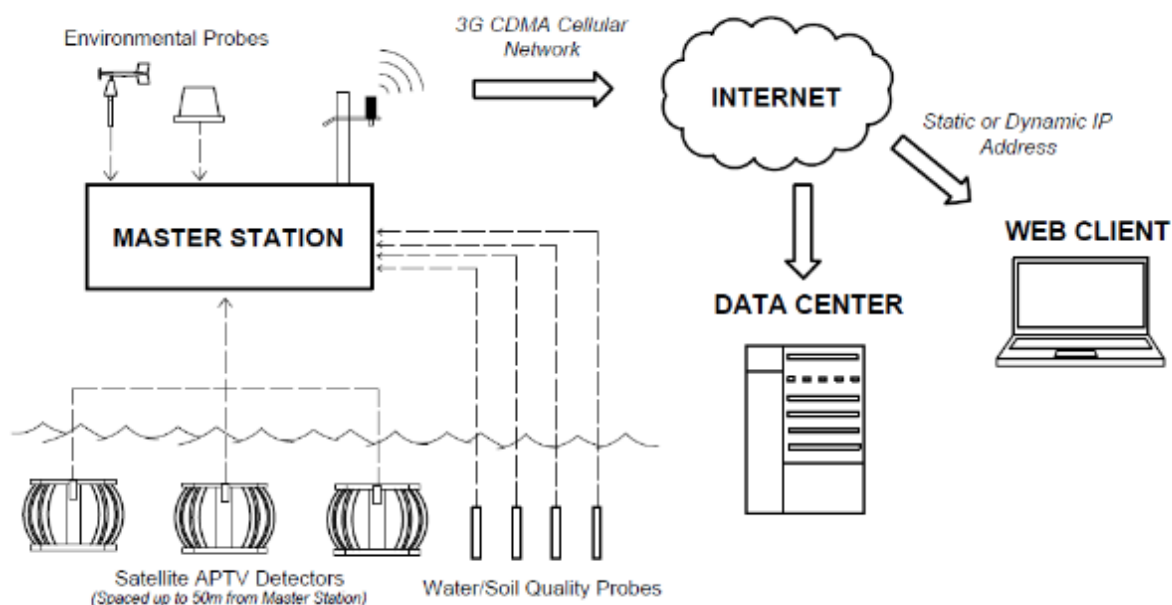


Figure 6-20 Communications diagram for full-scale remote APTV system designed for horizontal velocity field, water & soil quality and environmental measurements.



Figure 6-21 Theoretical field installation of APTV sensing network with seven velocity sensors positioned to capture horizontal velocity profile.

It should be noted that the Arc-type APTV is a first generation device and can be improved in accuracy and design. Further research may improve the design by building more hydrodynamic and accurate detector bodies utilizing 3D printer technology. Improved detector design may increase measurement accuracy by creating streamlined, uniform detector bodies designed for very minimal interfere with the detection of pulses. The improved detectors may also increase the directional range of the APTV, making the device more suitable for directionally variable flow such as found in Site 2. Additionally, research in use of more conductive, less dense tracers may increase the directional accuracy and extend the velocity range of the APTV to velocities well below $0.5 \text{ cm} \cdot \text{sec}^{-1}$. Finally, development of a computer software to make data processing more efficient would greatly reduce the time required for data post-processing.

All applications in this study thus far have focused on using salt tracers in freshwater systems. However with slight modifications the APTV may theoretically be designed to operate in saline estuary applications. This is accomplished by using a freshwater or de-ionized water tracer. As the tracer will be more buoyant than the estuary waters, the APTV design is inverted to capture the pulses released from the injection port as displayed in Figure 6-22. As the pulse passes the detectors, inverted tracer pulses will occur due to the decrease in conductivity of pulse.

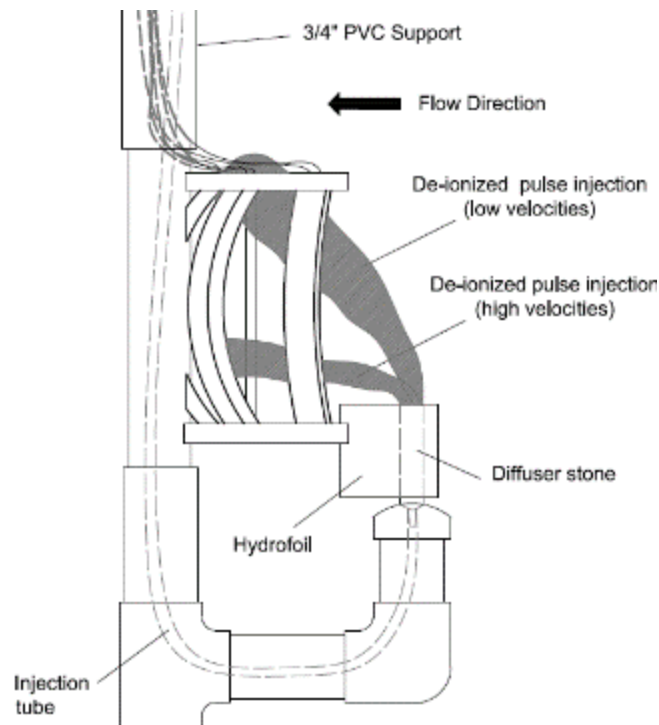


Figure 6-22 Side-view schematic of an APTV arc-type detector for operation in an estuary environment.

6.5 **Final Remarks**

The APTV sensors in this study shows promising signs to provide a cost effective, reliable alternative for measuring low flow velocities in the field environments using empirically derived calibration equations. The Δt_{PEAK} method shows good agreement when compared to Nortek Vector ADV measurements for the field environment for strait and variable flow conditions. The minimum velocity range was confirmed at $0.5 \text{ cm}\cdot\text{sec}^{-1}$ in a hydraulic flume and field, while a velocity of $5.3 \text{ cm}\cdot\text{sec}^{-1}$ was shown to be measureable in the flume. As a first generation device of APTV, there is opportunity to improve the accuracy and directional range of the APTV by techniques such as detector modification, hydrofoil design and more efficient post-processing techniques.

The results of the study indicate that the APTV is a promising new candidate for velocity and directional measurements in low flow environments such as wetlands, however comes with some limitations and has room for improvements to reach full capabilities. Due to the injection port spacing and density of the tracer, a limiting minimum velocity range of $0.5 \text{ cm}\cdot\text{sec}^{-1}$ was measured. This limit may be extended to capture lower velocities by decreasing the distance of the injection port, lengthening the detector wires, or by use of a tracer with equal density to the surrounding ambient water. Due to the hydrofoil design being initially designed for strait flows, the left and right detectors were found to have depressed velocity measurements which may be explained by turbulent eddies forming behind the hydrofoil for sideways flow directions. A revised hydrofoil design capable of reducing eddie formation behind the injection port for a flow range of 180° would overcome this limitation.

An APTV field station will also require a degree of operation and maintenance. Periodic refilling of the tracer reservoir will be required. As an example, a field station with a 20 gallon tracer reservoir, seven detectors, and a ten pulse sampling rate per hour would theoretically require tracer replacement every 16 days, not factoring in evaporative losses. Currently, some post-processing time is required to obtain velocity and directional measurements from the tracer pulses. This, however, may be sped up with the coding of a simple computer program to automatically analyze the tracer pulses to obtain velocity measurements. A summary list of the advantages and disadvantages of the APTV compared to other low flow meters is presented in Table 4.

Despite these limitations, the APTV has several operational advantages, especially with regards to conducting measurements in wetland environments. Firstly, the APTV has a significant cost advantage compared to acoustic Doppler technology. For a single point sampling volume, the APTV would only cost approximately 15% compared to the average cost of using an ADV, and when the number of sampling points increases to seven (7) the APTV costs drops down to approximately 5% of that of ADVs. Secondly, the APTV is more suited to horizontal profiling in shallow water conditions with dense vegetation. This is accomplished by spacing of sampling locations along a horizontal transect. Although ADCPs may be used for horizontal profiling by orientating the device sideways, several limitations prevent useful measurements when applied to a wetland system, mainly due to side lobe interferences. Side lobe interferences occur when parasitic side lobes reflect off of the bottom and water surface prior to the main beam transmitting across the full sampling volume, making data unusable at certain distances. As the water depth decreases these effects increase, which will likely render the ADCP unusable for such environmental conditions commonly found in the Everglades. In

addition, patches of dense EAV and SAV would block the transmission of acoustic pulses, thereby decreasing the sampling volume. Finally, the APTV does not have inherent limitations while operating in very low suspended solid conditions, such as with ADVs and ADCPs due to low signal strengths which reflect from suspended solids, resulting in low SNRs and higher errors. Conversely the APTV will have greater SNR for these environments.

6.6 References

- Ball M. H., R. W. Schaffranek, 2000. Flow-velocity data collected in the wetlands adjacent to canal C-111 in South Florida during 1997 and 1999. US Geological Survey Open File Report, 00-56.
- Barko J., D. Gunnison, S. Carpenter, 1991. Sediment interactions with submersed macrophyte growth and community dynamics. *Aquatic Botany*, 41, 41-65.
- Bayless E. R., W. Mandell, J. Ursic, 2011. Accuracy of flowmeters measuring horizontal groundwater flow in an unconsolidated aquifer simulator. *Groundwater Water Monitoring and Remediation*, 31(2), 48-62.
- Bokainan A., F. Geoola, 1984. Wake-induced galloping of two interfering circular cylinders. *Journal of Fluid Mechanics*, 146, 383-415.
- Blevins R., 1994. *Flow-induced Vibration*. Krieger, Malabar, Fla.
- Chanson H., M. Trevethan, S. Aoki, 2008. Acoustic Doppler velocimetry (ADV) in small estuary: Field experience and signal post-processing. *Flow Measurement and Instrumentation* 19, 307-313.
- Cliff R. H., D. E. Bazemore, 1993. Temporal and spatial patterns of wetland sedimentation, West Tennessee. *Journal of Hydrology* 141, no. 1-4, 179-196.

- Chimney M. J., G. Goforth, 2006. History and description of the Everglades nutrient removal project, a subtropical constructed wetland in south Florida (USA). *Journal of Ecological Engineering*, 27, 268-278.
- Devlin J. F., G. Tsoflias, M. McGlashan, and P. Schillig, 2009. An inexpensive multilevel array of sensors for direct ground water velocity measurement. *Ground Water Monitoring & Remediation* 29, no. 2, 73-77.
- Devlin J. F., P. C. Schillig, I. Bowen, C. E. Critchley, D. L. Rudolph, N. R. Thomson, G. P. Tsoflias, and J. A. Roberts, 2012. Applications and implications of direct groundwater velocity measurement at the centimetre scale." *Journal of contaminant hydrology* 127, no. 1, 3-14.
- Fischer H. B., E. J. List, R. Koh, J. Imberger, N. Brooks, 1979. *Mixing in Inland and Coastal Waters*. Academic, San Diego, Calif., 1979.
- Genereux D., E. Slater, 1999. Water exchange between canals and surrounding aquifer and wetlands in the Southern Everglades, USA. *Journal of Hydrology* 219, 153-168.
- Hatfield K., M. Annable, J. Cho, J., 2004. A direct passive method for measuring water and contaminant fluxes in porous media. *Journal of Contamination Hydrology*, 75, 155-181.
- Jury W. A., K. Roth, 1990. *Transfer functions and solute movement through soil: theory and applications*. Birkhäuser Verlag AG.
- Kerfoot W. B., 1994. Independent verification of heat pulse groundwater flowmeter results through long term observation and tracer tests on superfund sites. *Hydrocarbon Contaminated Soils*, 5, 37-49.
- Kerfoot W. B., V. A. Massard, 1985. Monitoring well influences on direct flowmeter measurements. *Ground Water Monitoring and Remediation*, 5(4), 74-77.

- Kempf A., C. E. Divine, G. Leone, S. Holland, and J. Mikac, 2013. Field performance of point velocity probes at a tidally influenced site. *Remediation Journal* 23, no. 1 37-61.
- Kovacic D. A., M. B. David, L. E. Gentry, K. M. Starks, R. A. Cooke, 2000. Effectiveness of constructed wetlands in reducing nitrogen and phosphorus export from agricultural tile drainage. *Alliance of Crop, Soil and Environmental Science Societies*, 29, no. 4, 1262-1274.
- Labaky W., J. F. Devlin, R. W. Gillham, 2007. Probe for measuring groundwater velocity at the centimeter scale. *Environmental science & technology* 41, no. 24, 8453-8458.
- Labaky W., J. F. Devlin, and R. W. Gillham, 2009. Field comparison of the point velocity probe with other groundwater velocity measurement methods. *Water Resources Research* 45, no. 4.
- Lee C. K., K. Low, N. Hew, 1991. Accumulation of arsenic by aquatic plants. *Science and The Total Environment*, 103, 215-227.
- Lee J. K., V. Carter, 1999. Field measurement of flow resistance in the Florida Everglades. *US Geological Survey Open File Report*, 99-181.
- McLelland S. J., A. P. Nicholas, 2000. A new method for evaluating errors in high-frequency ADV measurements. *Hydrological Processes*, 14, 351-366.
- McCormick, P.V., S. Newman, S. Miao, D.E. Gawlick, D. Marley, K.R. Reddy, T.D. Fontaine, 2002. Effects of anthropogenic phosphorus inputs on the Everglades. In: Porter, J.W., Porter K.G. (Eds.), *The Everglades, Florida Bay and Coral Reefs of the Florida Keys-An Ecosystem Sourcebook*. CRC Press, Boca Raton, FL, 83-126.
- Nepf H. M., J. A. Sullivan, R. A. Zavistoski. A model for diffusion within an emergent plant canopy. *Limnology and Oceanography*, 42(8), 85-95.

- Nepf H. M., 1999. Drag, turbulence, and diffusion in flow through emergent vegetation. *Water Resources Research* 35, no.2, 479-489.
- Nepf H. M., E.R. Vivoni, 2000. Flow structure in depth-limited, vegetated flow. *Journal of Geophysical Research* 105, no. c12, 28,547-28,557.
- Nikora V. I., D. G. Goring, 1998. ADV Measurements of turbulence: can we improve their interpretation?. *Journal of Hydraulic Engineering, ASCE*, 124, no. 6, 630-634
- Nixon S., 1980. Between coastal marshes and coastal waters – A review of twenty years of speculation and research on the role of salt marshes in estuarine productivity and water chemistry. *Estuarine and Wetland Processes*, 438-525.
- Orson R., R. Simpson, R. Good, 1992. A mechanism for the accumulation and retention of heavy metals in tidal freshwater marshes of the Upper Delaware River estuary. *Estuarine Coastal Shelf Science*, 34, 171-186.
- Philips J., 1989. Fluvial sediment storage in wetlands. *Water Resources Bulletin*, 25, 867-872.
- Rhemel M., 2007. Application of acoustic Doppler velocimeters for streamflow measurements. *Journal of Hydraulic Engineering*, 133, 1433-1438.
- Schaffranek R. W., A. L. Riscassi, 2003. Sheet flow in vegetated wetlands of the Everglades. *US Geological Survey*.
- Scheidt D. J., M. D. Flora, D. R. Walker, 1989. Water quality management for Everglades National Park. In: *Wetland Concerns and Successes*. American Water Research Association, 377-390.
- Scholes L., R. B. E. Shutes, D. M. Revitt, M Forshaw, D. Purchase, 1998. The treatment of metals in urban runoff by constructed wetlands. *Science of The Total Environment* 214, no. 1-3, 211-219.

- South Florida Water Management District, 2012. Performance and Optimization of the Everglades Stormwater Treatment Areas. 2012 South Florida Environmental Report, chap 5.
- Swift D. R., R. B. Nicholas, 1987. Periphyton and water quality relationships in the Everglades Water Conservation Areas. Tech Pub. 87-2, South Florida Water Management District, West Palm Beach, Fl.
- Vermeyen T, 2003. Acoustic Doppler velocity measurements collected near a municipal water intake, Lake Mead, Nevada-Arizona. Proc. of the IEEE/OES Seventh Working Conference on Current Measurement Technology.
- Water Survey of Canada, 2006. Comparison measurements between Sontek Flowtracker acoustic Doppler velocimeter and Price current meters. Water Survey of Canada Test Plan and Report.
- Williamson C. H. K., 1992. The natural and forced formation of spot-like “vortex dislocations” in the transition of a wake. *Journal of Fluid Mechanics*, 243, 393-441.

CHAPTER 7: CONCLUSIONS

In summary, the work included in this thesis present several new affordable options for both stormwater nutrient reduction including sloped, horizontal and floating media bed reactors, as well as stormwater monitoring including a groundwater velocity probe, low range surface water velocity, and automated water sample collection. These devices may be useful in providing affordable options for storm water management, allowing more sensing locations per budgets. The results of these technologies are presented below.

The MBRs were found to operate effectively in the field using solar powered submersible pumps to cycle stormwater through the media bed. Reductions in tested parameters were found to vary between each MBR. The SMBR reduced the mean concentrations of all tested parameters which included TP, SRP, TN, NH_4 , NO_x , Org-N, turbidity and chl-*a* during a 6-month study period, however only Turbidity and chl-*a* had confirmed statistical reductions in the means when tested at an α value of 0.05 using a one-tailed t-test. TP was reductions were found statistically significant at an α value of 0.15. The HMBR was found to reduce mean concentrations of TP, TN, NO_x , Org-N, turbidity and chl-*a*, while TN, Org-N, and chl-*a* were found to have statistical decreases in mean concentrations at an α value of 0.05 using a one-tailed t-test. Finally the FMBR was found to reduced the mean concentrations of TP, SRP, TN, NO_x , Org-N, and chl-*a* during a 6-month study period. TP had a confirmed statistical reduction in the means when tested at an α value of 0.05 using a one-tailed t-test. Overall the MBRs reduce the majority of parameters tested and are found to be an effective BMP method for inter-event pond treatment, however ultimate use will largely depend on cost and maintenance concerns. Further research is merited to analyze the effects of the effluent water

from MBRs to pond water quality when operated in direct re-cycle and direct discharge configurations.

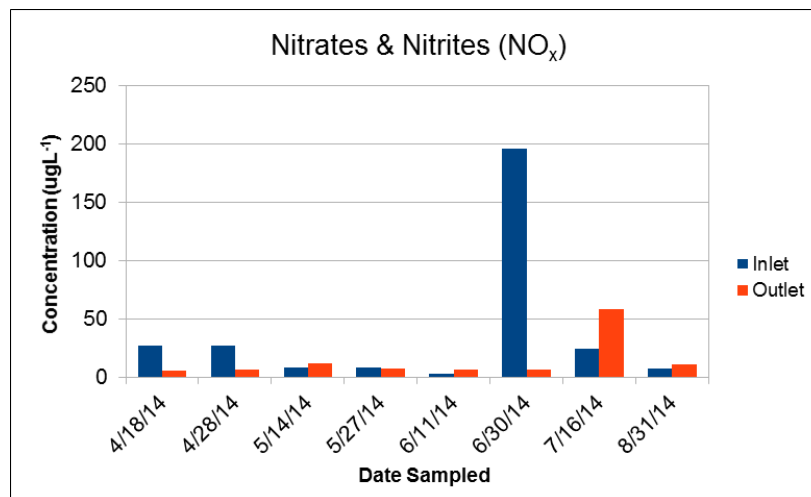
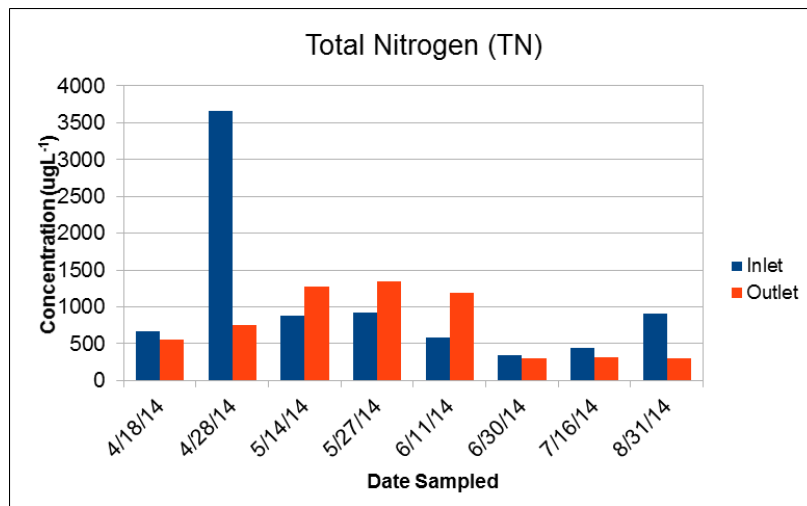
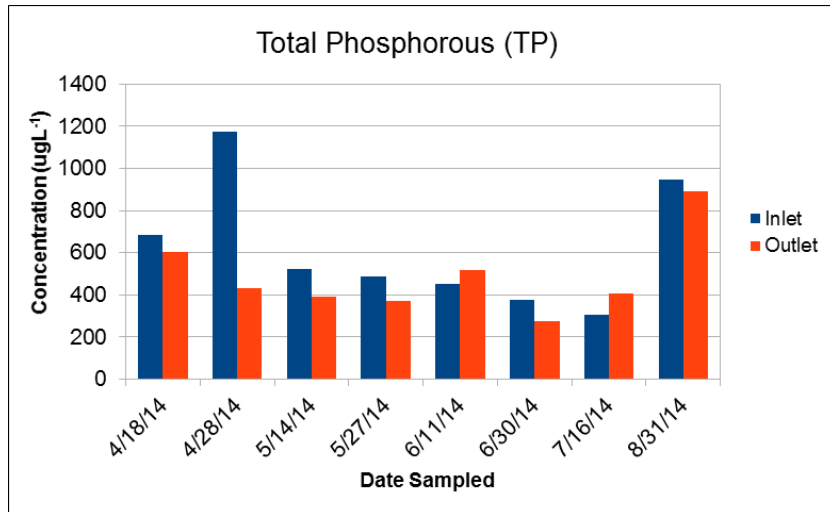
Initial trials of the GVP show promising signs of 2-D velocity magnitude, flow direction, hydraulic conductivity and to some extent lateral dispersion coefficient measurements on the centimeter scale. The GVP was shown to effectively measure the flow velocity using a moments method for non-cohesive sandy soil in a laboratory flume at 25°C from 26 to 459 cm d^{-1} (minimum and maximum values indicating pumping limitations with theoretical detections possible below or above tested ranges). Using a weighted averaging technique directional measurements of flow velocity were shown to be effective to within approximately 14° of expected values with hydraulic conductivity measurements within 1 order of magnitude to core laboratory samples. Use of the device is beneficial compared to traditional hydraulic gradient methods in establishing small scale spatial variability within aquifers, establishing low-range velocity measurements where pressure transducer resolutions present significant error, and environments with variable directional flow that hydraulic gradient measurements cannot account for and the device may be useful for field calibration samples for model and other developing technologies.

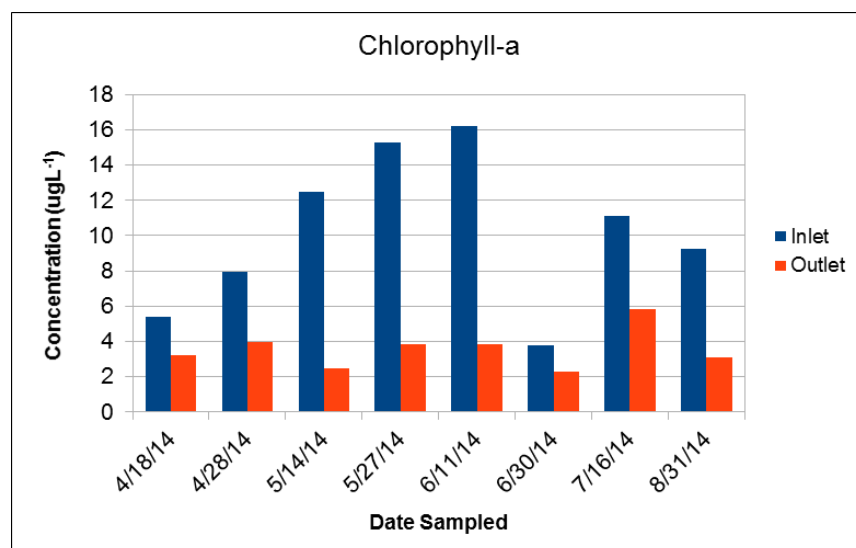
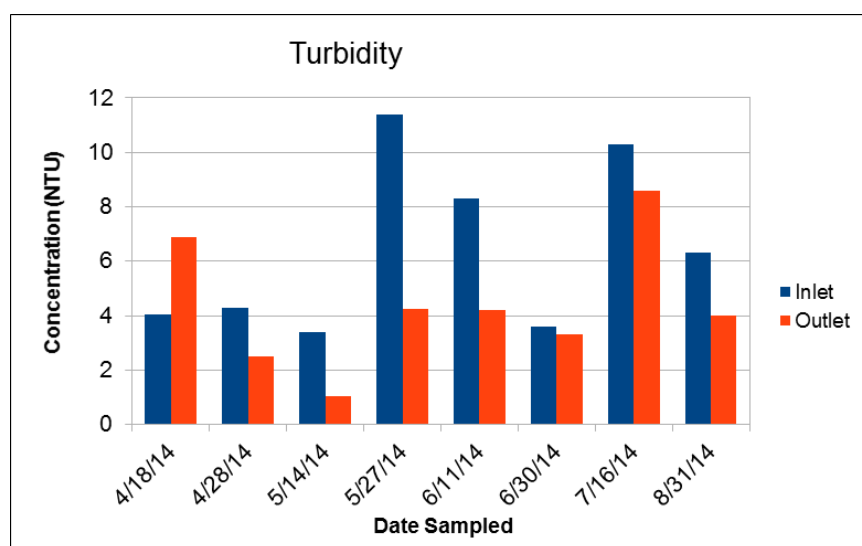
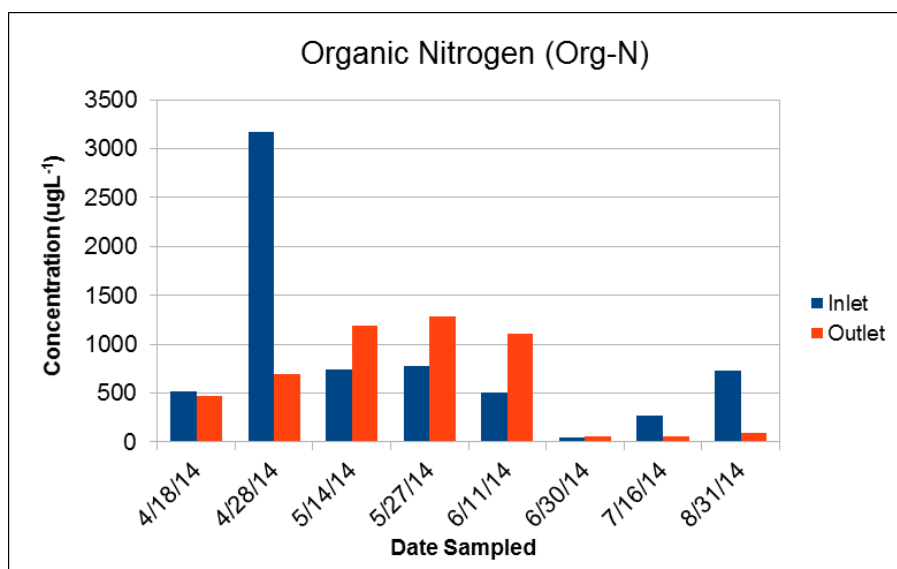
The wireless automated sampler network was found to operate effectively by text activation for predetermined sampling intervals in a pond during a storm event. The device was found to be much more affordable than current samplers on the market. The device may be useful in a number of applications, especially with respect to establishing pollutant flux gradients related to first flush phenomena within stormwater systems. Further work is merited to use the technology for field sample and analysis work.

Finally the Arc-Type APTV was found to be a cost effective and reliable alternative for measuring low flow velocities in the field environments using empirically derived calibration equations. The device is useful in replacing more expensive acoustic Doppler velocimeters for low range velocity ranges. The APTV may be particularly useful in coupling with mechanical flow velocimeters in order to allow capture of a full velocity range. Due to its affordable price the device would be useful in stormwater wetlands, allowing more sampling locations for the same price of other velocimeters. For a single point sampling volume, the APTV would only cost approximately 15% compared to the average cost of using an ADV, and when the number of sampling points increases to seven (7) the APTV costs drops down to approximately 5% of that of ADVs. Using a 3rd generation APTV and calibration equation technique, the device was found to measure to within 10% of velocity magnitude as measured by the ADVs across a 0.27 to 4.5 cm·sec⁻¹ range. Faster velocities were capable of measurement up to approximately 5.5 cm·sec⁻¹, however accuracy drops. Directional measurements were found to be within a 10° range of expected directional flow angles.

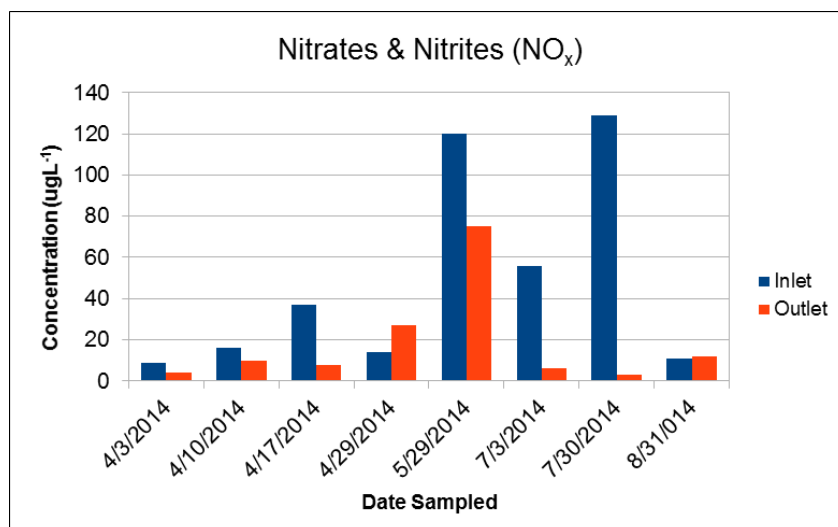
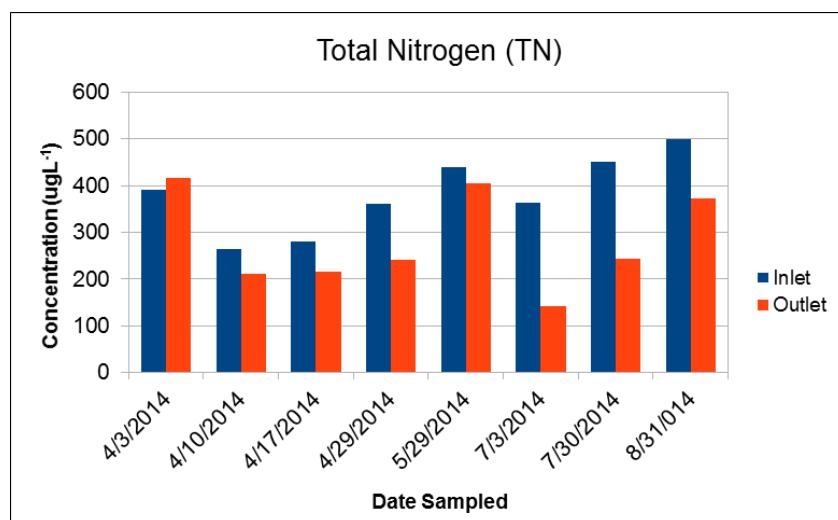
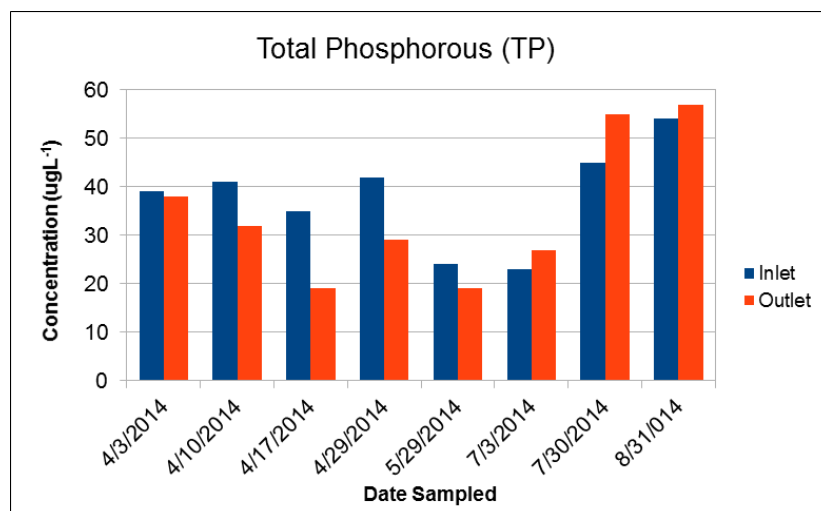
By applying such affordable technologies to stormwater management we may both decrease pollutant loading to surface waters while increasing our understanding of hydrologic behaviors. Further research and advancements may be made to the work presented in this thesis to increase accuracy, efficiency and usability.

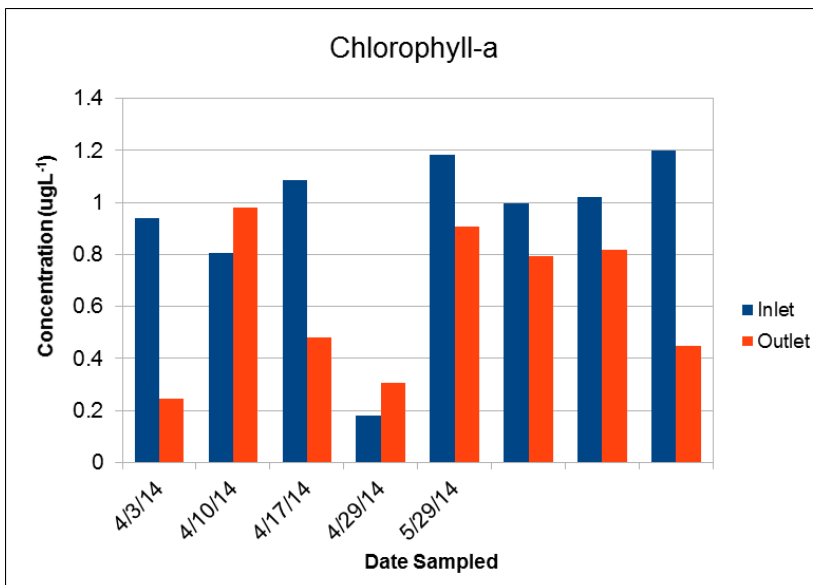
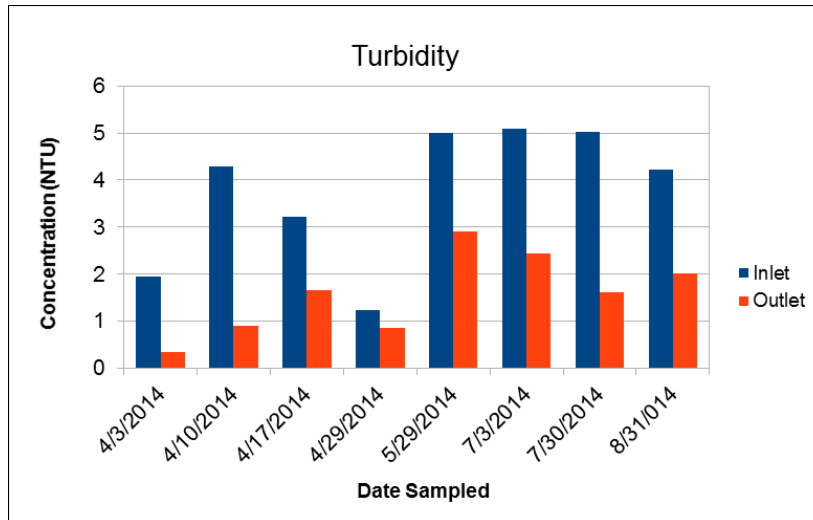
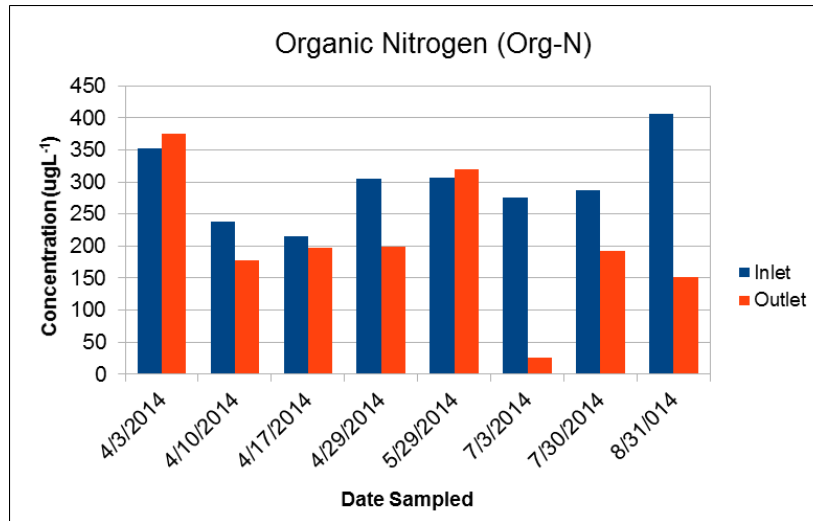
APPENDIX A: HMBR RESULTS



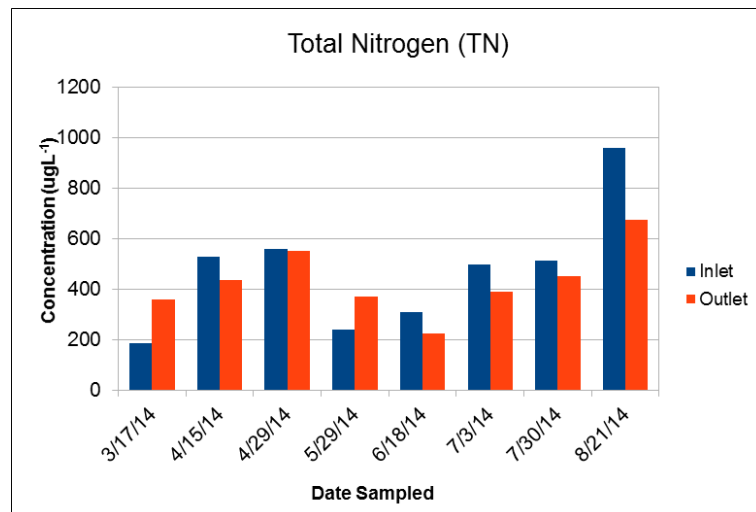
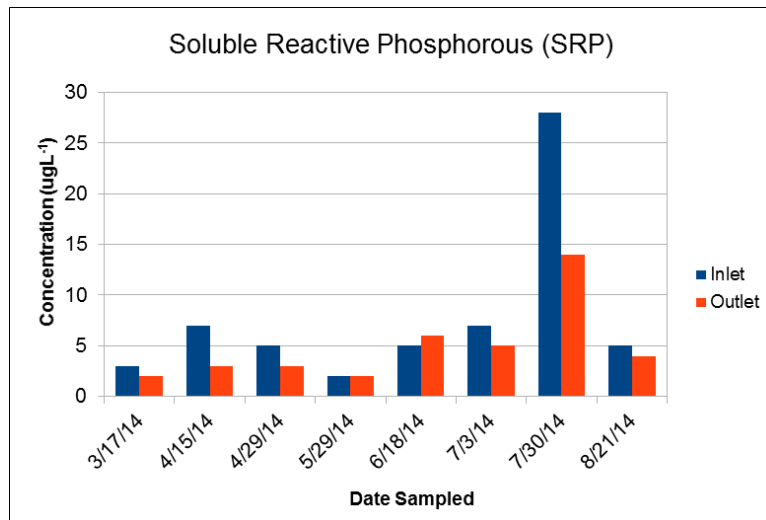
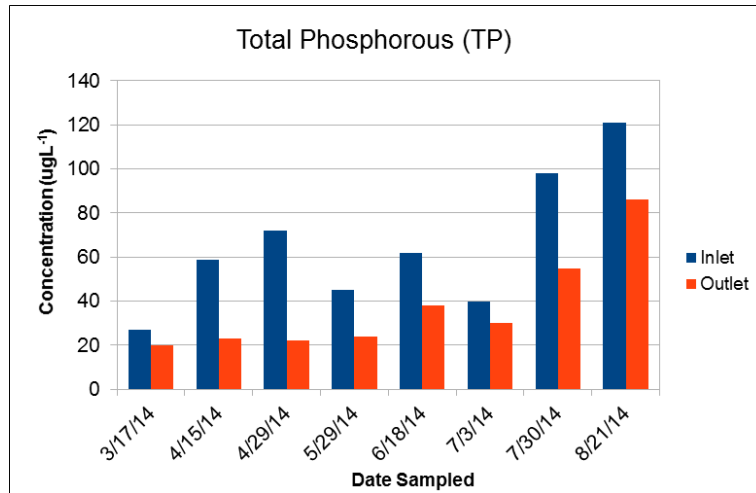


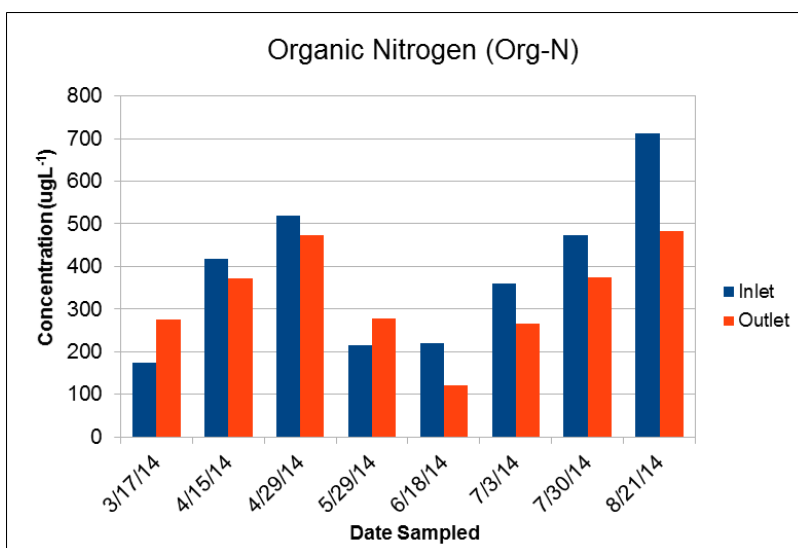
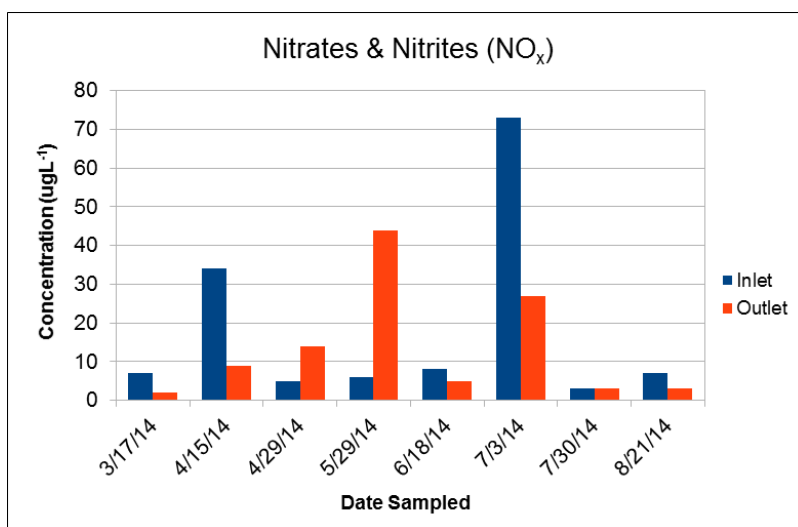
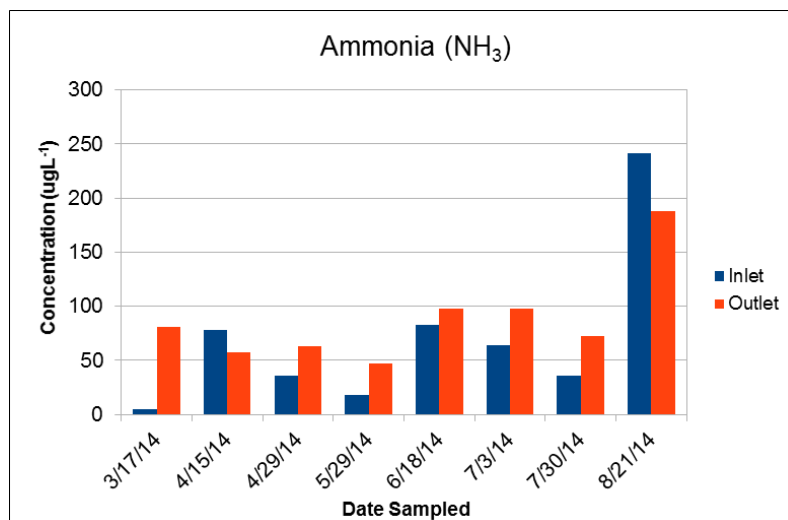
APPENDIX B: SMBR RESULTS

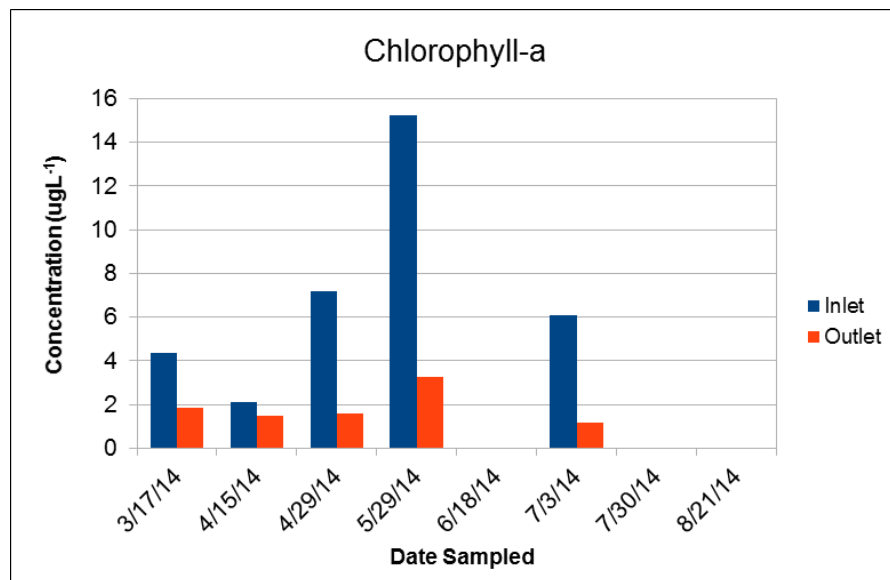
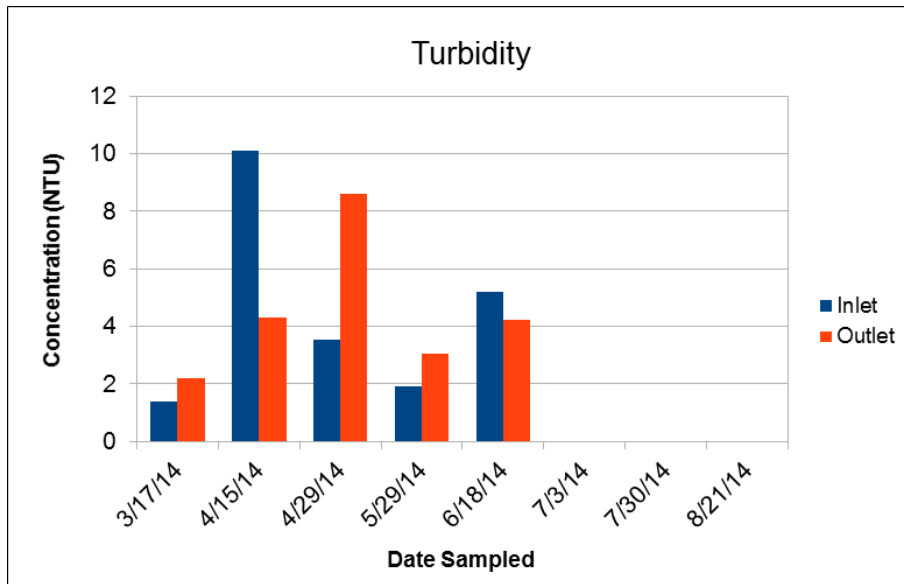




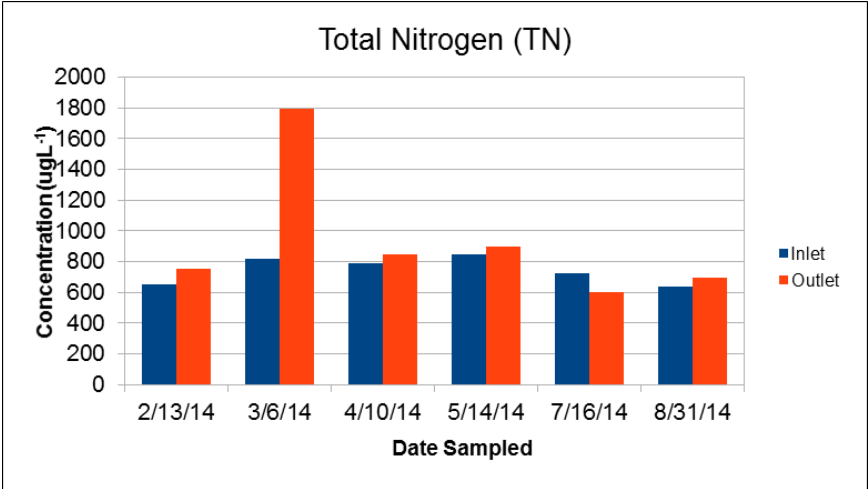
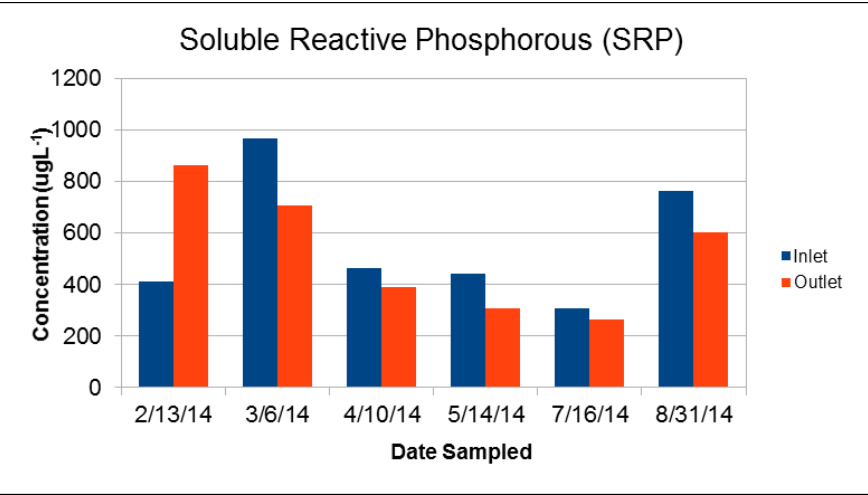
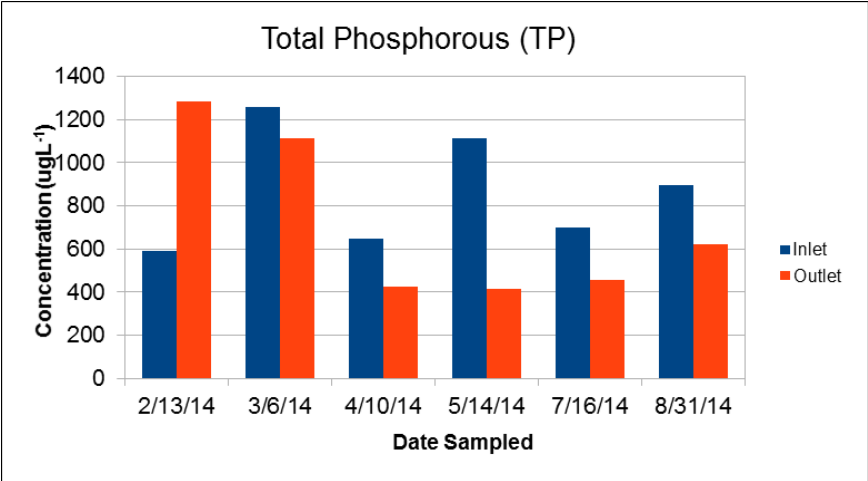
APPENDIX C: FMBR RESULTS

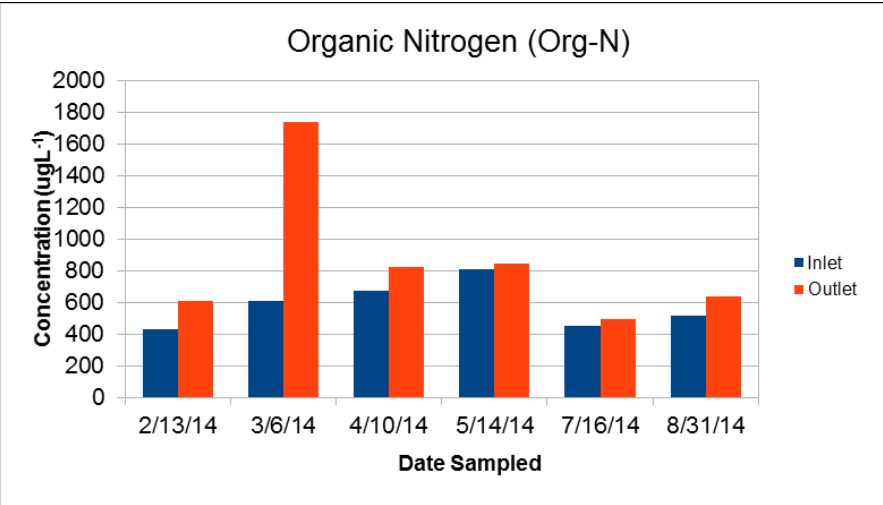
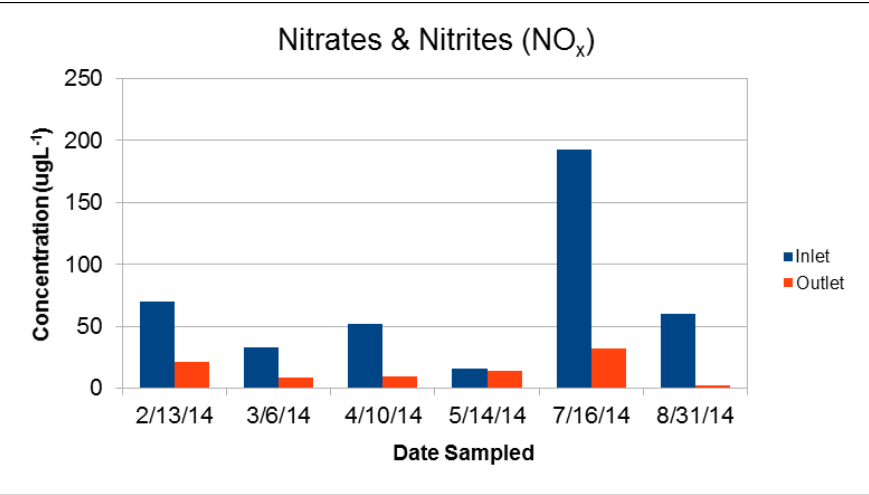
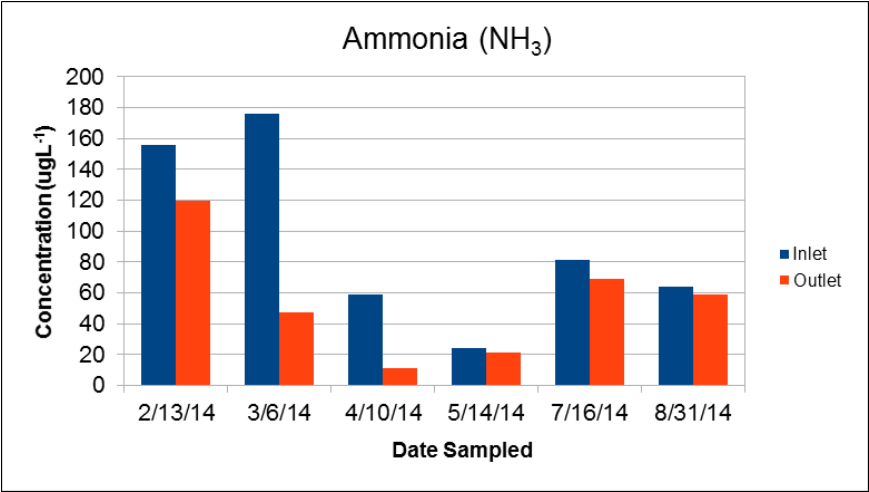




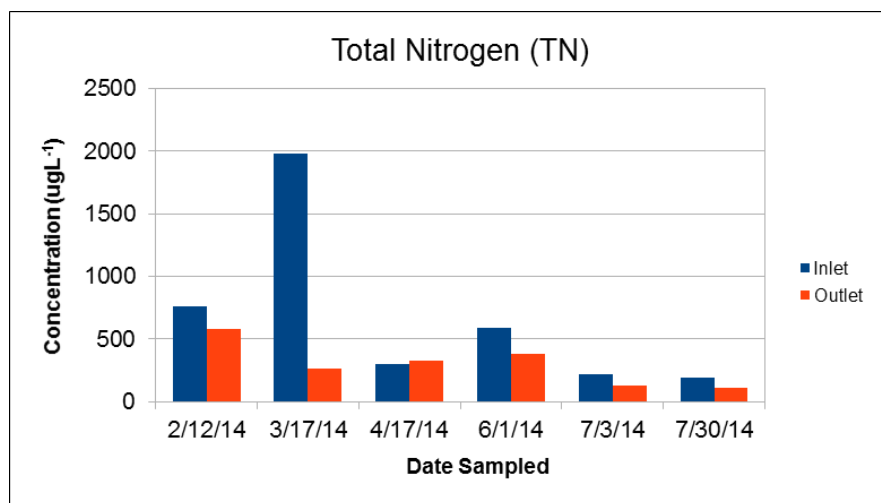
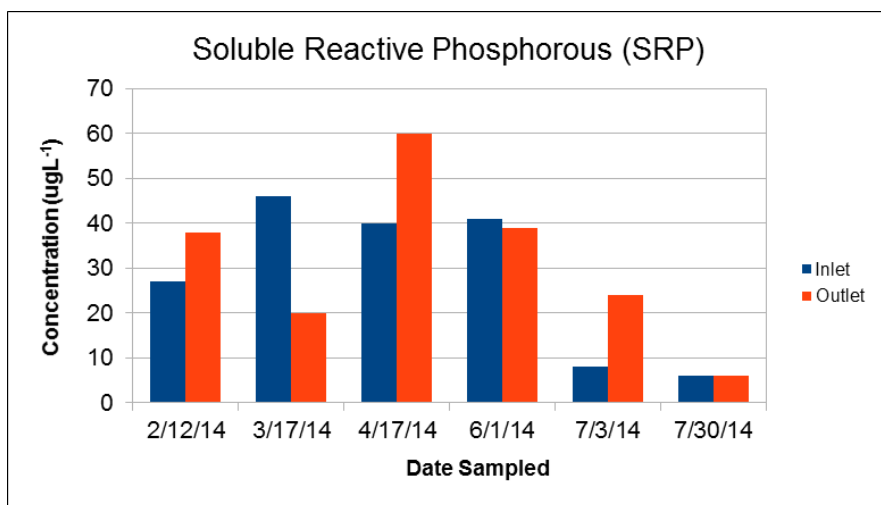
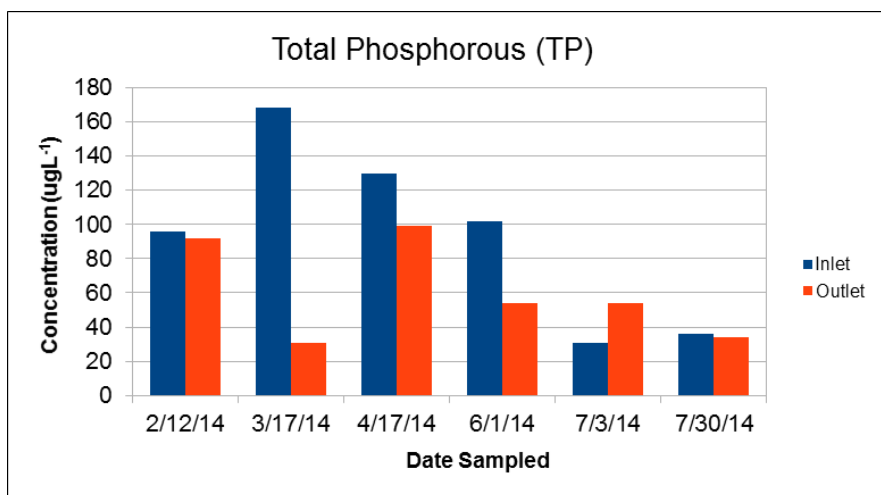


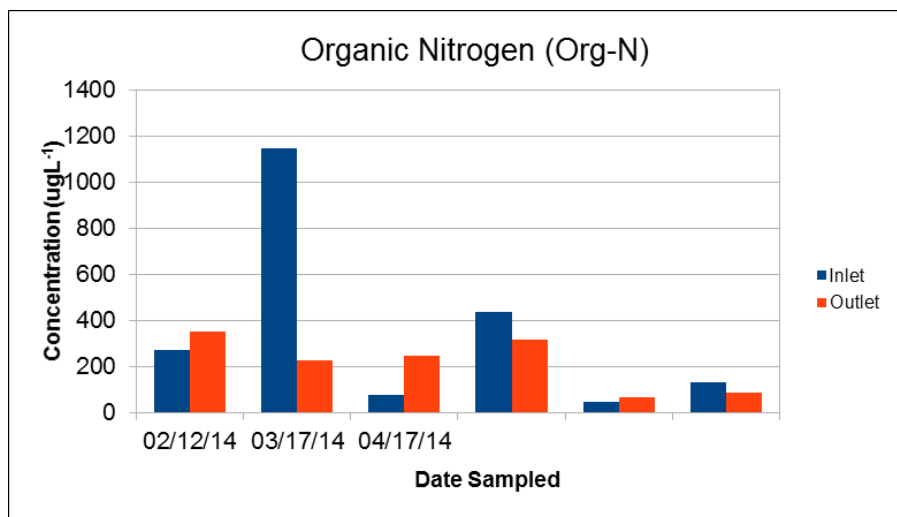
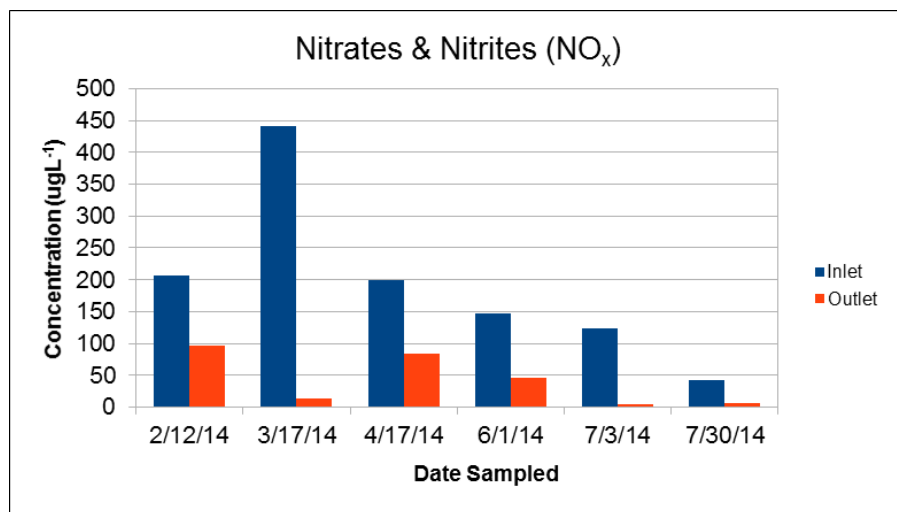
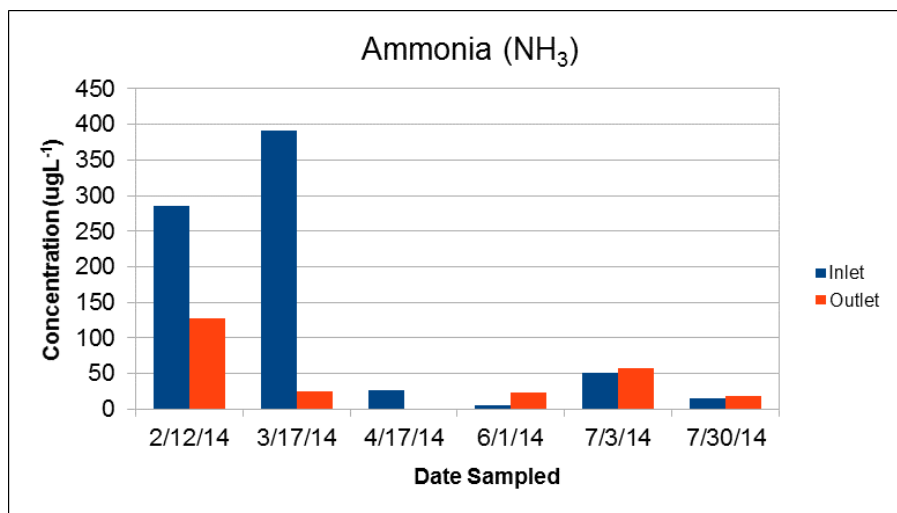
APPENDIX D: ZOLFO POND RESULTS





APPENDIX E: ORLANDO POND RESULTS





APPENDIX F: PALATKA POND RESULTS

